UNIVERSIDAD AUTÓNOMA
DE MADRID

FACULTY OF SCIENCES

DEPARTMENT OF MOLECULAR BIOLOGY

DISSERTATION TITLE:

STUDY OF PI3K PROTECTIVE ACTIONS IN Aβ42-INDUCED NEURODEGENERATION

by

Mercedes Arnés Fernández

May 2016

STUDY OF PI3K PROTECTIVE ACTIONS IN Aβ42-INDUCED NEURODEGENERATION

by

Mercedes Arnés Fernández

B.Sc. in Biology

B. Sc. in Biochemistry

A dissertation submitted to the Faculty of Sciences
at the Autonomous University of Madrid
in partial fulfillment of the requirements for the degree of
Doctor of Philosophy in Molecular Biosciences

May 2016

Supervisor: Dr. Sergio Casas Tintó

Co-supervisor: Dr. Ángel José Acebes Vindel

Advisor: Dr. Francisco Zafra Gómez

Cajal Institute

CSIC

SUMMARY

In this thesis we aimed to evaluate the ability of PI3K overexpression to induce synaptogenesis in a pathological context where synapses are degenerated due to Aβ42 accumulation. In addition we analyzed the mechanism underlying PI3K actions in Aβ42 affected synapses, and the overall effects that synaptic changes have from a whole organism perspective. Our data demonstrated that PI3K activation is beneficial in Aβ42 neurodegeneration since it prevented synapse loss, microtubule dynamics defects, and locomotion and lifespan reduction.

Furthermore, we described a novel effect of PI3K in Aβ aggregation that induces the generation of insoluble deposit. This change in conformation is suggested to occur due to a PI3K mediated phosphorylation in residue Ser-26 of Aβ backbone.

Synaptogenic and aggregation effects of PI3K in Aβ42 neurodegeneration are also reproduced in human neuroblastoma cells, proving that both actions are conserved in humans, and suggesting that it could be considered for future therapeutic studies in AD.

In addition, discovery of a transient neuronal enhancer activation event in epithelial cells during early development in *Drosophila*, helped us uncover new Aβ42 toxic effects in non-neuronal cells. In epithelial cells Aβ activated apoptosis and induced Wnt signaling misregulation. Both in epithelial cells and in neurosecretory cells Aβ42 deleterious effects were restored by PI3K.

SUMMARY (in Spanish)

En esta tesis doctoral se estudia la habilidad de PI3K, fosfatidilinositol-3 kinasa, para inducir sinapsis en un contexto patológico donde éstas se hallan deterioradas debido a la acumulación tóxica del péptido amiloide Aβ42. Además, se analiza el mecanismo de acción de PI3K en las sinapsis afectadas por Aβ42, y los efectos que se producen a nivel de organismo completo debidos a los cambios sinápticos. Nuestros datos demuestran que la activación de PI3K, y la en general de la ruta de señalización sinaptogénica, es beneficiosa en un contexto de neurodegeneración producido por Aβ42 ya que restaura la pérdida de sinapsis, los defectos causados en la dinámica de los microtúbulos, y la reducción en la locomoción y la esperanza de vida de los organismos.

Asimismo, se describe un efecto novedoso de PI3K sobre la agregación del β-amiloide, induciendo la generación de depósitos más insolubles, y por tanto menos tóxicos. Se sugiere que este cambio conformacional ocurre debido a la fosforilación de PI3K en el residuo Ser-26 del péptido Aβ.

Los efectos sinaptogénicos y agregantes causados por PI3K en la neurodegeneración mediada por Aβ también son reproducibles en las células de neuroblastoma humano (HT-SY5Y), indicando que ambos efectos están conservados en humanos y sugiriendo que podría ser utilizado en estudios terapéuticos futuros de la enfermedad de Alzheimer.

Por último, se descubre un proceso de activación transitoria de dos *enhancer* neuronales en células epiteliales durante el desarrollo temprano en *Drosophila*, lo que se utilizó para identificar un efecto tóxico novedoso de Aβ42 en células no-neuronales. La expresión del péptido amiloide activa la apoptosis e induce la desregulación de la vía de señalización de Wnt en células epiteliales. Ambos efectos deletéreos, originados por la actividad de Aβ42, son restaurados por la sobreexpresión de PI3K tanto en células epiteliales como en células neurosecretoras.

INDEX

ABBREVIATIONS

α7-nAChR	α7 nicotinic acetylcholine receptors
Aβ	Amyloid beta
Abl	Abelson kinase
AD	Alzheimer's Disease
Akt	Protein kinase B
AP1	Activator protein 1
APLP1	Amyloid precursor-like protein 1
APLP2	Amyloid precursor-like protein 2
APP	Amyloid Precursor Protein
Arm	Armadillo
AZs	Active zones
BMP	Bone morphogenetic protein
BRP	Bruchpilot
Bsk	Basket
cAMP	Cyclic adenosine monophosphate
CaMKII	Calcium/calmodulin-dependent kinase II
CNS	Central nervous system
cGMP	Cyclic guanosine monophosphate
CREB	cAMP response element-binding
CSF	Cerebrospinal fluid
Csp-3	Caspase 3
dda	Dendritic arborization dorsal cluster (sensory neurons)
EB1	End-binding protein 1
EDTA	Ethylenediamienetetraacetic acid
EEG	Electroencephalography
Elav	Embrionic lethal abnormal vision
EphB2	Ephrin-type B2 receptor
EphA4	Ephrin-type A4 receptor
FoxO	Forkhead box protein
Gbb	Glass bottom boat
GFP	Green fluorescent protein
GFP-nLs	Green fluorescent protein - nuclear localization sequence
GSK-3	Glicogen-3 kinase
G-TRACE	Gal4 technique for real-time and clonal expression
Hrp	Horseradish peroxidase
JNK	c-jun kinase
LTD	Long-term depression
LTM	Long-term memory
LTP	Long-term potentiation
MAPK	Mitogen-activated protein kinases

Mad	Mothers against decapentaplegic
Med	Medea
mGluR5	Metabotropic glutamate-5 receptor
MMSE	Mini-mental state evaluation
mTOR	Mammalian target of rapamycin
NFTs	Neurofibrillary tangles
NMDAR	N-methyl D-aspartate receptor
NMJs	Neuromuscular junctions
PBS	Phosphate buffered saline
PCP	Planar cell polarity
PET	Positron emission tomography
pH3	Phosphohistone 3
PI3K	Phosphoinositide-3 kinase
PIP2	Phosphatidylinositol 4,5-bisphosphate
PIP3	Phosphatidylinositol (3,4,5)-trisphosphate
PrP	Prion protein
PS-1	Presenilin 1
PSD-95	Postsynaptic density 95
p-tau	Phosphorylated tau
PTEN	Phosphatidylinositol-3,4,5-trisphosphate 3-phosphatase
RAGE	Receptor for advanced glycation end-products
RFP	Red fluorescent protein
RNAi	Interference RNA
SDS	Sodium dodecyl sulfate
trkB	Tropomyosin receptor B/ Tyrosine receptor kinase B
VLM	Ventral longitudinal muscle
Wit	Wishful thinking
Wg	Wingless

INTRODUCTION

---

1. NOW AND THEN OF ALZHEIMER'S DISEASE

Alzheimer's disease was first described in 1906 by Alois Alzheimer, who studied the brain of a 51 years-old female patient called Augusta D. She had suffered from memory loss, hallucinations, disorientation and paranoia, and had later died because of the injuries of a stay-in-bed condition and a pulmonary infection. In her brain, Alois Alzheimer described, the two hallmarks of the disease, extracellular β-amyloid plaques (Aβ), and intracellular neurofibrillary tangles (NFTs). His discoveries were presented, at the 37th meeting of the Society of Southwest Germany Psychiatrists in Tübingen. At that time, this type of dementia was thought to be a rare disease; more than a century later, Alzheimer's disease is the most prevalent neurodegenerative illness in the world, affecting an estimated population of 46 million people today. As recently published by the World Alzheimer's Report in 2015, there are 10.5 million patients in the European Union and 9.4 million patients in the United States suffering from this incurable disease, and these numbers are estimated to double every 20 years. The global incidence extends up to 5% of people over 60 years of age, being 2 in 3 women patients.

Known by being the most common type of dementia, Alzheimer's disease (AD) is characterized by a progressive neuronal loss that causes severe cognitive deficits and neuropsychiatric symptoms which induce memory loss, depression, anxiety, sleep alterations, hallucinations, aggressiveness and violence among other symptoms of neurodegeneration. The diagnosis of patients consists in the proved presence of amyloid-β and/or tau in the cerebrospinal fluid (CSF), together with mini-mental state evaluation (MMSE) for cognitive impairment measure, magnetic resonance imaging (MRI) for brain volume and positron emission tomography (PET) scans for amyloid-β plaques and/or brain glucose metabolism analysis.

Although the presence of amyloid-β and phosphorylated tau (p-tau) aggregates is considered to be the main sign of the disease, it has not yet been clarified if those are the causing agents of AD. Being the loss of memory the first symptom noticed by the eventual patient, it is very intriguing that this symptom becomes evident only 2 or 3 decades after amyloid-β presence is determined in a CSF sample. Thus, AD is a complex, multifactorial

syndrome studied nowadays by scientists around the globe to understand its mechanisms aiming to find ways to prevent the devastating effects.

1.1 MULTIPLE ETIOLOGIES

95% of diagnosed AD cases in people aged 60 or older are thought to be sporadic, being aging the main risk factor. Taking into account that AD develops over a long preclinical period, the question arises if instead of a causative relation, the disease can progress due to accumulative risk factors assessed in late or mid-life before the onset of the clinical symptoms. Many studies are carried out to decipher if factors as vascular health status, diabetes, obesity, physical and mental inactivity, depression, smoking, low educational level, diet or toxic environments are indeed risk factors of AD (Selkoe and Hardy, 2015, Scheltens et al., 2016).

More deeply evaluated risk factors include genetic factors like the presence of the allelic version APOE4, first discovered in 1993 (Corder et al., 1993) and later attributed 50% risk for AD in homozygous individuals, and 20-30% for APOE3 and APOE4 heterozygotes (Genin et al., 2011). APOE4 is a lipoprotein that mediates cholesterol metabolism in an isoform-dependent manner. The variant E4 associates with atherosclerosis, cognitive impairment, AD, faster multiple sclerosis progression and telomeres shortening. The ABCA7 lipid transporter has been identified as another genetic risk factor for AD (Hollingworth et al., 2011). APOE4 and ABCA7 alleles are associated with less efficient amyloid-β clearance, but in both cases, more evidence needs to be compiled to understand the biochemical details of their contribution in AD pathology.

Microglial elements of the complement cascade have recently been described also as genetic risks: CR1, CD33 and TREM2 increase expression upon amyloid-β plaques formation (Bertram et al., 2008, Lambert et al., 2009, Suarez-Calvet et al., 2016). Some other endosomal vesicle recycling elements implicated in APP (amyloid precursor protein) processing, like SORL1, BIN1 and PICALM, have been similarly associated with AD pathogenesis (Rogaeva et al., 2007, Lambert et al., 2013, Zhao et al., 2015).

In summary, all these factors could directly or indirectly alter amyloid-β homeostasis in late-onset (previously described as sporadic) AD patients, which serves as a proof-of-concept for the amyloid hypothesis as the mechanistic process underlying Alzheimer's disease, that will be addressed below.

1.2 β-AMYLOID PATHOPHYSIOLOGY

Dominantly inherited forms of AD and non-dominant forms of AD share the common hallmarks of the disease, β-amyloid plaque formation and neurofibrillary tangles (NFTs) of hyperphosphorylated tau aggregates. CSF detection of Aβ is the earliest biomarker for the disease, followed by p-tau. Both show exponential accumulation in the clinical progressive phase of the disease, being Aβ levels the biomarker that shows a faster increment in CSF.

NFTs were discovered in 1986 (Grundke-Iqbal et al., 1986) and described to be intraneuronal fibrillar aggregates of hyperphosphorylated tau protein. Tau is a microtubule-associated protein that, upon phosphorylation, alters microtubule dynamics by pathologically increasing their stability, and as a consequence leads to a less dynamic cytoskeleton and deficient transport. Several kinases are implicated in hyperphosphorylation of tau, including GSK-3, MAPK, CaMKII and Akt. NFTs are not only a marker of Alzheimer's disease but also a hallmark of other types of dementia and neurodegenerative diseases, generally referred to as tauopathies.

Aβ peptide is the only exclusive marker of AD known today. It is generated from the processing of the full-length amyloid precursor protein APP, a transmembrane protein processed in two sequential proteolytic cleavages by β and γ secretases (De Strooper et al., 2010); known as the amyloidogenic pathway. The first cleavage, mediated by β-secretase, generates a soluble (sAPPβ) fragment and a βAPP-CTF fragment. Subsequently, the γ-secretase produces other proteolytic cut upon the βAPP-CTF that leads to the formation of the Aβ fragment. This Aβ fragment is released from the intracellular domain of APP (AICD). Two forms of Aβ of 40 or 42 aminoacids can be produced (Aβ40 and Aβ42), but it is the relative amount of Aβ42 what is critical in AD progression.

In contrast, APP can also suffer non-amyloidogenic processing when it is first cleaved inside the Aβ sequence by the α-secretase, leading to a soluble (sAPPα) fragment and the membrane-tethered αAPP-CT fragment, that can be then proteolysed by the γ-secretase and give rise to p3 and AICD fragments.

It is important to note here that the amyloidogenic proteolytic pathway of APP also occurs under non-pathological conditions. Only when the equilibrium between its production through amyloidogenic processing of APP, and its degradation by neprilysin, insulin degrading enzyme or endothelin converting enzyme (Turner et al., 2004) becomes imbalanced, Aβ is regarded as a synaptotoxin, and the amyloid cascade is initiated (Hardy and Higgins, 1992).

Once generated, the Aβ peptide can accumulate, oligomerize and aggregate. Furthermore, the initial Aβ molecules can suffer modifications as truncations, isomerizations and/or phosphorylations that affect oligomerization and aggregation patterns (Kummer and Heneka, 2014).

*Aggregation of A*β

The relative increase in Aβ42/Aβ40 due to excessive accumulation of β-amyloid can lead to protein aggregation, which involves a misfolding process of Aβ into soluble and insoluble assemblies. Aβ innocuous monomers are composed by α-helical and/or unordered structure, while Aβ polymers have β-sheet conformation that promote homophilic interactions leading eventually to toxic oligomer formation (Pike et al, 1991). As the nucleation-dependent polymerization model states, monomers can suffer conformational changes of self-assembly and generate oligomers in a thermodynamically unfavorable manner. The resulting oligomers can then associate and create oligomeric nuclei that elongate and assemble larger aggregates in a more favorable and rapid process. The concentration of nuclei, or seeds, is crucial for determining the lag phase of aggregation. The addition of seeds would reduce the lag time and promote faster aggregation (Murphy and LeVine, 2010, Goedert, 2015).

The aggregation process is thought to be critical for AD development and progression, as the different Aβ species differ in toxicity (Goure et al., 2014). Monomers are innocuous, but as they self-associate into oligomers and pre-fibrillar aggregates, they become toxic. Insoluble Aβ plaques are now considered rather benign species that could serve as a sink but also a potential source of toxic soluble oligomers (Caughey and Lansbury, 2003, Stefani, 2010, Moreth et al., 2013, DaRocha-Souto et al., 2011).

Thus, there are three different Aβ pools with different aggregation kinetics that can cause from non-deleterious effect to very toxic damage to cells. From a biophysical point of view, small soluble aggregates could induce stronger synaptotoxic effects as they have a much larger surface to interfere with the surrounding cells than Aβ insoluble plaques.

Being the soluble species the most neurotoxic aggregates, strong effort has been directed to elucidate whether Aβ is accumulated extracellularly, intracellularly or in both compartments.

The amyloid cascade hypothesizes that plaques can sequester Aβ oligomers until reaching a physical limit after which the oligomers diffuse to the surrounding membranes and hydrophobic cell surfaces (Esparza et al., 2013).

Extracellular and Intracellular β*-amyloids*

First and direct evidence of extracellular Aβ is found in Aβ measurements of CSF analysis in AD patients (Engelborghs, 2013, Goedert, 2015). On the other hand, intracellular accumulation has also been found in high-resolution electron-microscopy studies in brain samples of AD patients, where Aβ appeared inside of the cell at synaptic-terminals (Gouras et al., 2010).

Classical extracellular localization of Aβ deposits occurs as a consequence of initial APP amyloidogenic proteolysis by β-secretase cleavage in the extracellular domain. Next, the subsequent cleavage of the intramembranous domain by γ-secretase releases the Aβ peptide into the extracellular space or vesicle lumen (Shoji et al., 1992, Haass et al., 2012). Intracellular deposits have also been detected in several studies (Wirths et al., 2004,

Crowther et al., 2005, LaFerla et al., 2007, Zhao et al., 2010). Their nature has not yet been fully clarified, as they could be a result of endosomal membrane-APP-derived Aβ aggregates, or they could be on the process of secretion, targeted for lysosomal degradation or even a result of a later uptake of previously secreted Aβ oligomers.

Whether the first toxic source of oligomers is the extracellular β-amyloid or the intracellular β-amyloid is a question still under debate.

1.3 Aβ-MEDIATED SYNAPTOTOXICITY

Aβ oligomers are gradually accumulated in limbic and association cortices, where they cause subtle effects to synapse efficacy. Higher deposition of oligomers can induce the formation of diffuse plaques that later promote microglial and astrocytic activation and inflammation. Together, all these events result in altered neuronal ion homeostasis and modified kinase and phosphatase activities that lead to NFTs formation, as a consequence, these events induce a widespread neuronal dysfunction and neuronal loss that ultimately manifest in cognitive impairment and dementia.

*Synaptotoxic Effects of A*β

It is well documented that Aβ oligomers produce early synaptic alterations that later develop into dramatic synapse loss. Although strong efforts have been directed to the study of the mechanisms by which β-amyloids elicit synaptotoxicity, it is still today a matter of deep analysis, as it seems a very complex sequence of events.

LTP (Long Term Potentiation) and LTD (Long Term Depression) electrophysiological recordings of synaptic strength and plasticity have shown interesting results upon Aβ oligomer's exposure. They measure activity-dependent reduction of efficacy in synapses in NMDAR (N-methyl D-aspartate receptor) -dependent long-term potentiation and NMDAR-dependent long-term depression, respectively. Several studies have proved that Aβ impairs LTP (Walsh et al., 2002, Cleary et al., 2005) but increases LTD (Hsieh et al., 2006) causing synaptic depression. The mechanisms by which Aβ enhances LTD are still to be

completely elucidated, but they comprise receptor internalization, desensitization or activation of perisynaptic receptors that lead, eventually, to spine loss.

Although electrophysiological recordings have highlighted the synaptotoxic actions of Aβ, it is still an open question whether they act in specific sets of cells or synapses or not. Several membrane receptors have been proposed to act as specific targets of Aβ in neurons: NMDA (De Felice et al., 2008, Decker et al., 2010), the prion protein (PrP) (Lauren et al., 2009), the metabotropic glutamate-5 receptor (mGluR5) (Renner et al, 2010), the receptor for advanced glycation end-products (RAGE), the neurotrophin receptor p75 (Yaar et al., 1997), the α7 nicotinic acetylcholine receptors (α7-nAChR) (Wang et al., 2000, Dineley et al., 2001), the postsynaptic membrane associated protein PSD-95 (Pham et al., 2010), the Ephrin-type B2 receptor (EphB2) (Cisse et al., 2011) and Ephrin-type A4 receptor (EphA4) (Vargas et al., 2014), and Insulin receptors (Giuffrida and McMahon, 2010), among others. None of them has been found to be necessary and sufficient to elicit Aβ toxicity (Benilova et al., 2012).

*A*β *Effects in Neuronal Networks*

Early Aβ synaptotoxicity yields to progressive degeneration of neuronal tissue, especially noticeable in the entorhinal cortex and the hippocampus, regions implicated in learning and memory.

Experimental evidence supports that Gabaergic neurons could be more vulnerable to Aβ, and that β-amyloids could act inhibiting network excitation by suppressing synaptic transmission strength and short-term plasticity (Palop and Mucke, 2010). In contrast, in vivo studies in hAPP (human APP) transgenic mice show evidence of epileptic activity upon Aβ exposure, in EEG recordings from cortex and hippocampus (Palop et al., 2007). Furthermore, cell culture and cortical slices have shown to increase their activity after Aβ treatment (Palop et al., 2007). These results suggest that Aβ can also elicit aberrant excitatory changes in neuronal circuits. This fact could generate a positive feedback loop, as an increment in neuronal activity have shown to produce enhancement of Aβ production, which would progressively induce abnormal patterns of neuronal activity. As a

result, this feedback loop could also affect compensatory inhibitory responses that would imply learning and memory circuits.

Aβ toxicity affect synapses depending on its own abundance, and on the synapse nature and vulnerability to Aβ (Palop and Mucke, 2010). Moreover, AD progression appears to affect different processes at different stages of the disease.

1.4 EMERGING HYPOTHESES FOR ALZHEIMER'S

Growing evidence suggests a strong association between insulin signaling components and AD pathogenesis, this relation suggests that the disease could develop as a metabolic syndrome where the patient presents insulin resistance or deficiency. It has been shown that extracellular Aβ oligomers are able to impair insulin receptor themselves (De Felice et al., 2008). Intracellular Aβ can interfere with phosphoinositide-dependent kinase (PDK) and Akt interaction, affecting insulin receptor signaling by inhibiting Akt activation (Lee et al., 2009). Also, the use of intranasal insulin in clinical trials has had positive results (Craft et al., 2012), as well as the use of a diabetes drug, rosiglitazone, that is able to lower Aβ oligomers levels in culture and rescues synapses and plasticity in vivo via PPAR-γ pathway (Xu et al., 2014).

Insulin signaling impairment could furthermore contribute to the dysfunction of downstream pathways including PI3K, Akt and Wnt/β-catenin or enhancement of GSK-3β activity, triggering tau hyperphosphorylation.

Multiple Wnt family components are dysregulated in AD and have been implicated in the characteristic cognitive decline and synaptic loss (Inestrosa and Varela-Nallar, 2014). β-catenin levels are reduced in mutated PS-1 carrying AD brains (Zhang et al., 1998) in addition Dickkopf-1 (Dkk1), an endogenous Wnt inhibitor, is found to be increased both in AD brains and mouse models (Caricasole et al., 2004, Rosi et al., 2010) and neuronal death and Aβ-induced tau phosphorylation can be prevented by Dkk1 knockdown (Caricasole et al., 2004).

Taken together, all these data suggest that dysregulation of insulin and Wnt/β-catenin pathways contribute to Aβ-induced synaptic loss and their components could constitute potential therapeutic targets against AD progression (Inestrosa and Varela-Nallar, 2014).

2. MOLECULAR TOOLS FOR SYNAPTOGENESIS

The search for new tools to restore the loss of synapses in neurodegenerative diseases has been very intense in the last years. In particular, synapse maintenance is critical for delaying the loss of spines and synaptic function that occurs along the normal ageing process.

Protein kinases are involved in plasticity mechanisms like neurogenesis, modulation of intrinsic excitability, long-lasting strengthening of pre-existing synapses or synaptogenesis. Some of them are calcium/calmodulin-dependent kinase II (CaMKII), cAMP-dependent protein kinase A (PKA), cGMP-dependent protein kinase (PKG), phosphoinositide-3 kinase (PI3K), cyclin-dependent kinase 5 (CdK5), protein kinase C (PKC) and brain atypical PKC (PKMζ), Fyn tyrosine kinase, casein kinase 2 (CK2) and p21-activated kinase (PAK) (Giese and Mizuno, 2013).

PI3K in particular, phosphorylates phosphatidylinositols that subsequently activate PDK (3-phosphoinositide-dependent kinase) and Akt, both downstream elements of the canonical PI3K/Akt pathway. PI3K activation is regulated by tyrosine kinase receptors like the BDNF receptor trkB. This activation is critical for long-term memory (LTM) formation as the impairment of PI3K/Akt signaling in trkB mutants suppress LTM (Musumeci et al., 2009). mTOR (mammalian target for rapamycin) and GSK3-β, downstream effectors of PI3K/Akt pathway, have also important functions in LTM and memory consolidation and retrieval (Bekinschtein et al., 2007, Hooper et al., 2008, Hong et al., 2012, Huang et al., 2013).

Furthermore, PTEN inhibition in hippocampal and cortical regions of mice showed over-activation of Akt signaling, causing macrocephaly, severe dendritic dystrophy and dramatic increase in spine density (Kwon et al., 2006).

Previous data from our lab have shown that PI3K and Akt activation elicit the increase of synapse number in larval NMJs and adult brain interneurons and projection neurons of *Drosophila melanogaster* (Martin-Pena et al., 2006, Acebes et al., 2011, Acebes et al.,

2012). In the same line, inhibitors of the PI3K/Akt pathway like GSK3-β reduced the number of synapses in both types of neurons. The results proved the synaptogenic actions of PI3K and Akt in an age-independent manner, as their activation at different times in the fruitfly life, generated new, supernumerary and fully functional synapses. The genetically driven increase in synapse number correlates with up-regulation of postsynaptic densities (PSDs) and glutamate receptors (Jordan-Alvarez et al., 2012). Other elements of the canonical PI3K/Akt pathway like PTEN, FoxO and mTOR, had no effect in the number of synapses, suggesting that a specific pathway for synapse number regulation was being characterized, in which PI3K, Akt and GSK3-β played central roles. Other studies report that the transcription factor AP1, Jun Kinase and Wnt signaling, also modulated by GSK3-β, are implicated in this synaptogenic pathway (Franciscovich et al., 2008). Moreover, BMP (bone morphogenetic protein) canonical signaling, transcriptional regulator Mad (SMAD1) and Type II BMP receptor Wit (wishfull thinking) are key regulators of synaptic development and maturation in the Drosophila NMJ (Berke et al., 2013).

Using the *Drosophila* larval NMJ, data from our lab have shown that PI3K-synaptogenic actions are part of a larger signaling pathway, connected with other previously known elements including: the Wit receptor, its ligand Gbb (glass bottom boat), and the MAPkinases cascade. In addition, an antagonistic pathway uses the transcription factors Mad and Medea, the co-factor Yorkie and the microRNA bantam to down-regulate key elements of the pro-synaptogenic pathway. Like its counterpart, this anti-synaptogenic pathway also makes use of a small GTPase and MAPKs signals including Ras-like-a, p38 and Licorne. Thus, the number of synapses results from the balanced output from the two signaling pathways.

Interestingly, the PI3K/Akt signaling pathway is well-conserved across species (Ruggero and Sonenberg, 2005) and PI3K synaptogenic actions have recently been tested in mammals with PTD4-PI3KAc administration (chapter 3 for details), resulting in conserved functions producing up-regulation of synaptic spines in mice primary hippocampal neuron cultures (Cuesto et al., 2011) and in vivo cognitive and learning abilities enhancement (Enriquez-Barreto et al., 2014).

Cytoskeletal associated proteins like kinesin-1 and dynein are cargo elements that allow transportation of synaptic components necessary for synapse formation, maintenance, growth and function. Disruption of intracellular transport has resulted in synaptic morphological abnormalities and BMP signaling perturbations (Kang et al., 2014). Similarly, direct regulators of cytoskeleton dynamics have important effects in synapses. For instance, GSK3-β can regulate microtubule dynamics by stabilizing Futsh; Wingless (Wg) regulates planar cell polarity (PCP) by activation of Dvl (Dishevelled) and c-Jun kinase (JNK) that directly controls microtubule stability. BMP can also regulate the cytoskeleton by inducing Wit activation, Mad (Mothers Against Decapentaplegic) and Med (Medea) translocation to the nucleus, where the complex Mad/Med regulates transcription of the RhoGEF Trio that controls actin remodeling (Long and Van Vactor, 2013).

3. AIM OF THIS THESIS

Our group has previously demonstrated that elements of the PI3K/AKT pathway control synapse number in addition to their well-known roles on cell survival and cell growth, thus, knowing that synapse loss is one of the first steps leading to neurodegeneration in AD, and that the accumulation of β-amyloid peptides from the APP has been related to the onset of the pathology, the aim of this thesis pose the question of whether PI3K synaptogenic actions could be effective against the synaptotoxic effects of Aβ42, both in *Drosophila* studies and in a human neuroblastoma *in vitro* system. The potential synaptogenic actions of PI3K will be addressed in an adult-onset AD model in *Drosophila* ausing the binary Gal4-UAS expression system, together with the $Gal80^{ts}$ repressor. This strategy will allow space and temporal control of the human Aβ42 peptide expression in the nervous system. Furthermore the scope will include the search for novel non-synaptogenic roles of PI3K activation in Aβ42 induced degeneration, in neurons and in non-neuronal tissues.

Box 1: APP

The Amyloid Precursor Protein (APP) belongs to the evolutionary conserved family of type I transmembrane glycoproteins that include the paralogs amyloid precursor-like proteins 1 and 2 (APLP1 & APLP2), which lack the Aβ sequence and appear to show redundant functions (Goldgaber et al., 1987, Wasco et al., 1993).

The extracellular region of the human protein contains a heparin-binding domain (HBD), a cooper binding domain (CuBD), an acidic domain (Ac), a Kutniz protease inhibitor domain (KPI) and an E2 domain. The intracellular region contains the YENPTY motif. The Aβ sequence is in the transmembrane region, between the YENPTY motif and the E2 domain.

Across species, Aβ sequence is only found in the human, *Mus musculus* and *Dario rerio* (Appa) homologs. Together with APLP1 and APLP2, *Caenorhabditis elegans* and *Drosophila melanogaster* homologs lack the Aβ sequence. The absence of Aβ conservation across species points out the fact that amyloidosis could not be the main function of APP. According to this, it has been extensively documented that APP has fundamental roles in cell functions that range from neurogenesis to morphogenesis, along with synaptogenesis, synapse maintenance, neurite growth and axonal guidance.

There are 3 major isoforms of human APP, which are generated by alternative splicing of exons 7 and 8: APP_{770}, APP_{751} and APP_{695}. The APP gene is located in chromosome 21 and is ubiquitously expressed since early stages of development, mainly in the brain and kidneys. APP_{695} is the most abundant isoform in neurons, and APP_{770} and APP_{751} are more abundant in glial cells.

Previous studies have demonstrated that Drosophila APP homolog APPL regulates synapse formation and neuromuscular junction (NMJ) appearance (Torroja et al., 1999a). APPL overexpression produces axonal transport disruption by interacting with kinesin heavy chain (Torroja et al., 1999b), and *Appl* null flies show decreased number of synaptic boutons in larval NMJs (Torroja et al., 1999a).

More recent work has described a new function of Drosophila APPL protein as modulator of the Wnt Planar Cell Polarity (PCP) signaling pathway in axonal outgrowth by modulation

of the receptor Dishevelled (Dsh) by Abelson kinase (Abl) mediated phosphorylation (Soldano et al., 2013).

Box 2: PI3K

PI3K or phosphoinositide-3 kinase is an intracellular family of proteins that includes four different classes: Class I are heterodimers of a catalytic subunit (p110) and a regulatory subunit (p85), responsible for the production of PI(3)P, PI(3,4)P_2 and PI(3,4,5)P_3. Class II members have three catalytic subunits and no regulatory subunits. Class III are heterodimers composed of a catalytic subunit (Vps34) and a regulatory subunit (Vps15/p150) that are involved in vesicles and protein trafficking. Finally, Class IV are serine/threonine kinases like mTOR, DNA-dependent protein kinase (DNA-PK), among others.

PI3K constitutes a cell-signaling crossroad, as it is implicated in proliferation, survival, cell growth, motility, differentiation, and intracellular transport (Grundke-Iqbal et al., 1986, Engelman et al., 2006, Acebes and Morales, 2012, Knafo and Esteban, 2012, Menon et al., 2014). The canonical activation of PI3K is mediated by RTKs (Receptors of tyrosine kinases) phosphorylation and the subsequent recruitment and conformational change of PI3K heterodimers. These events allow the phosphorylation of the catalytic subunit triggering PIP2 transformation to PIP3, which mediates Akt phosphorylation that later activates multiple downstream effectors as mTOR, CREB, FOXO… etc. Activators of the pathway are Insulin, EGF, IGF-1 and shh. Inhibitors of the pathway are GSK3-β and PTEN.

In *Drosophila,* there are 3 genes encoding PI3K. In particular, PI3K-92E encodes one PI3K isoform with a catalytic subunit (Dp110) and a regulatory subunit (Dp60) that present strong homology with of human class I PI3K p110 and p85 subunits respectively.

Box 3: Drosophila Adult NMJ

Larval neuromuscular junction (NMJ) has been utilized because of its easy accessibility, in numerous studies during decades to address synaptic plasticity mechanisms and development (Keshishian et al., 1996). However, to evaluate neurodegeneration and to distinguish from developmental defects, the adult NMJ is a more suitable tissue. Adult ventral longitudinal muscle (VLM) NMJs have been characterized (Hebbar et al., 2006, Wagner et al., 2015).

VLM NMJs have one single nerve entry point innervating the muscle and present large glutamatergic boutons (Hebbar et al., 2006). VLM NMJs synapses consist of presynaptic active zones (AZs) and associated postsynaptic membranes (Wagner et al., 2015). AZs are specialized membrane compartments at the axonal terminal where neurotransmitter release occurs, and present a T-bar electro dense structure when imaged with electron microscopy.

AZs are composed of evolutionarily conserved proteins like: ELKS/CAST/BRP (bruchpilot), Piccolo, Bassoon, CASK, Mint, RIM, Liprin-α and Syd-1; docking proteins such us Munc-13, Munc-18, SNAREs, SNAP25, Synaptobrevin/VAMP and syntaxin; cell adhesion molecules like SYG-1/Neph1, SYG-2/Nephrin, Neurexin and Neuroligin; actin and tubulin cytoskeletal components like actin, tubulin, myosin, spectrin, β-catenin and WVE-1/WAVE complex (Sudhof, 2012).

In vertebrates, NMJs contain elongated AZs to which neurotransmitter containing vesicles attach. Invertebrate NMJs are similar to central vertebrate synapses, although they present the T-bar shape, similar to the synaptic ribbon structures of sensory vertebrate neurons (Sudhof, 2012).

Box 4: *Drosophila melanogaster* AD Models

Many model organisms such as *Drosophila melanogaster*, *Caenorhabditis elegans*, *Dario rerio* (zebrafish) and *Mus musculus* (mouse) serve to model Alzheimer's disease (Hirth, 2010, Wisniewski and Sigurdsson, 2010, Rincon-Limas et al., 2012, De Felice and Munoz, 2016).

Drosophila in particular offers advantages over the other systems due to the shorter life cycle, lower cost, smaller body size and more importantly a wide spectrum of available genetic tools that allow faster genetic screens; moreover *Drosophila* can be use to test candidate therapies and drugs (Rincon-Limas et al., 2012, Ugur et al., 2016).

Fly models of AD have been generated following different strategies. Some studies coexpress human APP and human BACE (β-secretase), and describe consequent Aβ plaques formation and age-dependent neurodegeneration (Greeve et al., 2004) with decreased presynaptic connections, altered mitochondrial localization and reduced postsynaptic protein levels (Mhatre et al., 2014).

Other models are based on the human β-amyloid peptide expression. For this strategy, different Aβ constructs have been developped, the UAS-$A\beta_{40}$ (Iijima et al., 2004), that produces no plaque formation but causes age-dependent learning defects; the UAS-$A\beta_{42}$ that elicits synaptic alterations and locomotor, survival and learning impairments (Iijima et al., 2008) and other Aβ constructs that present AD associated mutations like the UAS-$A\beta_{42\text{-}Arc}$ and are more aggregation prone models (Crowther et al., 2005, Iijima et al., 2008).

Recently, the construct 2x-UAS-$A\beta_{42}$, has been generated and characterized (Casas-Tinto et al., 2011), consisting in a bi-cistronic system (2 tandem copies) of the human Aβ42 fused to a secretion signal. This model shows extensive neuronal cell death and induces XBP1 unconventional splicing. The 2x-UAS-$A\beta_{42}$ genetic construct, allows stronger neurotoxic phenotypes that develop faster than in other 1-copy models, facilitating the search for suppressor candidates.

All these studies have shed light on the molecular mechanisms underlying Aβ neurotoxicity, and moreover, to the possible targets and therapies that could be used to prevent its deleterious effects. Many researchers have described GSK3-β activation upon

Aβ expression, which can produce APP transport alterations by affecting kinesin-1 and dynein (Weaver et al., 2013). Others have shown that GSK3-β inhibition can restore some of the Aβ toxic effects, as well as lithium or Congo-Red treatment (Crowther et al., 2004, Sofola et al., 2010, Sofola-Adesakin et al., 2014). However, other authors found no restoration when they down-expressed shaggy (the *Drosophila* homolog of GSK3-β) in Aβ expressing neurons, claiming no Wnt-Aβ interaction in *Drosophila* AD models (Luchtenborg and Katanaev, 2014). PI3K inhibition by down-expression of p65 regulatory subunit has also been used in Aβ *Drosophila*, showing prevention of Aβ-induced LTD (Chiang et al., 2010).

SCOPE

The objectives of this thesis are the following:

1. To study the synaptogenic actions of PI3K in AZs in an adult-onset AD model
2. To analyze, from a whole organismal level, the potential beneficial effects of PI3K overexpression in Aβ42 neurodegeneration
3. To study of the synaptogenic actions of Medea down-regulation and mTOR overexpression in Aβ42-mediated neurodegeneration
4. To characterize a novel effect of PI3K activation in Aβ42 aggregation
5. To identify novel Aβ42 phenotypes in non-neuronal environments and evaluate the potential actions of PI3K in these contexts

MATERIALS AND METHODS

---

1. MATERIALS

Drosophila genetics, stocks and maintenance
- Gasl4/UAS system
- Gal80^{ts} system
- Flip-out clones and G-TRACE system
- Gal4 lines
- UAS lines

List of Primary and Secondary Antibodies
Cell Culture
PI3K Activating Peptides

2. METHODS

Preparation of Aβ42 Oligomers
Protein Extraction and Western Blot Analysis
- Insoluble vs Soluble separation
- Monomerization Protocol

RNA Isolation and cDNA Preparation
Quantitative RT-PCR
Immunostaining
Thioflavin-S Histochemistry
Larval Wing Disc Live Imaging
EB1-GFP Live Imaging
Negative Geotaxis Assays
Lifespan Analysis
Image Analysis
Adult NMJ Synapse Analysis
HT-SY5Y Viability Assay
HT-SY5Y Aβ42 Aggregation Assay
Aβ42 Extracellular Aggregation Assay
Statistical Analysis

MATERIALS

Drosophila genetics, stocks and maintenance

All fly stocks were maintained at 25°C (unless otherwise specified) on a 12/12-h light/dark cycle at constant humidity in standard medium (4% glucose, 55g/l yeast, 0,65% agar, 28 g/l wheat flour and 4 ml/l propionic acid).

Gal4/UAS system

For ectopic expression of genes, the Gal4/UAS binary system was used (Brand & Perrimon, 1993), in which the yeast transcriptional activator Gal4 is used to allow the expression of a gene of interest (gene X) under the regulation of UAS sequences (**U**pstream **A**ctivating **S**equence).

To report the activity of specific enhancers we have used 'enhancer-trap Gal4 lines'. These transgenic lines carry a P element including the cDNA of Gal4 transcriptional activator. This P-element is randomly mobilized through the genome and, as a consequence, specific insertions drive the expression of the Gal4 under the control of nearby endogenous tissue-specific enhancers. When Gal4 lines are crossed by UAS lines, the gene of interest, cloned downstream of UAS sequences, is expressed in the same pattern as the Gal4 activator. It is important to note that this gene will not be transcribed in the absence of the Gal4 protein.

Gal80^{ts} system

The Gal4/UAS system presents one important limitation, as it is not possible to induce its activation at specific times in the life cycle of the organism. To address this issue, another yeast protein, the Gal80, is used to specifically bind and repress Gal4 function.

By using a temperature-sensitive allele of Gal80 repressor under the control of the tubulin promoter (*tub-Gal80^{ts}*), the activation and repression of the Gal4/UAS system can be regulated by temperature. Gal80^{ts} protein is not functional at 29°C, so the Gal4/UAS system is active at this temperature. On the other hand, Gal80^{ts} is functional at 17°C, repressing the Gal4/UAS (McGuire et al., 2003).

This construct is highly instrumental in situations where the gene of interest is causing toxic or lethal effects that restrict the study to early stages of development. In these situations, Gal80^{ts} can be used to activate the expression of the gene of interest only at later stages of development. This was the case in the study of the toxic effects of Aβ42 during development.

Additionally, several GAL4 lines show dynamic expression, with patterns changing throughout development and adulthood (Chapter 8). The use of Gal80^{ts} construct can also prevent this event.

Flip-Out Clones & G-TRACE system

Flip-out clones consist in the excision of a given DNA sequence by Flipase induced mitotic recombination between **FRT** sites (**F**lipase **R**ecognition **T**arget), situated flanking the gene of interest (Struhl & Basler, 1993).

The Gal4 technique for real-time and clonal expression, or G-TRACE analysis system, consists on a UAS-RFP fluorescent protein construct; a UAS-*Flipase* and a tracking construct Act-FRT-STOP-FRT-GFP that reports the temporal activation of an enhancer over time. The *Gal4* activity induces the expression of the UAS-*Flipase* (Flp) and UAS-*RFP* (red) constructs. The Flp enzyme recognizes FRT sites and removes the STOP cassette, allowing the expression of Act>*GFP* (green) in these cells and, thus, expressing the GFP reporter independently from the enhancer that controlled the Gal4 driver under study. In this way, we can determine the current expression of an enhancer-*Gal4* in the moment of dissection (red, RFP) and the historical expression during development (Act>*GFP* (green)). Using this system, it has been described that some enhancer-*Gal4* lines show divergence of their expression domains at different stages of development (Evans et al., 2003).

The following stocks were used in this work:

GAL4 lines

Stock Name	**Bloomington Reference/Source**	**Reference**
elav^{c155}-Gal4 (Chr. X)	BL-458	*Lin et al., 1994*
D42-Gal4	BL-8816	*Chan et al., 2002*

Stock Name	Bloomington Reference/Source	Reference
leucokinin^{M7}-Gal4	F. Benjumea (CBMSO)	*de Haro et al., 2010*
engrailed-Gal4	BL-1973	*Lawrence et al., 1995*
rotund-Gal4	BL-7405	*St. Pierre et al., 2002*
elav-Gal4 (Chr. II)	BL-8765	*Luo et al., 1994*
elav-Gal4 (Chr. III)	BL-8760	*Luo et al., 1994*
Tubulin-Gal80^{ts}	BL-7019	*McGuire et al., 2003*

elav-Gal4;Gal80^{ts} was generated in the lab for this work with *elav*^{c155}-Gal4 (Chr. X) and *Tubulin*-Gal80^{ts} .

UAS lines:

Stock Name	Bloomington Reference/Source	Reference
UAS-*LacZ*	BL-1776	(Brand and Perrimon, 1993)
UAS-*PI3K*	BL-8294	(Parrish et al., 2009)
UAS-*mTOR*	BL-7013	(Hennig and Neufeld, 2002)
UAS-*bsk*	BL-9310	(Boutros et al., 1998)
UAS-*Medea*^{RNAi}	BL-31028	(Ni et al., 2009)
UAS-*Aβ42(2x)*	Dr. Pedro Fernández Fúnez	(Casas-Tinto et al., 2011)
UAS-*EB1-GFP*	Dr. Melisa Rolls	(Rolls et al., 2007)

UAS-*Aβ42(2x)*/UAS-*GFPnLs*, UAS-*PI3K*/UAS-*Aβ42(2x)*, UAS-*mTOR*/UAS-*Aβ42(2x) and* UAS-*Medea*^{RNAi}/UAS-*Aβ42(2x)* lines were generated in the lab for this work.

Other lines; G-TRACE (BL-28280)

List of Primary and Secondary Antibodies

Antibody	Tech.	Protein	Species	Dilution	Source
nc82	IHC	Bruchpilot	mouse	1:20	DSHB
hrp	IHC	Horseradish peroxidase	rabbit	1:200	DSHB

Antibody	Tech.	Protein	Species	Dilution	Source
6E10	IHC	Amyloid Beta	mouse	1:1500	Covance
	WB			1:1000	
csp-3	IHC	Activated caspase-3	rabbit	1:100	Cell Signaling
wg	IHC	Wingless	mouse	1:20	DSHB
pH3	IHC	phospho Histone-3	rabbit		Millipore
arm	IHC	armadillo	mouse	1:50	
elav	IHC	Elav	mouse	1:50	DSHB
pSer	IHC	phospho-Serine	mouse	1:200	Abcam
pTyr	IHC	phospho-Tyrosine	rabbit	1:200	Abcam
pSer8-Aβ	IHC	phospho-Serine8-Aβ42	mouse	1:1000	Jochen Lab
pSer26-Aβ	IHC	phospho-Serine26-Aβ42	rat	1:1000	Jochen Lab
β-Tub	WB	β-Tubulin	mouse	1:10000	Abcam

Secondary Antibodies

Alexa 488	IHC	Alexa Fluor 488 dye	mouse	1:300	TFS
Alexa 568	IHC	Alexa Fluor 568 dye	rabbit	1:300	TFS
Alexa 647	IHC	Alexa Fluor 647 dye	rat	1:300	TFS

Cell Culture

SH-SY5Y human neuroblastoma cells were purchased from ATCC (ref: CRL-2266). Cells were seeded at $5x10^4$ cells/cm^2 and used when cultures reached a 70–80% confluence. Culture media contained RPMI (Sigma-Aldrich, USA) supplemented with 0.5 mM glutamine (Sigma-Aldrich, USA), penicillin (50 mg/ml)/streptomycin (50 U/ml) from Sigma-Aldrich (USA), and 10% FBS (Sigma-Aldrich, USA). Cells were serum starved and differentiated with retinoic acid (10 μM) for 24 hours prior to treatment.

PI3K Activating Peptides

Activation of PI3K was achieved by using the peptide PTD4-PI3KAc (Cuesto et al., 2011). The peptide includes a PTD$-transduction domain that allows membrane permeabilization, PTD4 (Tyr-Ala-Arg-Ala-Ala-Ala- Arg-Gln-Ala-Arg-Ala), (Ho et al., 2001), fused to a phosphopeptide containing the intracellular phosphorylated SH2 domain of the PDGF receptor (Gly-Ser-Asp-Gly-Gly-pTyr-Met-Asp-Met-Ser), (Derossi et al., 1998). This peptide has been shown to induce class I PI3K activation, independently of tyrosine kinase dimerization, both *in vitro* and *in vivo* brains (Cuesto et al., 2011). Peptides were a gift from Dr. Miguel Morales Lab.

METHODS

Preparation of Aβ42 Oligomers

Soluble oligomers were prepared by dissolving 0.3 mg Aβ42, previously re-solubilized in formic acid, in 200 µl of hexafluoroisopropanol (HFIP) for 20 min. at room temperature. 200 µl of this Aβ42 solution were added to 1ml Milli-Q H_2O in a siliconized eppendorf tube. The samples were then stirred at 500 rpm using a Teflon coated micro stir bar for 8h at 22°C for evaporation of the HFIP and progressive formation of oligomers. Before using Aβ42 oligomers for cytotoxicity assays, the samples were sonicated to break and prevent incipient fibers (Kayed and Glabe, 2006).

Protein Extraction and Western Blot Analysis

Ten fly heads from each genotype were used to prepare homogenates. Fly heads were homogenized in 20 µl of lysis buffer containing PBS1x, Triton 1%, 150 mM NaCl and Complete Protease Inhibitors (Roche). Equal volume of Tricine-SDS and 5% β-mercaptoethanol loading buffer was added to each sample. Later, the samples were boiled at 95°C for 5 min. Protein extracts were fractionated by sodium dodecyl sulfate-polyacrylamide gel electrophoresis (SDS – PAGE) in 15% Bis–Tris under reducing conditions and electroblotted into 0,22 µm nitrocellulose membranes. Membranes were then blocked in PBS containing 5% non-fat milk, and probed against Aβ42 (6E10) and β-Tubulin. To improve reactivity of 6E10 antibody, membranes were boiled for 5 min in PBS before blocking. Immunoreactive bands were visualized by enhanced chemiluminescence (ECL, Amersham). Quantification of relative expression was done from three independent experiments using a loading control for normalization. The signal intensity was quantified using ImageJ (NIH) software.

Insoluble vs Soluble Protein Separation

Ten fly heads were hand homogenized in 40 µl of lysis buffer and centrifuged for 1 min. at 1300 rpm. The supernatant was stored as the Soluble Fraction. The remaining pellet was resuspended in 30 µl of PBS with 1% Triton X-100 and 30 µl 70% formic acid. After

sonication, vortex shaking and 800 rpm centrifugation for 1 min., the supernatant was dried with SpeedVac for 1 hour. The dried pellet was finally resuspended in 40 µl of PBS with 1% Triton X-100, sonicated and centrifuged again at 1300 rpm. The resulting supernatant was stored and named Insoluble Fraction.

Monomerization Protocol

20µl of Monomerization Buffer (9M Urea, 1% SDS, 25mM Tris-HCl, 1mM EDTA) was added to total, insoluble or soluble protein fractions. The samples were then sonicated and incubated for 1 hour at 55 °C, followed by centrifugation at 14000 rpm for 2 min. The supernatants were mixed with loading buffer and boiled at 95 °C for 5 min.

RNA Isolation and cDNA Preparation

Total RNA was isolated from 15 fly heads per genotype (Trizol, Invitrogen) and cDNAs were synthetized using M-MLV Retrotranscriptase (Invitrogen).

Quantitative RT- PCR

qPCR analysis was done using 7500 Real Time PCR System (Applied Biosystems) with cycling conditions of 95°C for 10 min and 40 cycles of 95°C for 15 s and 55°C for 1 min. qPCR results were analyzed with 7500 v2.0.6 software (Applied Biosystems).

Immunostaining

Third instar larval tissues and adult brains were dissected and fixed with 4% formaldehyde in phosphate-buffered saline for 20 minutes, washed 3 times with 0,1% triton, and mounted in Vectashield mounting medium with DAPI, or incubated with primary and secondary antibodies. (Tables in chapter 3 - Materials)

Preparations were imaged in a Leica SP5 confocal microscope.

Thioflavin S Histochemistry

7-day old and 15-day old female fly brains were fixed in 4% formaldehyde and permeabilized in PBS containing 0.4% Triton X-100. The brains were incubated in 50% EtOH containing 0.1% TS (Sigma) for 10 min. and later washed in 50% EtOH and PBS.

Larval Wing Disc Live Imaging

First and second instar larval wing imaginal discs were visualized and imaged following a previously published protocol (Nienhaus et al., 2012). Preparations were imaged in a Leica SP5 confocal microscope.

EB1-GFP Live Imaging

Third instar larvae were washed in PBS, dried and placed in a drop of halocarbon oil 700 and 10% chloroform mixture. Dendritic arborization dorsal cluster sensory neurons (ddA) live imaging was performed in the dorsal side of the extended larva with a 60x oil immersion objective in a spinning disk microscope.

Laser intensity was maintained to 15% in all experiments. The time-lapse acquisition was done for a total time of 3 min. with 2 sec. interval time.

Negative Geotaxis Assays

A total number of 30 to 48 female flies per genotype were grown at 29°C since eclosion, allowing the Gal4/UAS system to activate the expression of the corresponding genes thanks to the inactivation of the $Gal80^{ts}$ repressor. Females were separated and placed in plastic vials containing ten to fifteen of them, and kept at 29°C, 70% humidity, under a 12/12-h light/dark cycle. The counting was done at 25°C every 2-3 days in a plastic vial that was gently tapped to the bottom. The number of flies that reached the 4 cm. high line was counted after 10 sec. of climbing; at the same time, the number of flies that started climbing but did not reached the 4cm line, and the number of flies that stayed at the bottom of the tube, were also annotated. Every counting was repeated 8 times. The experiment was repeated at least three times.

Lifespan Analysis

A total number of 30 to 48 female flies per genotype were grown at 29°C since eclosion, allowing the Gal4/UAS system to activate the expression of the corresponding genes. Flies were separated in groups of ten to fifteen females, and placed in food vials. Each vial was kept at 29°C, 70% humidity, under a 12/12-h light/dark cycle. Food vials were changed

every 2-3 days, and the dead flies were counted at that time. Experiments were carried out in triplicates.

Statistical analysis was performed using Mantel-Cox test with GraphPad software.

Image Analysis

Fluorescence quantification was performed with Imaris (Bitplane) software. Images were processed with ImageJ.

Adult NMJ Synapse Analysis

Adult female flies of 7, 15 and 25 (± 0-3) days of age were dissected under the microscope. In order to isolate the abdominal muscles and its corresponding innervating motor neurons. Briefly, adult flies were anesthetized with CO_2 and immobilized with dissection pins in Silgar polymere plates with their dorsal side up. Flies when then submerged in a drop PBS-1X containing formaldehyde (4%), allowing the fixing process to start. A dorso-longitudinal cut was done along the abdomen and dissection pins were used to open the abdomen in a wide-open-book manner. Fat and non-required tissues were removed. After a total fixation process of 20 minutes, the abdomens were washed with PBS-1X containing 0,1% triton and transferred to 4-well plates for immunostaining.

Synapses were revealed by the primary mouse monoclonal antibody nc82, which recognizes the CAST homolog bruchpilot protein, a constituent of the active zone of the synapse. Anti-HRP rabbit antibody was used to label and identify the motor neuron membrane.

Finally, the samples were mounted in Vetashield medium after incubation with secondary antibodies anti-mouse Alexa 488 and anti-rabbit Alexa 568.

To quantify the active zone area, total nc82 positive signal was measured in the third segment VLM-NMJs (adult ventral longitudinal muscle neuro muscular junctions) with Imaris (Bitplane) software. This estimation procedure was required as some of the mutant conditions render a diffuse nc82 signal over the motor neuron membrane as oppose to the regular individual spots appearance (see text).

HT-SY5Y Viability Assay

SH-SY5Y human neuroblastoma cells were seeded in a 96-well plate when cultures reached a 70–80% confluence, and incubated overnight with RPMI culture media supplemented with 10% FBS (see Materials for more details). Cells were differentiated with retinoic acid (10µM) and RPMI containing 2% FBS. 24h later, PTD4-PI3KAc peptide was added to the wells for pre-treatment studies. Aβ42 oligomers were added to the media 24h after the first treatment of PTD4-PI3KAc. For co-treatment experiments, PTD4-PI3KAc peptide was added at the same time as Aβ42 oligomers. Finally, for Post-treatment studies, PTD4-PI3KAc peptide was added to the media 24h after oligomer addition. Concentration of PTD4-PI3KAc peptide was 50µg/ml in all the cases. Concentration of Aβ42 oligomers was 18µg/ml, 36µg/ml or 72µg/ml.

HT-SY5Y Aβ42 Aggregation Assay

SH-SY5Y human neuroblastoma cells were seeded in a 12-well plate with coverslips when cultures reached a 70–80% confluence, and incubated overnight with RPMI culture media supplemented with 10% FBS (see Materials for more details). Cells were differentiated with retinoic acid (10µM) and RPMI containing 2% FBS for 48 hours prior to the addition of any stimuli. Aβ42 oligomers (36µg/ml) and PTD4-PI3KAc (50µg/ml) were added to the media. Cells were incubated with the stimuli for another 48h period and then the coverslip followed the standard immunostaining protocol (described above).

The 6E10 positive signal was analyzed in the total surface of the coverslip and quantified with Imaris software.

Aβ42 Extracellular Aggregation Assay

Cells were seeded and differentiated as previously described in *HT-SY5Y Aβ42 Aggregation Assay* (above). In this case, 4 different approaches were designed:

1. Cells supernatant was transferred to a new well, with a coverslip, after 48h of differentiation. Aβ42 oligomers were added to the supernatant and incubated for 48h before immunstaining. This experiment was an internal control for Aβ42 aggregation.

2. Differentiated cells were treated with PTD4-PI3KAc and incubated for 48h, the supernatant was then transferred to a new well, with a coverslip, were Aβ42 oligomers were added and incubated for another 48h prior to immunostaining. This experiment was named PI3K pre-treatment.
3. The Supernatant of differentiated cells was transferred to a new well, with a coverslip, after 48h of differentiation. In the new well, the supernatant was treated with PTD4-PI3KAc and Aβ42 oligomers at the same time, and incubated for 48h before immunostaining. This experiment was named PI3K co-treatment.
4. Differentiated cells were treated with Aβ42 oligomers for 48h prior to transfer the supernatant to a new well, with a coverslip. The supernatant was then treated with PTD4-PI3KAc and incubated for another 48h before immunostaining. This experiment was named PI3K post-treatment.

The 6E10 positive dots in the total surface of the coverslip were analyzed and counted with Imaris software.

Statistical Analysis

All data are shown as mean ± standard deviation of the mean.

Statistical significance was calculated using a unpaired Student's two-tailed *t*-test, with significant differences between compared groups noted by *$P \leq 0.05$, **$P \leq 0.01$, and ***$P \leq 0.001$.

RESULTS

CHAPTER 4 STUDY OF THE SYNAPTOGENIC ACTIONS OF PI3K IN AZs IN AN ADULT-ONSET AD MODEL

Previous studies have demonstrated the synaptogenic functions of PI3K in invertebrate and mammal neurons (Martin-Pena et al., 2006, Acebes et al., 2011, Cuesto et al., 2011). These new synapses were functional and supernumerary, as quantified in larval NMJ active zones (Martin-Peña et al, 2006; Jordan-Alvarez et al, 2012), and adult antennal lobe inhibitory interneurons in *Drosophila* (Acebes et al., 2011), and in CA1 hippocampal cultured neurons in mice (Cuesto et al., 2011). Thus, PI3K overexpression becomes a synaptogenic tool than could be used in pathological situations where synapses are affected.

In this work we ask if the synaptogenic functions of PI3K are effective in a neurodegenerative model of Alzheimer's disease in *Drosophila* where human Aβ42 peptide is overexpressed and induces synapse loss.

4.1 PI3K prevents Aβ42 induced neurodegeneration

To determine if PI3K can rescue the loss of synapses induced by Aβ42, we overexpressed a constitutively active form of PI3K and the human Aβ42 peptide within the pan-neural pattern of the *elav*-Gal4 driver. To discard an effect during development, we used the temperature sensitive $Gal80^{TS}$ construct to activate the expression of the desired genes only in adult stages. As detailed in Chapter 3 (Materials & Methods), flies were grown at 17°C, and transferred to 29°C when they reached adulthood to allow the expression of the Gal4.

To estimate the number of synapses, we aged adult flies for 7, 15 and 25 days (± 0-3 days), and dissected adult abdomens to later visualize the third segment ventral longitudinal muscle (VLM) NMJs. Synapses were revealed by the monoclonal antibody nc82, which recognizes a CAST homolog localized in the active zones (presynaptic region) of the motor neuron. Anti-HRP antibody was used to label and identify the motor neuron membrane.

To quantify the active zone area, nc82 total positive signal was measured in third segment ventral longitudinal muscle (VLM) NMJs. (Chapter 3 for more details).

At 7 days (**Fig. R1 A**-**D**,**E**), all genotypes had similar numbers of synaptic area, and no significant changes were found, suggesting that neither of the genotypes (Aβ42, PI3K, or PI3K/Aβ42) had altered synapse formation. However, at a later time-point, Aβ42 expressing flies showed significant decrease in the total synaptic area when compared to matching controls that had reached 15 days. At the same time, PI3K flies showed a significant increase in total synaptic surface, in concordance with previous published data (Martín-Peña et al, 2006). Interestingly, PI3K and Aβ42 co-expression showed very significant differences compared to Aβ42 (**Fig. R1 A'**-**D**',**E**). This recovery in the synaptic area indicated that the synaptogenic effect of PI3K could prevent the synapse loss induced by Aβ42 in adult motor neurons at day 15 of expression. PI3K/Aβ42 showed no significant changes when compared to control flies, meaning that the synapses in PI3K/Aβ42 genotype stayed in the similar values than control healthy flies.

Observing puncta morphology, we noticed that Aβ42 flies showed disorganized non-spherical positive dots of bruchpilot signal (**Fig. R1 C'**). This deposit-like morphology was not observed in any of the other genotypes, nor in 7 days aged Aβ42 flies (**Fig. R1 A**-**D**,**A'**,**B'**,**D'**,**A''**-**D''**).

4.2 PI3K prevention of Aβ42-induced synaptic loss is age-independent

Even though Aβ42 flies died soon after 15 days of age (at 29°C) (Chapter 5), we wanted to test if the effect of PI3K/Aβ42 in synapses was maintained at later time-points (**Fig. R1 A''**-**D''**,**E**). At 25 days, PI3K flies maintained significantly larger values of synaptic area compared to matching controls. At this time-point PI3K/Aβ42 genotype was still able to keep similar values of synaptic area to controls, and no significant differences were observed between the two groups. These results suggest that PI3K expression prevents Aβ42 synaptotoxic effects also at later time-points. Taking into consideration that PI3K/Aβ42 flies died under these conditions soon after 25 days (Chapter 5), we can

conclude that PI3K effects in preventing Aβ42 synaptotoxicity are effective in an age-independent manner.

Taking all these results together (**Fig. R1**), we confirm that Aβ42 expression causes progressive morphological alterations and synapse loss in adult motorneurons, and have demonstrated that these deleterious effects can be prevented by PI3K activation.

4.3 Changes in synapses are not due to transcriptional regulation

In order to investigate the molecular mechanism for PI3K rescue of Aβ42-induced synapse elimination, we wondered first if the transcription of synaptic genes was affected. Quantitative RT-PCR using mRNA from adult heads was used to analyzed three AZs components: *bruchpilot*, *liprin* and *synaptobrevin* (Kidokoro, 2003, Fouquet et al., 2009) mRNA levels. Flies from all the genotypes in the study were aged to 15 days with the same adult-onset design used in previous experiments.

Our qRT-PCR results indicated that there are no significant changes in mRNA expression for any of the studied genes (**Fig. R2 A**-**C**), suggesting that PI3K synaptic restoration is not due to changes in transcription of the synaptic genes *bruchpilot*, *liprin* or *synaptobrevin*.

4.4 PI3K prevents the Aβ42-induced microtubule dynamics defects

Since Aβ42 can alter the intracellular transport, we wondered if PI3K could prevent these alterations as a mechanism to restore synapses (shown in Fig. R1).

To this end, we performed live time-lapse imaging in whole-mount larvae to analyze microtubule dynamics using the UAS-EB1-GFP construct. EB1 is a plus-end microtubule binding protein that reports microtubule dynamics (see Chapter 3 for details). Briefly, EB1 binds to the plus-end of a growing microtubule, but detaches from shrinking microtubules resulting in dynamic GFP signals known as “comets” (**Fig. R3 A**).

EB1-GFP comets of third instar larval ddA (dendritic arborization dorsal cluster) sensory neurons were recorded under a microscope equipped with a spinning disk. Length, duration, velocity and density of EB1-GFP comets were quantified with Imaris® software.

Track speed in PI3K and PI3K/Aβ42 genotypes showed significant changes when compared to controls, but no statistical significance was found in Aβ42. Furthermore, no statistical significance was observed when PI3K and PI3K/Aβ42 comets were compared (**Fig. R3 B-E**,**F**). Values of track length and track duration did not change in any of the studied genotypes (**Fig. R3 G**,**H**).

Moreover, we analyzed track density by counting the number of comets relative to dendritic surface, as the EB1-GFP overexpression allows some background signal that serves as a reporter of the dendritic size (**Fig. R3**). Aβ42 expressing neurons showed a significant decrease in comet density compared to controls. Interestingly, PI3K and PI3K/Aβ42 did not show significant changes when compared to controls (**Fig. R3 I**), indicating that PI3K/Aβ42 was able to prevent the decrease in comet density induced by Aβ42.

The absence of significant changes in track length and track duration indicates that the growing process of the microtubule, once started, is affected neither by Aβ42 nor by PI3K or PI3K/Aβ42 expression (**Fig. R3 G**,**H**). The polymerization of tubulin units to the growing microtubule appears to be in this case, a process independent of Aβ42 or PI3K overexpression. In the same line, the speed of growing processes in microtubules appears to be independent of Aβ42, but can be affected by PI3K or PI3K/Aβ42 combined (**Fig. R3 F**).

We conclude from these findings (**Fig. R3**) that Aβ42 produces changes in microtubule dynamics by reducing the number of growing events per surface unit, which is a direct evidence of intracellular transport deficits. Interestingly, PI3K/Aβ42 neurons had the same number of growing microtubules per surface unit as control, pointing that PI3K activation can prevent microtubule dynamics defects induced by Aβ42, thus allowing a functional intracellular transport.

CHAPTER 5 ANALYSIS OF LOCOMOTION ACTIVITY AND SURVIVAL EFFECTS OF PI3K OVEREXPRESSION IN Aβ42 INDUCED NEURODEGENERATION

The promising results shown in chapter 4 urged us to further analyze the effect of PI3K overexpression at a whole organismal level. In other *Drosophila* AD models, neurodegenerative phenotypes have been characterized by locomotion performance and lifespan studies. In order to compare our adult-onset Aβ42 overexpression model with the rest of AD models described, and to evaluate if PI3K activation can protect, not only synapses morphology but also their function, we tested the locomotor activity of adult flies and the lifespan of the 4 genotypes under study.

5.1 Aβ42-induced locomotion activity reduction is delayed by PI3K overexpression

To test if the protected synapses were functional when Aβ42 was expressed in combination with PI3K, we analyzed locomotion performance in adult flies.

Three different groups of flies were annotated: 1) flies that reached the 4 cm line threshold within the given time, blue histograms, 2) flies that did not reach this line but climbed along the tube, orange histograms, and 3) flies that stayed at the bottom of the tube, black histograms (**Fig. R4 A**).

Results showed that Aβ42 expressing flies developed a locomotor activity reduction as soon as 11 days of age, appearing for the first time in this study, a significant group of flies that stayed at the bottom of the tube during the climbing assay (black histograms) (**Fig. R4 D**). The total percentage of flies that could not climb at all increased progressively as the flies aged, and this proportion of flies was higher than 50% at 18 days of age (**Fig. R4 D**).

When combined with Aβ42, PI3K overexpression delayed the appearance of the non-climbing phenotype to 15 days, which reached 50% of the total population at 25 days of age, 7 days later than the Aβ42 expressing flies (**Fig. R4 E**).

Control and PI3K flies did not show any sign of locomotor deficits until 30 days of age, as expected for healthy flies grown at 29°C (**Fig. R4 B**,**C**).

The total number of flies that climbed above the line was reduced in Aβ42 flies when compared to matching controls and PI3K. This effect was delayed with PI3K/Aβ42 expression (**Fig. R4 B**-**E**).

Pie charts for 15 days and 20 days data show more specific values (**Fig. R4 F**-**M**). As the flies aged, the locomotor affectation became more evident in all genotypes. Aβ42 genotype showed a very rapid reduction of the climbing performance that was also aggravated in time. PI3K/Aβ42 genotype developed also a reduction in the climbing performance when compared to controls, but this reduction was delayed in time when compared to Aβ42 flies (**Fig. R4**).

5.2 PI3K expression increases lifespan of Aβ42 flies

Aβ42 is known to affect very aggressively the organism lifespan when expressed with pan-neural drivers as elav-Gal4 (Iijima et al., 2004), but the overexpression of PI3K or the combination of both had not been investigated before, so we studied the effect of these genotypes with the same adult-onset design.

As expected, Aβ42 genotype showed a significant decrease in lifespan when compared to control (**Fig. R5 B**). On the other hand, PI3K overexpression alone showed significant increase in survival (**Fig R5 A**). PI3K overexpression when combined to Aβ42, significantly ameliorated the negative lifespan effect attributed to Aβ42 (**Fig. R5 D**). However, this recovery in survival did not reach control values, and significant differences were observed when PI3K/Aβ42 was compared to controls (**Fig. R5 C**).

Taken together, these data (**Fig. R5**) indicate that PI3K overexpression ameliorates Aβ42 lifespan reduction. The recovery in survival, although very significant when compared to Aβ42, does not reach lifespan values of control flies. Moreover, PI3K alone showed significant increase in lifespan in comparison with controls (**Fig. R5 E**).

5.3 PI3K in human neurons prevents the cell survival reduction induced by Aβ42

Knowing that PI3K synaptogenic actions are conserved in human neurons, and that our Drosophila AD model is based in human Aβ42 expression, we wondered if the effect of PI3K preventing Aβ42 neurodegeneration was also conserved.

To examine if the effects of PI3K in neurons exposed to Aβ42 oligomers were reproduced in human cells, we cultured the human neuroblastoma cell line SH-SY5Y.

Cells were grown and differentiated with retinoic acid and 1% serum for 48h prior to stimulation with treatments. Once differentiated, neurons were treated with Aβ42 oligomers. As expected, treatment with Aβ42 oligomers - reduced viability after 48 hours. To stimulate PI3K activity in these cells and evaluate cell viability, we used the peptide PTD4-PI3KAc, which was previously proved to trigger PI3K activation both in vitro and in vivo (Cuesto et al., 2011, Enriquez-Barreto et al., 2014). PTD4-PI3KAc peptide was administered at 3 different time points, naming the 3 time-point treatments as 1) pre-treatment, 24h before Aβ42, 2) co-treatment, at the same time as Aβ42 and 3) post-treatment, 24h after Aβ42.

Aβ42 oligomers where prepared following Kayed & Gable, 2006 protocol (see chapter 3 for details) and added to the cell culture 72 hours after cell seeding (48 hours after differentiation), at 3 different concentrations, to study the potential effects of PI3K activation under these conditions.

The percentage of cells alive after the treatment with Aβ42 oligomers was significantly decreased when Aβ42 peptide concentration was 36µg/ml or 72µg/ml, compared to control cells. These results confirmed the acuity of the oligomer preparation protocol and were used as positive internal controls in the experiment (**Fig. R6**).

As expected, Aβ42 oligomers did not affect cell viability at low concentrations (18µg/ml).

PTD4-PI3KAc peptide administration produced no significant changes in cell viability when the treatment occurred 48h or 72h after differentiation, but produced a significant increase in viability when administer 24h after differentiation. This effect can be attributed to the brief period of starvation and differentiation that the cells had at this moment (24h) that could allow cells to respond to mitogen stimuli, like PI3K pathway effectors.

Results from the viability Cell Titer assay showed that PI3K activation could prevent Aβ42-induced cell death when administer either before or at the same time than Aβ42 oligomers, if the concentration of oligomers was 36μg/ml. No protection was found at higher concentrations (72μg/ml) (**Fig. R6**)

Together, these data indicate (**Fig. R6**) that PI3K activation can protect cell viability from Aβ42 oligomers toxic effect in human neurons. This protection can be achieved if PTD4-PI3KAc peptide was added 24 hours before Aβ42 treatment, or at the same time as Aβ42 treatment, when oligomers concentration was 36μg/ml.

CHAPTER 6 STUDY OF THE SYNAPTOGENIC ACTIONS OF MEDEA DOWN-REGULATION AND mTOR OVEREXPRESSION IN Aβ42 NEURODEGENERATION

Activation of PI3K proved to prevent Aβ42-induced synapse loss and delayed locomotor performance deficits, as well as ameliorated longevity, as shown in bruchpilot quantification in adult NMJs, climbing, and lifespan assays, respectively. Furthermore, SH-SY5Y cells were also protected from Aβ42-induced cell death when PI3K was activated before or together with Aβ42 treatment.

Being PI3K at the crossroads of many pathways, one could argue that the preventive effects shown by the overexpression of this kinase could be explained by the activation of the canonical pathway of PI3K, that is known to elicit pro-survival and cell growth responses. Thus, we wondered if classical effectors of PI3K pathway could reproduce the protective functions of PI3K, or if on the other hand, more synaptogenic proteins previously proved to increase synapse number, could attain the preventive actions of PI3K.

6.1 Synaptogenic proteins, but not canonical PI3K effectors, prevent Aβ42-induced synapse loss

To explore the PI3K partners in the neuroprotective effect against Aβ42, synapses were quantified when mammalian Target of Rapamycin (mTOR), a downstream protein of the canonical pathway of PI3K/Akt, was overexpressed. mTOR, does not exhibit synaptogenic effects when overexpressed in Drosophila NMJs (Martín-Peña 2007), and thus is not considered a player in the synaptogenic pathway. Using the same procedure as in Chapter 4.1, the total bruchpilot signal was quantified from adult abdominal NMJs of 15 days-old flies. This is a time-point where PI3K synaptogenic effect was first observed. Like in all previous experiments, the pan-neural elav-Gal4 driver was used under the Gal80^{ts} control, allowing the expression of the corresponding UAS constructs, only after fly eclosion.

Results showed that mTOR overexpression (**Fig. R7 B**,**E**,**G**) was not able to prevent Aβ42 synapto-toxicity, as we found a very significant decrease in synapse surface in mTOR/Aβ42

(**Fig. R7 E**,**G**) NMJs compared to controls. When overexpressed alone, mTOR (**Fig. R7 B**,**G**) showed no significant differences in the active zones quantification compared to controls, confirming previous reports.

Synapse surface was also evaluated with Medea down-expression. Medea is an anti-synaptogenic protein, homolog of human Smad 4 (Hudson et al., 1998), that binds to Mad and, together, regulate gene transcription. It acts downstream of PI3K, and is directly inhibited by the E3-Ubiquitin ligase Hiw (Highwire), which can bind to Medea and cause its degradation impeding NMJ growth (McCabe et al., 2004).

On the other hand, $Medea_{RNAi}$ in combination with Aβ42 (**Fig. R7 F**) prevented the synapse loss (**Fig. R7 D**), as we found no significant differences between $Medea_{RNAi}$/Aβ42 and control, while there was very significant differences when compared to Aβ42 (**Fig R7 G**). $Medea_{RNAi}$, when expressed alone (**Fig. R7 C**) did not show significant changes in synapses (**Fig. R7 A**,**C**, **G**).

These observations (**Fig. R7**) indicate that $Medea_{RNAi,}$ but not mTOR, prevents Aβ42-induced synaptotoxicity. Medea down-expression alone did not affect synapse surface, but mTOR produced a very significant decrease in synapse values.

6.2 Aβ42-induced locomotor decline is prevented by Medea knockdown

The promising results extracted from the NMJ active zones quantification shown by Aβ42 in combination with $Medea_{RNAi}$ urged us to analyze the functionality of these flies in a locomotor assay.

The same procedure used in Chapter 5.1 was applied to mTOR, mTOR/Aβ42, $Medea_{RNAi}$ and $Medea_{RNAi}$/Aβ42 genotypes (**Fig. R8 A**).

The results showed a reduction in the climbing performance of mTOR/Aβ42 flies when compared to controls (**Fig. R8 H**,**B**). Also, we found that flies started to show a no-climbing phenotype, and stayed at the bottom of the tube, as early as 9 days of expression (black histograms in **Fig. R8 H**). mTOR overexpression alone, also showed a reduction in the total

number of flies reaching the 4cm line (**Fig. R8 E**), with flies staying at the bottom of the tube at 15 days of expression.

On the other hand, $Medea_{RNAi}$/Aβ42 combination showed no differences when compared to control flies in any of the three populations counted: above the 4 cm. line, below the 4 cm. line, and at the bottom of the tube (**Fig. R8 B**,**M**). $Medea_{RNAi}$ alone showed a climbing phenotype, as expected because of its role in synapse number regulation (**Fig. R8 B**, **J**).

Taken together these data (**Fig. R8**) indicate that other synaptogenic agents, such us down-expression of Medea prevent the deterioration of the locomotor performance characteristic of Aβ42 toxicty. By contrast, this is not the case for classical effectors of the PI3K pathway like mTOR.

6.3 Medea knockdown prevents Aβ42-induced lifespan reduction

Already known the longevity effects of PI3K in Aβ42 flies, we wondered if mTOR overexpression or Medea down-expression could also be affecting Aβ42 flies lifespan.

To address this issue, survival studies were conducted following the same protocol as in Chapter 5.2, this time with mTOR, mTOR/Aβ42, $Medea_{RNAi}$ and $Medea_{RNAi}$/Aβ42 genotypes.

The analysis of the survival curves demonstrated a significant decrease in lifespan in mTOR/Aβ42 flies, as well as in mTOR overexpression alone (**Fig. R9 A**,**B**). When compared to Aβ42 flies, mTor/Aβ42 group showed a significant decrease (**Fig. R9 E**) indicating that mTOR could act as an enhancer in lifespan reduction by Aβ42.

$Medea_{RNAi}$/Aβ42, on the other hand, blocked the Aβ42 reduction effect in lifespan, showing no significant differences when compared to control flies (**Fig. R9 D**). $Medea_{RNAi}$ alone demonstrated no significant differences either (**Fig. R9 C**). Comparing Aβ42 and $Medea_{RNAi}$/Aβ42 lifespan we found a very significant increase (**Fig. R9 F**), as expected from previous comparisons of $Medea_{RNAi}$/Aβ42 with control flies.

These results (**Fig. R9**) indicate that Medea down-expression, a synaptogenic tool, abolishes the lifespan limiting effect of Aβ42 expressing flies. On the opposite side, mTOR

overexpression, a downstream activation of PI3K/Akt canonical pathway, cannot prevent Aβ42 toxicity, but rather accentuates it.

Experiments of synapse quantification (**Fig. R1** & **Fig. R7**), climbing performance (**Fig. R4** & **Fig. R8**) and survival (**Fig. R5** & **Fig. R9**) have tested the ability of Medea down-expression and PI3K overexpression, two synaptogenic strategies, to counteract the degenerative effects of Aβ42. Both proteins, previously proved to upregulate synapse growth, have demonstrated to effectively decrease the synapto-toxicity produced by Aβ42, allowing a better locomotor performance and increasing lifespan.

CHAPTER 7 ANALYSIS OF A NOVEL EFFECT OF PI3K IN Aβ42 AGGREGATION

As described in Chapter 1, a key feature in AD pathology is Aβ42 accumulation, which exponentially increases during the preclinical phase. Excessive accumulation of Aβ42 can lead to oligomer formation. Oligomers are the most toxic species of β-amyloid, as they are known to directly affect synapses, and they can suffer modifications such as truncations, isomerization and/or phosphorylations that alter oligomerization and aggregation.

Being Aβ42 levels critical for the progression and outcome of the pathology, we wondered if PI3K preventive actions in synapses had any effect on Aβ42 accumulation or aggregation.

7.1 PI3K activation increases Aβ42 levels without affecting transcription

To understand the effect that PI3K could be causing in Aβ42 accumulation, we analyzed by immunohistochemistry the total signal of Aβ42 in 15 days-old brains using the commonly used 6E10 antibody. This antibody recognizes the N-terminus of the amyloid peptide. As this epitope is not found in APLP Drosophila protein, no signal is expected in control brains.

Aβ42 adult brains (**Fig. R10 A**-**D**) showed a noticeable positive signal for 6E10, which was completely absent in control or PI3K overexpressing brains (**Fig. R10 A**,**B**). Surprisingly, this positive signal was increased and expanded in PI3K/Aβ42 brains (**Fig. R10 C**,**D**).

To confirm this result, same aged adult heads homogenates were analyzed by Western blot (**Fig. R10 E**). Quantification of the total Aβ42 protein showed 2.5 fold increase in PI3K/Aβ42 compared to Aβ42 alone.

In order to investigate a putative effect in transcription, qRT-PCR was performed with same aged adult head homogenates and the results showed no changes in total Aβ42 mRNA, discarding this possibility (**Fig. R10 F**).

Therefore, these data indicate (**Fig. R10**) that PI3K overexpression causes a total Aβ42 protein increase, demonstrated by immunostaining and Western-blot, without affecting its transcription levels, as analyzed by quantitative RT-PCR.

7.2 PI3K overexpression increases Aβ42 insoluble fraction

Being aware that different Aβ aggregation assemblies can lead to very different scenarios (**Fig. R11 A**), we postulated the hypothesis that the increase in total Aβ42 protein found in PI3K/Aβ42, could be explained by having a higher proportion of insoluble, and thus less toxic, aggregates.

To prove this hypothesis we stained 7 and 15 days-old brains with Thioflavin-S (**Fig. R11 B-C'**), a dye that specifically binds to proteins with β-sheet conformation. The dye labels Aβ42 fibers and plaques that constitute the insoluble fraction of β-amyloid aggregates. Quantification of the positive Thioflavin-S signal demonstrated a significant increase in the insoluble fraction of Aβ42 deposits at 15 days of age in the PI3K/Aβ42 brains compared to age-matched Aβ42 alone (**Fig. R11 E**).

This result was confirmed by Western-blot of insoluble protein extractions from 15 days-old adult heads. The quantification showed a 4-fold increase in the insoluble fraction of Aβ42 in PI3K/Aβ42 genotype (**Fig. R11 D**).

Taken together, these data (**Fig. R11**) confirm the hypothesis that PI3K triggers a change in Aβ42 aggregation into a more insoluble species.

7.3 PI3K-induced Aβ42 aggregation changes are reproduced in human neurons

Having previously proved that PI3K activation can prevent Aβ42-induced cell death, we wondered if the aggregation effect that PI3K elicits in Aβ42 conformers could also be reproduced in human neurons.

To assess that, we cultured and differentiated human neuroblastoma cells (SH-SY5Y) with retinoic acid and 2% serum for 48h prior to stimulation with the treatments. Once

differentiated, neurons were treated with Aβ42 oligomers (36μg/ml) and PTD4-PI3KAc peptide (50μg/ml) (see Chapter 3 for details). Cover-slides were used in the seeding plates to later perform immunostainings with 6E10 antibody. Cells were treated with both stimuli added at the same time and incubated for 48h. Afterwards, cells were fixed with formaldehyde 4% following a standard protocol of immunostaining (**Fig. R.12 A**). 6E10 positive deposits were counted and surface per deposit was measure with the Imaris software.

As expected, no 6E10 positive deposits were found in cells treated either with vehicles or with PTD4-PI3K alone (**Fig. R12 E-F'**). For practical reasons only Aβ42 and PTD4-PI3KAc/Aβ42 experiments were compared (**Fig. R12 G-H'**).

PTD4-PI3KAc in combination with Aβ42 oligomers treatment, showed a significant decrease when comparing the total number of deposits found in Aβ42 treatment (**Fig. R12 B**). Interestingly, the total surface of deposits did not change between Aβ42 treatment and PTD4-PI3KAc + Aβ42 treatment (**Fig. R12 C**). However, deposit surface distribution showed that in PTD4-PI3KAc + Aβ42 treatment there were bigger deposits that differed from Aβ42 treatment by threefold, fourfold and even six fold increase in size (**Fig. R12 D**).

These data (**Fig. R12**) indicate that the Aβ42 aggregative properties shown by PI3K in adult flies are reproduced in human SH-SY5Y neurons, where the peptide PTD4-PI3KAc can induce three to six fold increase in the deposit size.

7.4 PI3K-induced changes in Aβ42 aggregation can be reproduced outside of cells

To further analyze the aggregation effect that PI3K activation triggers in Aβ42 oligomers, and to test if these actions could take place in the extracellular space, were the majority of deposits are generated, we designed a set of experiments to decipher if PTD4-PI3KAc peptide was indeed capable to promote Aβ42 aggregation extracellularly.

Following a previously described protocol, human neuroblastoma cells (SH-SY5Y) were cultured with retinoic acid and 2% serum for 48h prior to stimulation with treatments. Once differentiated, neurons were treated with Aβ42 oligomers (36μg/ml) and PTD4-PI3KAc peptide (50μg/ml) (see Chapter 3 for details).

Four different culture classes were designed: 1) internal control for Aβ42 oligomers aggregation, 2) Aβ42 oligomers with PTD4-PI3KAc pre-treatment, 3) Aβ42 oligomers with PTD4-PI3KAc co-treatment, and Aβ42 oligomers with PTD4-PI3KAc post-treatment (**Fig. R13 A**). Supernatants were stained with 6E10 antibody, and analyzed with Imaris software.

The internal control of Aβ42 oligomers showed no significant 6E10 positive deposits, meaning that in the given time of 48h, extracellular aggregates that could be generated were not detected.

When total number of deposits in the PTD4-PI3K pre-treatment, co-treatment and post-treatment experiments was measured, (**Fig. R13 B**) we found no significant differences in any of the experiments. Moreover, similar negative results appeared when the total area of deposits was compared among the three experiments (**Fig. R13 C**).

However, the three experiments showed significant differences when the ratio "number of deposits/deposit area" was studied (**Fig. R13 D**). When more detailed analysis was performed, in order to evaluate the deposit surface distribution (**Fig. R13 E**), PTD4-PI3K co-treatment showed a twofold, fourfold or even a ten-fold increase in deposit size, when compared to PTD4-PI3KAc pre-treatment and post-treatment. PTD4-PI3KAc post-treatment showed the smallest deposits among the three experiments of the study (**Fig. R13 E**).

Taken together, these data indicate that PTD4-PI3KAc peptide promotes Aβ42 aggregation extracellularly (**Fig. R13**). This increase in aggregation upon PI3K treatment leads to larger Aβ42 deposits that range from two to ten-fold increments in size. These findings also suggest that PTD4-PI3KAc co-treatment is the most aggregative strategy for Aβ42 oligomers.

7.5 pSer-Aβ42 increases following PI3K overexpression

Knowing that phosphorylation has been documented to be one of the factors that can affect Aβ42 seeding in the initial phase of the plaque formation, we argue that PI3K kinase

activity could be directly affecting this phosphorylation and thus inducing Aβ42 plaque seeding.

To test this hypothesis, we looked for residues suitable to be phosphorylated in Aβ42 according to the NetPhos 2.0 Server prediction software (www.cbs.dtu.dk). This study suggested 3 putative residues: pSer8 (Score: 0.963), pTyr10 (Score: 0.870) and pSer26 (Score: 0.787) (**Fig. R14 A**).

Phospho-Tyrosine and phospho-Serine specific antibodies were used in 15 days-old brains in order to analyze changes in the signal in the four genotypes under study. Confocal images (**Fig. R14 B**-**E'**) indicated that only in PI3K/Aβ42 brains (**Fig. R14 E**,**E'**) the phospho-Serine signal was incremented. Interestingly, the phospho-Serine signal in PI3K/ Aβ42 brains had deposit-like morphology. Phospho-Tyrosine signal was very similar in all genotypes and no deposit-like morphology was found (**Fig. R14 F**-**I'**).

Co-localization of 6E10 and both phospho-Serine and phospho-Tyrosine was not feasible due to the requirement of formic acid for 6E10 immunostaining, which strongly alters phospho-peptides and membrane stability (data not shown).

We can conclude from these results (**Fig. R14**) that PI3K overexpression in an Aβ42 background drives the accumulation of phospho-Serine positive deposits.

7.6 PI3K specifically triggers Ser26-Aβ42 phosphorylation

The NetPhos 2.0 Server predicts two different serine residues that could become phosphorylated. Thus, we took advantage of the recently developed and kindly gifted pSer8-Aβ42 and pSer26-Aβ42 antibodies, by Dr. Jochen Walter lab (Kumar et al, 2013) and performed immunostainings.

No changes were found in pSer8-Aβ42 immunostainings in Aβ42 or PI3K/Aβ42 genotypes (**Fig. R15 A''**,**B''**). Phospho-Ser26-Aβ42 immunostainings showed deposits with positive signal in both Aβ42 and PI3K/Aβ42 (**Fig. R15 A'**,**B'**). Unfortunately, pSer26-Aβ42 antibody could not give direct results due to the fact that it can detect both phosphorylated and non-phosphorylated Aβ42.

Taken together, these data (**Fig. R15**) indicate that PI3K does not trigger the phosphorylation of Aβ42 in residue serine 8, proved by immunostaining with the only specific antibody available at this time, and thus, having proved before that PI3K generates phospho-serine positive deposits, and that there are only two potential serine residues in Aβ42, a phosphorylation in pSer26-Aβ42 seems plausible.

CHAPTER 8 CHARACTERIZATION OF Aβ42 PHENOTYPES IN NON-NEURONAL TISSUES AND STUDY OF PI3K EFFECT IN THESE ENVIRONMENTS

Although it is not fully understood today whether extracellular or intracellular β-amyloids are the first toxic Aβ species, it is widely accepted that Aβ42 accumulations can aggregate in extracellular spaces. Moreover, the two models used in this study can mimic this type of accumulations, as the UAS-Aβ42 construct consists of two tandem copies of the human Aβ42 sequence fused to a peptide signal for secretion, and the Aβ42 oligomers were added extracellularly to HT-SY5Y cultured cells, allowing in both scenarios extracellular circulation and aggregation of Aβ species.

In this work, we have demonstrated the PI3K preventive actions of Aβ42 synaptotoxicity, and moreover, the effects of PI3K in Aβ42 aggregation, both in human *in vitro* studies and in *Drosophila in vivo* analysis. However, being aware that Aβ42 can diffuse, circulate and eventually reach other types of cells that could become sensitive to Aβ42 toxicity, we wondered if 1) Aβ42 expression could affect non-neuronal cells, and if 2) PI3K activation could also prevent the potential Aβ42-induced toxicity in these non-neuronal contexts.

In this chapter we evaluated Aβ42 toxicity in neuro-secretory cells and epithelial cells, and checked if PI3K co-expression could prevent these potential deleterious effects. For this purpose we characterized in detail the expression domains of two drivers, *elav*-Gal and D42-Gal4, along development in epithelial cells of the wing disc.

8.1 Aβ42-induced inflated abdomen phenotype is prevented by PI3K overexpression

To our surprise, adult flies overexpressing Aβ42 with the pan-neural elav-Gal4 driver, together with the temperature sensitive Gal80^{ts} construct, which allowed expression of the UAS-Aβ42 only after adult eclosion, showed a largely inflated abdomen as they aged (**Fig. R16 A,B**). To our knowledge, this is the first report of Aβ42 causing an abdominal phenotype in flies. We also observed that the flies presented not-retractable proboscis, and that this phenotype did not appear in PI3K/Aβ42 flies (**Fig. R16 C**). By contrast, PI3K

and PI3K/Aβ42 flies showed no abdomen inflation (**Fig. R16 A**). These data indicate that PI3K can restore the abdomen volume inflation and the loss of proboscis retraction caused by Aβ42 (**Fig. R16 A-C**).

Knowing that a very similar phenotype is caused by irregular secretion due to blockade of the secretory system in flies, we wondered if this could be the case for Aβ42. To assess that, we overexpressed Aβ42 in abdominal leucokinergic cells (*leucokinin*^{M7}-Gal4), a set of peptidergic neuro-secretory cells that extend their projections to the CNS and the periphery, where they reach abdominal muscle 8. The terminals of these cells do not present bouton-like structures and they lack synapsin and sybsynaptic reticulum (Landgraf et al., 2003).

The overexpression of Aβ42 in leucokinin cells reproduced the increase in abdominal volume previously described with *elav*-Gal4 driver (**Fig. R16 D**,**E**). Furthermore, PI3K/Aβ42 combination prevented the inflation phenotype (**Fig. R16 D**,**E**). The loss of retraction in the proboscis of Aβ42 flies was also observed with *leucokinin*-Gal4 driver, and akin to elav-Gal4, PI3K/Aβ42 prevented this effect (**Fig. R16 F**). These observations suggest that Aβ42 can cause deleterious effects in cells lacking regular synapses, like leucokinin neuro-secretory cells, and that this phenotype can be restored by PI3K overexpression (**Fig. R16**).

The surprising observation of Aβ42 effects in non-neuronal cells, made us wonder about the possibility that other non-neuronal tissues could also be sensitive to Aβ42 toxicity.

However, the elav-Gal4 expression domain with which the non-neuronal Aβ42 phenotypes were identified was at odds with the widely accepted neuronal specificity of this driver. To address this contrast, we re-examined in detail the expression domain of this driver.

8.1.1 The nervous system enhancer *elav* is transiently active in epithelial cells

The Drosophila gene *elav*, orthologue of *ELAVL* gene family in humans, is expressed throughout the brain (Robinow and White, 1988, Van Tine et al., 1998, Han et al., 1996, Muresu et al., 1994, Robinow and White, 1991). We confirmed the reported *elav*-Gal4 expression in brain neurons (**Figure R17 A**,**A'**) with the G-TRACE system, which reports the

temporal activation of the enhancer-Gal4 under study (Chapter 3 for details). The current (red positive cells) and historical (green positive cells) records of *elav* enhancer activity showed high correspondence between both signals. These data indicate that cells fated to be neurons in the brain are determined during development and this fate is maintained during CNS development.

Further, we analyzed epithelial tissues to determine the specificity of this *elav* enhancer. The data showed widespread positive green cells (**Figure R17 B**) and randomly distributed red positive cells in wing imaginal discs (**Figure R17 B'**). These red (RFP) and green (GFP) signals demonstrate that the *elav* enhancer had been expressed in wing disc cells sometime along development.

To determine at what stage during development this ectopic enhancer activation occurs, we analyzed 1st and 2nd instar larvae wing discs (24 and 48 hours after egg laying, AEL) (**Figure R17 C**-**D'**). G-TRACE reporters showed that the *elav* enhancer was active as early as 1st (**Figure R17 C**,**C'**) and 2nd (**Figure 17 D**,**D'**) instar larvae. Red and green cells are found in the wing disc suggesting that the enhancer activity is triggered at the initial stages of development.

Together, these results indicate that the *elav* enhancer is active in epithelial cells during development and maintains its activity by the third larval instar, albeit to a lesser extent, as RFP-positive cells are less numerous than GFP-positive cells (**Fig. R17 A**-**D'**). GFP-positive cells represent the wing disc cells where the enhancer has been active at some point during development, but has eventually become inactive. RFP-positive cells represent the wing disc cells where, at the moment of dissection, *elav* enhancer was active.

We noticed that the expression pattern of GFP and RFP cells across different discs of different larvae was not reproducible. Although this variability could result from heterogeneous environmental conditions among individuals, we further evaluated this feature comparing left and right wing discs from the same individual. The number of GFP-positive cells was comparable between the two wing discs of the same animal, yet, the pattern differs (**Figure R17 E**-**F**,**G**). Moreover, we compared left and right wing discs of the *elav*-Gal4 inserted in another chromosome (Chr.II), in order to check if the ectopic

activation of the classical neuronal enhancer *elav* was affected by the insertion locus (**Fig. R17 H**,**I**). In this case, we also found strong variability in GFP-positive cells when comparing left and right wing discs, and no RFP-positive cells were detected. GFP and RFP cells patterns differed also when we compared *elav*-Gal4 enhancer inserted in Chr. III versus *elav*-Gal4 in Chr. II. (**Fig. R17 E**-**I**, **J**).

This result (**Fig. R17 E**-**J**) supports the notion that the *elav* enhancer activation during development is not a deterministic phenomenon and it rather appears to be a random process.

Finally, to determine if the ectopic wing disc expression of the *elav* enhancer induces the expression of Elav protein, we stained larval tissues with anti-Elav antibody. Third instar larval brains showed that *elav* enhancer is active in neurons as expected (**Figure 17 K**) and brain cells express Elav protein (**Figure 17 K'**). However, while wing discs show *elav* enhancer activity (**Figure 17 L**), the Elav protein staining was negative (**Figure 17 L'**).

These results suggest that early ectopic wing disc activation of *elav* enhancer does not imply transcription of the corresponding gene, at least as judged by its encoded protein (**Fig. 17 K**-**L'**).

8.1.2 *Toll-6* enhancer (D42-Gal4) is transiently activated in wing imaginal discs during first 12h after egg-laying

To test if the phenomenon observed with the *elav* enhancer is general to other enhancers, we selected the line *D42*-Gal4, which corresponds to a *Toll-6* gene enhancer (Sanyal, 2009), as another case also described as nervous system specific. Neurons in the third instar larval brain activated D42 during early development (**Figure R18 C**). Similar to *elav*, D42 is also activated in wing disc cells during early development but not at third instar larvae (**Figure R18 H**), as only GFP-positive cells are detected. In addition, D42-Gal4 domain in the wing disc is also different between left and right discs in the same animal (data not shown).

Next, to determine the temporal activation of the D42 enhancer, we used the repressor, Gal80^{ts}, and analyzed the resulting G-TRACE pattern for D42 enhancer (**Fig R18 A**). As

controls, we maintained the larvae at 17°C (negative control, **Figure R18 D**) or at 29°C (positive control, **Figure R18 H**). The negative control shows no G-TRACE signal and the positive control yields full enhancer expression in the brain. We set five time points (OFF, 12hOFF, 24hOFF, 48hOFF and ON) corresponding to the hours that the system is kept silenced (**Fig. R18 A**). Our results show that, if the system is silenced during 48h (**Fig. R18 E**), 24h (**Fig. R18 F**) or 12h (**Fig. R18 G**) of larval development, the ectopic expression of D42 does not occur (**Figure R18 D**-**H**, quantified in **I**). These data suggest that D42 activation occurs during the first 12 hours of larval development, mainly (**Fig. R18**).

8.1.3 *Toll-6* gene product is not necessary for wing disc development

To resolve if *Toll6* gene expression is necessary for the development of the wing disc, we expressed a *Toll6* specific iRNA under the control of D42-Gal4. Staining with anti-caspase 3 and anti-wingless antibodies, did not detect any apoptosis or *wg* pattern defect and the adult wing morphology was normal (**Figure R19 A**-**H**). These results suggest that, even though the *Toll6* enhancer D42 shows activity in the wing disc during development, *Toll6* gene expression is not switched on during wing development, at least to the point of manifesting a visible phenotype in disc size, shape, wg pattern or adult wing morphology.

To further determine if the ectopic enhancer expression implies a transient expression of another gene under UAS control, we used *Basket (Bsk).* This gene product induces apoptosis by driving a core component of the JNK pathway, (Moreno et al., 2002). Driven under D42-Gal4 we stained with anti-caspase-3 and with anti-Wingless to evaluate wing disc development. The early activation of D42-Gal4/*Toll-6* lead to Bsk-dependent apoptosis, as revealed by caspase-3 staining, to abnormalities in the Wg pattern and resulted in defective adult wings (**Fig R19 E**-**I**).

Together, these findings indicate that two classical neuronal enhancers, elav-Gal4 and D42-Gal4, are transiently activated in wing epithelial cells during early development. The expression activation of the corresponding native genes, *elav* and *Toll-6* do not appear to yield detectable proteins, but can be used to achieve ectopic gene expression (**Fig. R17**, **R18** and **R19**).

Thus, *elav*-Gal4 and D42-Gal4 lines can be used as genetic tools to transiently express any given gene in epithelial cells of the wing disc during early development. The transient activation period of the enhancers varies with each enhancer and depends on chromosomal location of the insertion.

8.2 Adult wing defects in Aβ42 flies are restored by PI3K overexpression

Taking advantage of the transient activation of *elav*-Gal4 and D42-Gal4 enhancers in epithelial cells, we wondered if Aβ42 also elicits defects in tissue growth and development in the wing discs. We tested the Aβ42 deleterious effect with the D42-Gal4 driver and analyzed adult wings morphology.

Adult wings of Aβ42 flies grown at 29°C presented severe abnormalities (**Fig. R20**). PI3K flies showed no defects in adult wing, and only 5% of PI3K/Aβ42 flies showed noticeable defects in their wings (**Fig. R20**)

These findings confirmed that Aβ42 affects non-neuronal tissues, and further, the effects in epithelial cells can be reduced by PI3K overexpression.

8.3 PI3K overexpression reduces Aβ42-induced apoptosis in epithelial cells of the wing disc

Thanks to the transient activation of D42-Gal4 in the wing disc, we confirmed that Aβ42 could degenerate epithelial cells that later developed into malformed adult wings. Thus, we wondered if these effects could trigger caspase-3 activation.

For that, we stainned discs with anti-caspase-3 antibody using the engrailed-Gal4 driver, a domain that occupies the posterior compartment of the wing disc (**Fig. R21 A**-**B'**).

We observed caspase-3 activation upon Aβ42 expression in third instar larvae wing discs (**Fig. R21 A**, **A'**). PI3K/Aβ42 wing disc region showed reduced caspase-3 activation when compared to Aβ42, although some caspase-3 positive signal was still detected (**Fig. R21 B**,

B'). The control region (anterior compartment of the wing disc) showed no caspase-3 activation (**Fig. R21 A**-**B'**).

Knowing that PI3K can induce proliferation, we further looked for phosphorylated histone-3 (pH3) signals (**Fig. R21 C**-**D'**). Histone-3 becomes phosphorylated in the mitotic processes during chromatin condensation and is often used as a reporter of cell proliferation (Hans and Dimitrov, 2001).

Both, Aβ42 (**Fig. R21 C**, **C'**) and PI3K/Aβ42 (**Fig. R21 D**, **D'**) genotypes showed pH3 positive cells. Likewise, control areas (anterior compartment) showed pH3 signals (**Fig. R21 C**-**D'**). Thus, no alterations in normal pH3 signal were found due to the overexpression of either Aβ42 or PI3K and Aβ42 combination.

Taken together, these observations indicate that Aβ42 can induce caspase-3 activation in epithelial cells, and that this activation can be reduced with PI3K overexpression. In addition, neither Aβ42 nor PI3K/Aβ42 induce proliferation as no increment in pH3 positive cells is found when we compare to control areas (**Fig. R21**).

8.4 PI3K overexpression restores Wnt signaling impairment caused by Aβ42 in epithelial cells of the wing disc

Several Wnt family components are dysregulated in AD (reviewed in Inestrosa and Varela-Nallar, 2014), and some of these elements have also been implicated in synaptogenesis (Franciscovich et al, 2008). Being the wing disc of Drosophila a very suitable system for signaling studies, we investigated if Aβ42 and PI3K/Aβ42 could affect Wnt signaling.

In line with previous experiments, we stained third instar larval wing discs with specific anti-Wingless and anti-Armadillo/β-catenin antibodies (**Fig. R22**).

We observed alterations of the Wingless pattern in Aβ42 area (P compartment) (**Fig. R22 A**, **A'**) when compared to the control area (A compartment). Moreover, the armadillo/β-catenin signal is reduced in the Aβ42 area (**Fig. R22 C**,**C'**).

PI3K overexpression, in combination with Aβ42, showed normal Wingless pattern across the wing disc, both in PI3K/Aβ42 and control areas (**Fig. R22 B**,**B'**). Furthermore,

armadillo/β-catenin signal showed homogeneous levels in control and PI3K/Aβ42 areas (**Fig. R22 D**,**D'**).

Together, these data indicate that Aβ42 misregulates Wnt signaling in epithelial cells, and that these alterations are restored with PI3K co-expression (**Fig. R22**).

DISCUSSION

1. **SYNAPTOGENESIS IN Aβ42 NEURODEGENERATION**
2. **NOVEL EFFECT OF PI3K IN Aβ42 AGGREGATION**
3. **Aβ42 EFFECTS IN NON-NEURONAL CELLS. NEW NON-SYNAPTIC ACTIONS OF PI3K OVER Aβ42 CYTOTOXICITY.**

Knowing that in AD synapse loss is one of the first steps in the progression of the neurodegenerative process, and that previous studies have demonstrated the age independent synaptogenic actions of PI3K in *in vitro* and *in vivo* studies (Martin-Pena et al., 2006, Acebes et al., 2011, Cuesto et al., 2011), we studied the potential beneficial effects of PI3K overexpression in an adult-onset model of AD in *Drosophila*.

Taking advantage of the binary Gal4/UAS expression system, in combination with the Gal80^{ts} construct, that allows temporal control of the Gal4 protein synthesis (see Chapter 3), human Aβ42 peptide was expressed in the nervous system of adult flies. The importance of this experimental design rise from the fact that Aβ42 expression is inhibited during the developmental stages of *Drosophila* (embryo, larva and pupa) and is only activated when flies reach adulthood and eclosionate from their puparium. Other study has used a similar strategy with the GeneSwitch system (Sofola et al., 2010), which controls Gal4/UAS system activation by mifepristone (RU486) treatment. However, the majority of AD models, in *Drosophila* and other organisms, follow constitutive expression of the Aβ peptide, APP, PS1, tau, in their mutated or wild type forms (Ashe and Zahs, 2010, Wisniewski and Sigurdsson, 2010, De Felice and Munoz, 2016). Aβ42 formation, although achieved at all moments in life, is only known to exhibit toxic effects when it exponentially increases due to rapid production or insufficient degradation. Aβ42 accumulation has only been detected in elderly individuals, and never at younger ages. For that, the use of Gal80^{ts}/Gal4/UAS system in *Drosophila* can be very useful in modeling AD neurodegenerative progression.

1. Synaptogenesis in Aβ42 Neurodegeneration

In this work, we show *in vivo* evidences of the synaptogenic effect of PI3K activation in a pathological context were synapses are toxically affected by Aβ42. Morphological observation of active zones (Bruchpilot puncta) across genotypes and time-points demonstrated that Aβ42 expression at 15 days elicits ultraestructural misorganization of AZs, and that PI3K/Aβ42 combination reverted this defect. Presynaptic affectation by

Aβ42 has not been as deeply studied as the postsynaptic effects, where Aβ42 directly interacts with NMDA, mGluR5, PrP, p75 and other receptors (Benilova et al., 2012) impairing LTP and inducing LTD enhancement (see Chapter 1 "Introduction"). Thus, direct effects in the presynaptic region, or in postsynaptic densities, that could therefore indirectly affect AZs, could both cause the changes shown in active zone surface. A previous study in our lab has demonstrated that presynaptic PI3K activation promotes the assembly of glutamate receptors (Jordan-Alvarez et al., 2012). These findings mean that, although we are not sure if Aβ42 is affecting the presynaptic or the postsynaptic region in the first place, PI3K activation can elicit changes in both synapse sides. Therefore, a direct interaction of PI3K and Aβ42 is possible.

Our results could be a consequence of an indirect interaction between PI3K and Aβ42, where the synaptogenic actions of PI3K would be fighting against the synaptic loss triggered by Aβ42; nevertheless they could also be caused by a direct interaction, as has been suggested by other groups. PTEN is a lipid phosphatase that inhibits PI3K activation (Maehama and Dixon, 1998), and it has been found to directly mediate Aβ42 synaptic and cognitive impairments (Knafo et al., 2016). PTEN can regulate LTD (Jurado et al., 2010) and when studied in AD models, PTEN can be targeted by Aβ42 to synaptic spines. Furthermore, pharmacological administration of a PTEN membrane-permeable peptide, unable to interact with Aβ42 through PDZ domains, rescues the synaptic deterioration (Knafo et al., 2016). Morevover GSK3-β (PI3K/Akt pathway inhibitor) is known to elicit anti-synaptogenic actions in *Drosophila* and mice (Martin-Pena et al., 2006, Cuesto et al., 2015), and participates in LTP and long-term memory (Hooper et al., 2008). Likewise, Jun kinase/AP-1 and Wnt signaling are also members of the synaptogenic pathway, as they are regulated by GSK3 (Franciscovich et al., 2008). In AD, GSK3 is known to phosphorylate tau and therefore regulate microtubule dynamics (Llorens-Martin et al., 2014) therefore, it has become one of the most tested therapeutic targets in AD.

PIP3, synthetized by PI3K, regulates PSD-95 accumulation and synaptic AMPA receptors in spines, affecting synaptic strength (Arendt et al., 2010). In this line, cyclic adenosine monophosphate (cAMP) response element-binding protein (CREB) has been showed to play important roles in memory formation and consolidation (Levenson et al., 2004, Korzus et al., 2004). This cAMP/PKA/CREB pathway that regulates histone acetylation and

thus gene transcription, has also been studied in Alzheimer's models (Chen et al., 2012) and is being used as a target for potential therapeutic treatments (Teich et al., 2015).

Our data suggest that neither Aβ42 nor PI3K promote mRNA changes in AZ components (*bruchpilot*, *liprin* and *synaptobrevin*), although transcriptional regulation cannot be excluded from the possible mechanisms associated to Aβ42 and PI3K. These transcriptional alterations, or even post-transcriptional regulations could modify synaptic proteins availability, turnover, degradation and/or trafficking, leading to the synaptic changes described in our results.

Our microtubule dynamics data showed that Aβ42 larvae had a reduced number of comet density. This affectation was reverted in PI3K/Aβ42, suggesting that PI3K overexpression can restore Aβ42 induced microtubule alterations.

Defects in microtubule dynamics are known to elicit trafficking dysfunctions. Also, Brp and other components of the AZs and PSDs need to be transported via microtubules, and changes in tubulin cytoskeleton stability can generate problems not only in the formation of new AZs or PSDs structures, but also in synaptic protein turnover. Our data confirm that Aβ42 affects microtubule dynamics, and more specifically demonstrate that Aβ42 reduces the number of growing events, leading to a less dynamic, and thus ineffective, cytoskeleton. This would suggest that Brp transport to the AZ could be affected and might explain the reduced synaptic area in adult NMJs. More importantly, PI3K overexpression led to a total recovery in microtubule dynamics, allowing the normal transportation and/or turnover of synaptic proteins. However, our results do not demonstrate a direct interaction between Aβ42 or PI3K with EB1.

Knowing that PI3K alone promotes an increase in synapse number, which was confirmed in this work, our data suggest that this could also be causing lifespan increase. PI3K is at the crossroads of different signaling pathways that elicit a wide range of cellular processes such as: cell growth, proliferation, differentiation, cell survival and intracellular trafficking (Acebes and Morales, 2012). Thus, the demonstrated synaptogenic actions that counteract Aβ42 neurotoxicity could trigger the activation of PI3K/Akt classical effectors and its cellular consequent cellular responses.

In this study, we further tested the effect of a classical PI3K effector, mTOR. Although mTOR in implicated in memory, previous studies in our lab have demonstrated that mTOR overexpression does not generate new synapses, therefore is not considered to be a part of the synaptogenic pathway.

Synapse quantification, locomotion assay and lifespan performance of flies expressing Aβ42 together with mTOR, showed that this non-synaptogenic tool failed to restore neurodegeneration. This means that PI3K neuroprotective effect in synapses does not follow the canonical signaling path.

On the other hand, to verify if synaptogenesis was the process preventing Aβ42 toxicity, we took advantage of the knockdown of Medea, a genetic tool that had been previously demonstrated to exert novel synaptogenic actions (McCabe et al., 2003). Further studies in our lab have confirmed that Medea participates with its molecular partner, Mad (mother against decapentaplegic) in the same synaptic signaling cascade that PI3K, although they have opposing roles. Medea is considered an antisynaptogenic protein, and thus, we decided to test its downexpression, to increase synapse number and study the effects in our Aβ42 model. Interestingly, Medea downregulation resulted in synapse restoration and total prevention of Aβ42 induced effects in locomotion activity and lifespan. Taking all these data together, synaptogenesis has been proved to prevent Aβ42 neurotoxic effects and to rescue functional defects associated to neurodegeneration.

mTOR and Medea experiments help us understand the mechanism by which PI3K serves as a protective protein from Aβ42 neurotoxicity. Nonetheless, it is important to remember that PI3K can mediate many other intracellular processes. Hence, it is possible that pro-survival signaling could also cause the beneficial actions that PI3K exhibits in lifespan. In the future, further studies will address this issue and decipher whether synaptogenesis and survival cues can be separated.

PI3K/Akt/mTOR signaling is conserved across phyla (Ruggero and Sonenberg, 2005), and so seem to be PI3K synaptogenic actions, since studies in Drosophila, mice and human cells have corroborated this fact (Cuesto et al., 2011, Jordan-Alvarez et al., 2012, Enriquez-Barreto et al., 2014). Moreover, in this work we have evaluated the preventive actions of PI3K in Drosophila and in human neuroblastoma cells, to Aβ42mediated

neurodegeneration. Our findings demonstrated that PI3K activation can be proposed as a target to prevent AD progression, and that PTD4-PI3KAc peptide is a powerful tool in this matter.

Besides, Medea downexpression could also become a potential target for AD therapies, as it restores synapses locomotion and lifespan of Aβ42 affected flies. In addition, Medea downregulation has shown to block BMP signaling (ref) which is in turn altered in AD (ref).

On the other hand, mTOR appears to enhance the neurotoxic effects of Aβ42 in lifespan, and when overexpressed alone, showed similar reduction in synapses than Aβ42 flies. These findings go in the same line of published data from other labs, where mTOR has been found to participate in memory formation and consolidation, and has also been described to be a target of Aβ42. Thus, mTOR inhibition appears as a potential target for further AD studies.

2. Novel effect of PI3K in Aβ42 aggregation

In this work, we show evidences for a new role of PI3K in Aβ42 accumulation. Our *in vivo* and *in vitro* results have demonstrated the ability of PI3K to induce faster aggregation of Aβ42 assemblies, leading to a more insoluble aggregative pattern change. Interestingly, this increase in insoluble Aβ42 species correlates with better lifespan, locomotor and synaptic data, suggesting that PI3K induced change in aggregation might be beneficial by for AD.

Previous studies consider fibrillar insoluble deposits of Aβ42 rather benign species (DaRocha-Souto et al., 2011, Moreth et al., 2013), in contrast to soluble and more toxic Aβ42 oligomers. Although larger and more insoluble accumulations could be very difficult to degrade by the three known Aβ42 degrading enzymes: neprilysin, insulin degrading enzyme or endothelium converting enzyme (Turner et al., 2004) they have been proposed to serve as a sink for oligomers.

Many efforts are being directed to decipher the structural changes of Aβ42 leading to different aggregation patterns that could therefore change its accumulation, toxicity and

in the end, AD progression.

Aβ monomers are mainly α-helical structures and/or unordered structures that can suffer conformational changes, that in turn, promote hemophilic interactions and eventually lead to Aβ oligomer formation. Due to these conformational changes, the resulting polymers become rich in β-sheet structures.

Besides, post-translationally modified Aβ species have been identified (Kummer and Heneka, 2014, Kuo et al., 2001) including truncation (Hartig et al., 2010), racemization (Murakami et al., 2008), isomerization (Shimizu et al., 2000), pyroglutamination (Kuo et al., 1997), metal-induced oxidation (Dong and Bai, 2003) and phosphorylation (Milton, 2001, Kumar et al., 2011).

Phosphorylation in particular can be potentially achieved at 3 different sites in the Aβ42 aminoacid sequence: serines at position 8^{th} and 26^{th}, and tyrosine at position 10^{th}. In addition, Aβ has been previously found to undergo phosphorylation by protein kinase A and cyclin-dependent kinase (cdc) 2 *in vitro* (Milton, 2001). Specially, phosphorylation at serine-8 by protein kinase A was observed in free extracellular Aβ rather than in its precursors (APP or β-CTF) and promoted the formation of toxic aggregates. Also, phosphorylated deposits from APP transgenic mice were found concentrated in the center of the plaque (Kumar et al., 2011). Phosphorylation in this particular residue (ser-8) has been documented to induce Aβ resistance to degradation by insulin degrading enzyme (Kumar et al., 2012).

Another study described cdc 2 phosphorylation at residue serine-26 in an *in vitro* approach (Milton, 2001). In this case, no detailed analysis was performed about the potential changes in aggregation, although cell treatment with olomoucine prevented cytotoxicity and Aβ phosphorylation, suggesting that aggregative forms favored by ser-26 phosphorylation enhance Aβ toxicity. In contrast, our data suggest that PI3K-induced phosphorylation in ser-26 ameliorates Aβ neurodegenerative effects and promotes insoluble Aβ assemblies formation.

Recent *in vitro* analysis of Aβ40 phosphorylated at ser-26 has described that this modification impairs fibrillization while stabilizing monomer and non-toxic soluble

aggregates. Computational studies predicted that a phosphate-group at residue 26 could rigidify the region and interfere with a fibril-specific salt-bridge (Rezaei-Ghaleh et al., 2014).

A specific region in the Aβ sequence comprising residues 25-29 generates a bend-like structure that juxtaposes the hydrophobic faces of the two cross-β units. This bend formation is important for the pathogenic aggregation of Aβ (Murray et al., 2009, Fawzi et al., 2008). Other studies have further emphasized the importance of the 'Glycine 25 - Serine 26' dipeptide in Aβ42 monomer structure organization by finding changes in aggregative properties upon biochemical modifications in these two residues (Roychaudhuri et al., 2014). They have proposed a potential use of drugs that could alter the interactions of this dipeptide with neighboring side-chain atoms or with the core sequence of the peptide.

Moreover, specific mutations in APP, specifically in this region, are known to induce aggregation propensity, such us Arctic (E22G), Italian (E22K), Dutch (E22Q), Osaka (E22Δ) and Iowa (D23N). These variants can cause early onset familial AD (Benilova et al., 2012).

Thus, given the biochemical and biophysical properties of Aβ peptide, more studies should explore new therapies triggering specific residue modifications like phosphorylation or dephosphorylation which, in turn, could change Aβ aggregation patterns to less toxic assemblies. These strategies combined with drugs to enhance Aβ clearance and degradation would potentially be very beneficial for AD patients.

Protein kinases (PKs) in general play important roles in cell cycle control, gene regulation and learning and memory (Giese and Mizuno, 2013, Johnson and Barford, 1993) and they can assert their phosphorylation activities inside of the cell or even outside of the cell, where they can phosphorylate cell-surface proteins or soluble extracellular substrates (Redegeld et al., 1999, Shaltiel et al., 1993, Walter et al., 1994). These Ecto-PKs and Exo-PKs, that catalyze their activities at the external cell surface or in the extracellular media respectively, can use extracellular ATP, which is present in the brain at nanomolar concentrations and can also increase locally upon certain stimuli (Gourine et al., 2007, Melani et al., 2005, el-Moatassim et al., 1992).

Thus, extracellular phosphorylation of Aβ is biochemically possible by protein kinases. Although in depth studies are needed in order to completely understand the structural changes that Aβ phosphorylation could have in amyloid aggregation and AD progression.

3. Aβ42 effects in non-neuronal cells. New non-synaptogenic actions of PI3K in Aβ toxicity

Almost thirty years ago, expression of APP in non-neuronal cells was first reported and short after, secretion of its putative Aβ peptides was also described (Card et al., 1988, Busciglio et al., 1993). Even so, until very recently, it was widely accepted that neurons were the only cells producing the majority of Aβ in an activity-dependent manner (Kamenetz et al., 2003). Nowadays, several studies have demonstrated that also glial cells: astrocytes, oligodendrocytes and microglia play important roles in AD pathology (De Strooper and Karran, 2016). In this work, we did not evaluated the effects PI3K in Aβ induced expression in glial cells, since PI3K activation has already been studied in glial cells in *Drosophila* and it is known to induce proliferation, for which is being used as a model for glioblastoma (Read et al, 2009).

AD patients' causes of death are mostly attributed to bronchopneumonia and cardiovascular disease (Brunnstrom and Englund, 2009, Attems et al., 2005). Deleterious effects in non-neuronal tissues could contribute to explain the cause of the eventual death of the patient.

To evaluate the toxic effect of Aβ42 in non-neuronal tissues, we evaluated the affectation in neurosecretory cells and epithelial cells of the wing disc of the β-amyloid Expression of Aβ42 in leucokinergic cells lead to inflated abdomens, and epithelial expression of Aβ resulted in caspase-3 activation, as well as Wnt signaling misregulation. Although it is thought that Aβ affects cells differentially, it is not well understood what are the factors leading this cell specificity. Our data suggest that even if the mechanistic features of Aβ toxicity could be different, other types of cells out of the nervous system are also susceptible.

We have observed changes in Wnt signaling and apoptosis activation upon Aβ expression, two mechanisms also involved in Aβ degeneration in neurons. Interestingly, PI3K activation restored also Aβ toxicity in both leucokinergic cells and epithelial cells. Taken together, these observations indicate that PI3K is able to counteract Aβ toxic effects not only in neurons, but also in neurosecretory and epitheial cells, although more studies are needed to further analyze the novel non-synaptogenic mechanisms of PI3K activation as a preventive agent against Aβ toxicity.

4. Perspectives

Taking together the data presented in this thesis, new questions arise in order to seek more detailed understanding of the PI3K actions in β-amyloid neurodegeneration, since activation of Phosphoinositide-3 kinase has shown to induce synaptogenic protection and aggregative effects, but we ask if both outcomes are related, being one the consequence of the other, or if PI3K synaptogenic and aggregation effects are independent. Knowing that other synaptogenic strategies, like Medea down-expression, also elicit Aβ42 protective effects, we wonder if in this scenario Aβ42 aggregative properties are also affected, and then, what could be triggering the aggregation change?

Interestingly, although PI3K can revert the loss of synapses to normal control values, its actions are not sufficient to produce total recovery in locomotion and lifespan. Another open question arises asking what other negative effects of Aβ42, if any, are not being restored by PI3K? In the case of Medea knockdown experiments, synapses were also reverted to control levels, and locomotion and survival Aβ effects are totally prevented. Thus, is Medea downregulation triggering better functional effects in synapses that those triggered by PI3K? or is Medea downregulation mediating other synaptic-independent effects that contribute to Aβ42 protection?

Newly described deleterious effects of Aβ42 in neurosecretory cells and epithelial cells, two non-synaptic environments, bring numerous questions: Does Aβ42 affect epithelial and neurosecretory cells in AD patients? Are those effects triggering the same intracellular effectors? Is Aβ42 affecting other cell-to-cell communication structures in these non-synaptogenic contexts? Our data also suggest that *Drosophila* leucokinergic cells and epithelial cells can be used to further study Aβ42 effects, as especially wing disc cells have

been long studied and characterized, and a wide variety of genetic tools can be used to address new questions Aβ42 pathology in this tissue.

Finally, PI3K actions in a synaptotoxic scenario could also be studied in other neurodegenerative models like Parkinson disease, amyotrophic lateral sclerosis, Huntington disease or frontotemporal dementia. Moreover, since many of these diseases develop extracellular and/or intracellular protein aggregates, PI3K actions could also be studied in these models to evaluate if it could mediate changes in aggregation propensity in proteins other that Aβ peptide.

CONCLUSIONS

1. PI3K overexpression prevents Aβ42-induced synaptic loss in an age-independent manner.
2. Synaptic protection by PI3K overexpression restores microtubule dynamics; however, it does not affect transcriptional regulation of the synaptic proteins bruchpilot, liprin or synaptobrevin.
3. PI3K synaptogenic actions delay the Aβ42-induced locomotion degeneration and lifespan.
4. PI3K activation can also elicit survival recovery in human neurons treated with Aβ42 oligomers.
5. Medea down-expression, but not canonical PI3K effectors like mTOR, prevents Aβ42 mediated synaptic degeneration and recovers the β-amyloid deleterious effects.
6. PI3K overexpression causes changes in Aβ aggregation to a more insoluble non-toxic pattern.
7. PI3K effect in Aβ42 aggregation is reproduced in *in vitro* studies with human neurons, where PI3K can promote Aβ42 aggregation outside of the cell.
8. PI3K overexpression induces the phosphorylation of Aβ42 in residue Serine 26 which is critical for Aβ42 aggregation.
9. Aβ42 is also toxic in non-neuronal environments, where PI3K overexpression also prevents Aβ toxicity.
10. Classical neural enhancers show transient ectopic activity in non-neuronal tissues.

CONCLUSIONS (in Spanish)

1. La sobre-expresión de PI3K previene la pérdida sináptica inducida por Aβ42 de manera independiente a la edad.

2. La protección sináptica producida por la sobre-expresión de PI3K restaura la dinámica de los microtúbulos; sin embargo, no afecta a la regulación transcripcional de las proteínas sinápticas Bruchpilot, Liprina o Sinaptobrevina.

3. La acción sinaptogénica de PI3K retrasa los defectos degenerativos de Aβ42 en la actividad locomotora y en la esperanza de vida.

4. La activación de PI3K produce la recuperación de la supervivencia en neuronas humanas tratadas con oligómeros de Aβ42.

5. La bajada de expresión de Medea, pero no la sobre-expresión de los efectores canónicos de PI3K, como mTOR, previene la degeneración sináptica mediada por Aβ42 y recupera los efectos deletéreos de β-amiloide.

6. La sobre-expresión de PI3K provoca cambios en la agregación de Aβ hacia un patrón más insoluble y por tanto, considerado menos tóxico.

7. Los efectos de PI3K en la agregación de Aβ42 también se reproducen en estudios *in vitro* con neuronas humanas, donde PI3K puede promover la agregación de Aβ fuera de la célula.

8. La sobre-expresión de PI3K induce la fosforilación de Aβ42 en el residuo Serina-26, que es crítico para la agregación del péptido amiloide.

9. Aβ42 causa efectos deletéreos en ambientes no-neuronales, donde la sobre-expresión de PI3K también es capaz de prevenir su toxicidad.

10. *Enhancers* neuronales clásicos muestran una actividad ectópica transitoria en tejidos no-neuronales, como el epitelio del disco de ala de *Drosophila*.

BIBLIOGRAPHY

ACEBES, A., DEVAUD, J. M., ARNES, M. & FERRUS, A. 2012. Central Adaptation to Odorants Depends on PI3K Levels in Local Interneurons of the Antennal Lobe. *The Journal of Neuroscience,* 32**,** 417– 422.

ACEBES, A., MARTIN-PENA, A., CHEVALIER, V. & FERRÚS, A. 2011. Synapse Loss in Olfactory Local Interneurons Modifies Perception. *The Journal of Neuroscience,* 31**,** 2734 –2745.

ACEBES, A. & MORALES, M. 2012. At a PI3K crossroads: lessons from flies and rodents. *Rev Neurosci,* 23**,** 29-37.

ARENDT, K. L., ROYO, M., FERNANDEZ-MONREAL, M., KNAFO, S., PETROK, C. N., MARTENS, J. R. & ESTEBAN, J. A. 2010. PIP3 controls synaptic function by maintaining AMPA receptor clustering at the postsynaptic membrane. *Nat Neurosci,* 13**,** 36-44.

ASHE, K. H. & ZAHS, K. R. 2010. Probing the biology of Alzheimer's disease in mice. *Neuron,* 66**,** 631-45.

ATTEMS, J., KONIG, C., HUBER, M., LINTNER, F. & JELLINGER, K. A. 2005. Cause of death in demented and non-demented elderly inpatients; an autopsy study of 308 cases. *J Alzheimers Dis,* 8**,** 57-62.

BEKINSCHTEIN, P., KATCHE, C., SLIPCZUK, L. N., IGAZ, L. M., CAMMAROTA, M., IZQUIERDO, I. & MEDINA, J. H. 2007. mTOR signaling in the hippocampus is necessary for memory formation. *Neurobiol Learn Mem,* 87**,** 303-7.

BENILOVA, I., KARRAN, E. & DE STROOPER, B. 2012. The toxic Abeta oligomer and Alzheimer's disease: an emperor in need of clothes. *Nat Neurosci,* 15**,** 349-57.

BERKE, B., WITTNAM, J., MCNEILL, E., VAN VACTOR, D. L. & KESHISHIAN, H. 2013. Retrograde BMP signaling at the synapse: a permissive signal for synapse maturation and activity-dependent plasticity. *J Neurosci,* 33**,** 17937-50.

BERTRAM, L., LANGE, C., MULLIN, K., PARKINSON, M., HSIAO, M., HOGAN, M. F., SCHJEIDE, B. M., HOOLI, B., DIVITO, J., IONITA, I., JIANG, H., LAIRD, N., MOSCARILLO, T., OHLSEN, K. L., ELLIOTT, K., WANG, X., HU-LINCE, D., RYDER, M., MURPHY, A., WAGNER, S. L., BLACKER, D., BECKER, K. D. & TANZI, R. E. 2008. Genome-wide association analysis reveals putative Alzheimer's disease susceptibility loci in addition to APOE. *Am J Hum Genet,* 83**,** 623-32.

BOUTROS, M., PARICIO, N., STRUTT, D. I. & MLODZIK, M. 1998. Dishevelled activates JNK and discriminates between JNK pathways in planar polarity and wingless signaling. *Cell,* 94**,** 109-18.

BRAND, A. H. & PERRIMON, N. 1993. Targeted gene expression as a means of altering cell fates and generating dominant phenotypes. *Development,* 118**,** 401-15.

BRUNNSTROM, H. R. & ENGLUND, E. M. 2009. Cause of death in patients with dementia disorders. *Eur J Neurol,* 16**,** 488-92.

BUSCIGLIO, J., GABUZDA, D. H., MATSUDAIRA, P. & YANKNER, B. A. 1993. Generation of beta-amyloid in the secretory pathway in neuronal and nonneuronal cells. *Proc Natl Acad Sci U S A,* 90**,** 2092-6.

CARD, J. P., MEADE, R. P. & DAVIS, L. G. 1988. Immunocytochemical localization of the precursor protein for beta-amyloid in the rat central nervous system. *Neuron,* 1**,** 835-46.

CARICASOLE, A., COPANI, A., CARACI, F., ARONICA, E., ROZEMULLER, A. J., CARUSO, A., STORTO, M., GAVIRAGHI, G., TERSTAPPEN, G. C. & NICOLETTI, F. 2004. Induction of Dickkopf-1, a negative modulator of the Wnt pathway, is associated with neuronal degeneration in Alzheimer's brain. *J Neurosci,* 24**,** 6021-7.

CASAS-TINTO, S., ZHANG, Y., SANCHEZ-GARCIA, J., GOMEZ-VELAZQUEZ, M., RINCON-LIMAS, D. E. & FERNANDEZ-FUNEZ, P. 2011. The ER stress factor XBP1s prevents amyloid-beta neurotoxicity. *Hum Mol Genet,* 20**,** 2144-60.

CAUGHEY, B. & LANSBURY, P. T. 2003. Protofibrils, pores, fibrils, and neurodegeneration: separating the responsible protein aggregates from the innocent bystanders. *Annu Rev Neurosci,* 26**,** 267-98.

CHEN, S. H., WU, H. M., OSSOLA, B., SCHENDZIELORZ, N., WILSON, B. C., CHU, C. H., CHEN, S. L., WANG, Q., ZHANG, D., QIAN, L., LI, X., HONG, J. S. & LU, R. B. 2012. Suberoylanilide hydroxamic acid, a histone deacetylase inhibitor, protects dopaminergic neurons from neurotoxin-induced damage. *Br J Pharmacol,* 165**,** 494-505.

CHIANG, H. C., WANG, L., XIE, Z., YAU, A. & ZHONG, Y. 2010. PI3 kinase signaling is involved in Abeta-induced memory loss in Drosophila. *Proc Natl Acad Sci U S A,* 107**,** 7060-5.

CISSE, M., HALABISKY, B., HARRIS, J., DEVIDZE, N., DUBAL, D. B., SUN, B., ORR, A., LOTZ, G., KIM, D. H., HAMTO, P., HO, K., YU, G. Q. & MUCKE, L. 2011. Reversing EphB2 depletion rescues cognitive functions in Alzheimer model. *Nature,* 469**,** 47-52.

CLEARY, J. P., WALSH, D. M., HOFMEISTER, J. J., SHANKAR, G. M., KUSKOWSKI, M. A., SELKOE, D. J. & ASHE, K. H. 2005. Natural oligomers of the amyloid-beta protein specifically disrupt cognitive function. *Nat Neurosci,* 8**,** 79-84.

CORDER, E. H., SAUNDERS, A. M., STRITTMATTER, W. J., SCHMECHEL, D. E., GASKELL, P. C., SMALL, G. W., ROSES, A. D., HAINES, J. L. & PERICAK-VANCE, M. A. 1993. Gene dose of apolipoprotein E type 4 allele and the risk of Alzheimer's disease in late onset families. *Science,* 261**,** 921-3.

CRAFT, S., BAKER, L. D., MONTINE, T. J., MINOSHIMA, S., WATSON, G. S., CLAXTON, A., ARBUCKLE, M., CALLAGHAN, M., TSAI, E., PLYMATE, S. R., GREEN, P. S., LEVERENZ, J., CROSS, D. & GERTON, B. 2012. Intranasal insulin therapy for Alzheimer disease and amnestic mild cognitive impairment: a pilot clinical trial. *Arch Neurol,* 69**,** 29-38.

CROWTHER, D. C., KINGHORN, K. J., MIRANDA, E., PAGE, R., CURRY, J. A., DUTHIE, F. A., GUBB, D. C. & LOMAS, D. A. 2005. Intraneuronal Abeta, non-amyloid aggregates and neurodegeneration in a Drosophila model of Alzheimer's disease. *Neuroscience,* 132**,** 123-35.

CROWTHER, D. C., KINGHORN, K. J., PAGE, R. & LOMAS, D. A. 2004. Therapeutic targets from a Drosophila model of Alzheimer's disease. *Curr Opin Pharmacol,* 4**,** 513-6.

CUESTO, G., ENRIQUEZ-BARRETO, L., CARAMES, C., CANTARERO, M., GASULL, X., SANDI, C., FERRUS, A., ACEBES, A. & MORALES, M. 2011. Phosphoinositide-3-kinase activation controls synaptogenesis and spinogenesis in hippocampal neurons. *J Neurosci,* 31**,** 2721-33.

CUESTO, G., JORDAN-ALVAREZ, S., ENRIQUEZ-BARRETO, L., FERRUS, A., MORALES, M. & ACEBES, A. 2015. GSK3beta inhibition promotes synaptogenesis in Drosophila and mammalian neurons. *PLoS One,* 10**,** e0118475.

DAROCHA-SOUTO, B., SCOTTON, T. C., COMA, M., SERRANO-POZO, A., HASHIMOTO, T., SERENO, L., RODRIGUEZ, M., SANCHEZ, B., HYMAN, B. T. & GOMEZ-ISLA, T. 2011. Brain oligomeric beta-amyloid but not total amyloid plaque burden correlates with neuronal loss and astrocyte inflammatory response in amyloid precursor protein/tau transgenic mice. *J Neuropathol Exp Neurol,* 70**,** 360-76.

DE FELICE, F. G. & MUNOZ, D. P. 2016. Opportunities and challenges in developing relevant animal models for Alzheimer's disease. *Ageing Research Reviews,* 26**,** 112-114.

DE FELICE, F. G., VIEIRA, M. N. N., BOMFIM, T. R., DECKER, H., VELASCO, P. T., LAMBERT, M. P., VIOLA, K. L., ZHAO, W. Q., FERREIRA, S. T. & KLEIN, W. L. 2008. *Proc Natl Acad Sci U S A,* 106**,** 1971-1976.

DE STROOPER, B. & KARRAN, E. 2016. The Cellular Phase of Alzheimer's Disease. *Cell,* 164**,** 603-15.

DE STROOPER, B., VASSAR, R. & GOLDE, T. 2010. The secretases: enzymes with therapeutic potential in Alzheimer disease. *Nat Rev Neurol,* 6**,** 99-107.

DECKER, H., LO, K. Y., UNGER, S. M., FERREIRA, S. T. & SILVERMAN, M. A. 2010. Amyloid-beta peptide oligomers disrupt axonal transport through an NMDA receptor-dependent mechanism that is mediated by glycogen synthase kinase 3beta in primary cultured hippocampal neurons. *J Neurosci,* 30**,** 9166-71.

DINELEY, K. T., WESTERMAN, M., BUI, D., BELL, K., ASHE, K. H. & SWEATT, J. D. 2001. Beta-amyloid activates the mitogen-activated protein kinase cascade via hippocampal alpha7 nicotinic acetylcholine receptors: In vitro and in vivo mechanisms related to Alzheimer's disease. *J Neurosci,* 21**,** 4125-33.

DONG, H. T. & BAI, Y. 2003. [Clinical research of the influence of cognizing potential on AD patients by electroacupuncture treatment]. *Zhongguo Ying Yong Sheng Li Xue Za Zhi,* 19**,** 94-6.

EL-MOATASSIM, C., DORNAND, J. & MANI, J. C. 1992. Extracellular ATP and cell signalling. *Biochim Biophys Acta,* 1134**,** 31-45.

ENGELBORGHS, S. 2013. Clinical indications for analysis of Alzheimer's disease CSF biomarkers. *Rev Neurol (Paris),* 169**,** 709-14.

ENGELMAN, J. A., LUO, J. & CANTLEY, L. C. 2006. The evolution of phosphatidylinositol 3-kinases as regulators of growth and metabolism. *Nat Rev Genet,* 7**,** 606-19.

ENRIQUEZ-BARRETO, L., CUESTO, G., DOMINGUEZ-ITURZA, N., GAVILAN, E., RUANO, D., SANDI, C., FERNANDEZ-RUIZ, A., MARTIN-VAZQUEZ, G., HERRERAS, O. & MORALES, M. 2014. Learning improvement after PI3K activation correlates with de novo formation of functional small spines. *Front Mol Neurosci,* 6**,** 54.

ESPARZA, T. J., ZHAO, H., CIRRITO, J. R., CAIRNS, N. J., BATEMAN, R. J., HOLTZMAN, D. M. & BRODY, D. L. 2013. Amyloid-beta oligomerization in Alzheimer dementia versus high-pathology controls. *Ann Neurol,* 73**,** 104-19.

FAWZI, N. L., PHILLIPS, A. H., RUSCIO, J. Z., DOUCLEFF, M., WEMMER, D. E. & HEAD-GORDON, T. 2008. Structure and dynamics of the Abeta(21-30) peptide from the interplay of NMR experiments and molecular simulations. *J Am Chem Soc,* 130**,** 6145-58.

FOUQUET, W., OWALD, D., WICHMANN, C., MERTEL, S., DEPNER, H., DYBA, M., HALLERMANN, S., KITTEL, R. J., EIMER, S. & SIGRIST, S. J. 2009. Maturation of active zone assembly by Drosophila Bruchpilot. *J Cell Biol,* 186**,** 129-45.

FRANCISCOVICH, A. L., MORTIMER, A. D., FREEMAN, A. A., GU, J. & SANYAL, S. 2008. Overexpression screen in Drosophila identifies neuronal roles of GSK-3 beta/shaggy as a regulator of AP-1-dependent developmental plasticity. *Genetics,* 180**,** 2057-71.

GENIN, E., HANNEQUIN, D., WALLON, D., SLEEGERS, K., HILTUNEN, M., COMBARROS, O., BULLIDO, M. J., ENGELBORGHS, S., DE DEYN, P., BERR, C., PASQUIER, F., DUBOIS, B., TOGNONI, G., FIEVET, N., BROUWERS, N., BETTENS, K., AROSIO, B., COTO, E., DEL ZOMPO, M., MATEO, I., EPELBAUM, J., FRANK-GARCIA, A., HELISALMI, S., PORCELLINI, E., PILOTTO, A., FORTI, P., FERRI, R., SCARPINI, E., SICILIANO, G., SOLFRIZZI, V., SORBI, S., SPALLETTA, G., VALDIVIESO, F., VEPSALAINEN, S., ALVAREZ, V., BOSCO, P., MANCUSO, M., PANZA, F., NACMIAS, B., BOSSU, P., HANON, O., PICCARDI, P., ANNONI, G., SERIPA, D., GALIMBERTI, D., LICASTRO, F., SOININEN, H., DARTIGUES, J. F., KAMBOH, M. I., VAN BROECKHOVEN, C., LAMBERT, J. C., AMOUYEL, P. & CAMPION, D. 2011. APOE and Alzheimer disease: a major gene with semi-dominant inheritance. *Mol Psychiatry,* 16**,** 903-7.

GIESE, K. P. & MIZUNO, K. 2013. The roles of protein kinases in learning and memory. *Learn Mem,* 20**,** 540-52.

GIUFFRIDA, A. & MCMAHON, L. R. 2010. In vivo pharmacology of endocannabinoids and their metabolic inhibitors: therapeutic implications in Parkinson's disease and abuse liability. *Prostaglandins Other Lipid Mediat,* 91**,** 90-103.

GOEDERT, M. 2015. Alzheimer's and Parkinson's diseases: The prion concept in relation to assembled Ab, tau, and a-synuclein. *Science,* 349**,** 601-610.

GOLDGABER, D., LERMAN, M. I., MCBRIDE, O. W., SAFFIOTTI, U. & GAJDUSEK, D. C. 1987. Characterization and chromosomal localization of a cDNA encoding brain amyloid of Alzheimer's disease. *Science,* 235**,** 877-80.

GOURAS, G. K., TAMPELLINI, D., TAKAHASHI, R. H. & CAPETILLO-ZARATE, E. 2010. Intraneuronal beta-amyloid accumulation and synapse pathology in Alzheimer's disease. *Acta Neuropathol,* 119**,** 523-41.

GOURE, W. F., KRAFFT, G. A., JERECIC, J. & HEFTI, F. 2014. Targeting the proper amyloid-beta neuronal toxins: a path forward for Alzheimer's disease immunotherapeutics. *Alzheimers Res Ther,* 6**,** 42.

GOURINE, A. V., DALE, N., LLAUDET, E., POPUTNIKOV, D. M., SPYER, K. M. & GOURINE, V. N. 2007. Release of ATP in the central nervous system during systemic inflammation: real-time measurement in the hypothalamus of conscious rabbits. *J Physiol,* 585**,** 305-16.

GREEVE, I., KRETZSCHMAR, D., TSCHAPE, J. A., BEYN, A., BRELLINGER, C., SCHWEIZER, M., NITSCH, R. M. & REIFEGERSTE, R. 2004. Age-dependent neurodegeneration and Alzheimer-amyloid plaque formation in transgenic Drosophila. *J Neurosci,* 24**,** 3899-906.

GRUNDKE-IQBAL, I., IQBAL, K., TUNG, Y. C., QUINLAN, M., WISNIEWSKI, H. M. & BINDER, L. I. 1986. Abnormal phosphorylation of the microtubule-associated protein T (tau)inAlzheimer cytoskeletal pathology. *Proc Natl Acad Sci U S A,* 83**,** 4913-4917.

HAASS, C., KAETHER, C., THINAKARAN, G. & SISODIA, S. 2012. Trafficking and proteolytic processing of APP. *Cold Spring Harb Perspect Med,* 2**,** a006270.

HAN, J., KNOPS, J. F., LONGSHORE, J. W. & KING, P. H. 1996. Localization of human elav-like neuronal protein 1 (Hel-N1) on chromosome 9p21 by chromosome microdissection polymerase chain reaction and fluorescence in situ hybridization. *Genomics,* 36**,** 189-191.

HARDY, J. A. & HIGGINS, G. A. 1992. Alzheimer's disease: the amyloid cascade hypothesis. *Science,* 256**,** 184-5.

HARTIG, W., GOLDHAMMER, S., BAUER, U., WEGNER, F., WIRTHS, O., BAYER, T. A. & GROSCHE, J. 2010. Concomitant detection of beta-amyloid peptides with N-terminal truncation and different C-terminal endings in cortical plaques from cases with Alzheimer's disease, senile monkeys and triple transgenic mice. *J Chem Neuroanat,* 40**,** 82-92.

HEBBAR, S., HALL, R. E., DEMSKI, S. A., SUBRAMANIAN, A. & FERNANDES, J. J. 2006. The adult abdominal neuromuscular junction of Drosophila: a model for synaptic plasticity. *J Neurobiol,* 66**,** 1140-55.

HENNIG, K. M. & NEUFELD, T. P. 2002. Inhibition of cellular growth and proliferation by dTOR overexpression in Drosophila. *Genesis,* 34**,** 107-10.

HIRTH, F. 2010. Drosophila melanogaster in the study of human neurodegeneration. *CNS Neurol Disord Drug Targets,* 9**,** 504-23.

HOLLINGWORTH, P., HAROLD, D., SIMS, R., GERRISH, A., LAMBERT, J. C., CARRASQUILLO, M. M., ABRAHAM, R., HAMSHERE, M. L., PAHWA, J. S., MOSKVINA, V., DOWZELL, K., JONES, N., STRETTON, A., THOMAS, C., RICHARDS, A., IVANOV, D., WIDDOWSON, C., CHAPMAN, J., LOVESTONE, S., POWELL, J., PROITSI, P., LUPTON, M. K., BRAYNE, C., RUBINSZTEIN, D. C., GILL, M., LAWLOR, B., LYNCH, A., BROWN, K. S., PASSMORE, P. A., CRAIG, D., MCGUINNESS, B., TODD, S., HOLMES, C., MANN, D., SMITH, A. D., BEAUMONT, H., WARDEN, D., WILCOCK, G., LOVE, S., KEHOE, P. G., HOOPER, N. M., VARDY, E. R., HARDY, J., MEAD, S., FOX, N. C., ROSSOR, M., COLLINGE, J., MAIER, W., JESSEN, F., RUTHER, E., SCHURMANN, B., HEUN, R., KOLSCH, H., VAN DEN BUSSCHE, H., HEUSER, I., KORNHUBER, J., WILTFANG, J., DICHGANS, M., FROLICH, L., HAMPEL, H., GALLACHER, J., HULL, M., RUJESCU, D., GIEGLING, I., GOATE, A. M., KAUWE, J. S., CRUCHAGA, C., NOWOTNY, P., MORRIS, J. C., MAYO, K., SLEEGERS, K., BETTENS, K., ENGELBORGHS, S., DE DEYN, P. P., VAN BROECKHOVEN, C., LIVINGSTON, G., BASS, N. J., GURLING, H., MCQUILLIN, A., GWILLIAM, R., DELOUKAS, P., AL-CHALABI, A., SHAW, C. E., TSOLAKI, M., SINGLETON, A. B., GUERREIRO, R., MUHLEISEN, T. W., NOTHEN, M. M., MOEBUS, S., JOCKEL, K. H., KLOPP, N., WICHMANN, H. E., PANKRATZ, V. S., SANDO, S. B., AASLY, J. O., BARCIKOWSKA, M., WSZOLEK, Z. K., DICKSON, D. W., GRAFF-RADFORD, N. R., PETERSEN, R. C., et al. 2011. Common variants at ABCA7, MS4A6A/MS4A4E, EPHA1, CD33 and CD2AP are associated with Alzheimer's disease. *Nat Genet,* 43**,** 429-35.

HONG, J. G., KIM, D. H., LEE, C. H., PARK, S. J., KIM, J. M., CAI, M., JANG, D. S. & RYU, J. H. 2012. GSK-3beta activity in the hippocampus is required for memory retrieval. *Neurobiol Learn Mem,* 98**,** 122-9.

HOOPER, C., KILLICK, R. & LOVESTONE, S. 2008. The GSK3 hypothesis of Alzheimer's disease. *J Neurochem,* 104**,** 1433-9.

HSIEH, H., BOEHM, J., SATO, C., IWATSUBO, T., TOMITA, T., SISODIA, S. & MALINOW, R. 2006. AMPAR removal underlies Abeta-induced synaptic depression and dendritic spine loss. *Neuron,* 52**,** 831-43.

HUANG, J. K., MA, P. L., JI, S. Y., ZHAO, X. L., TAN, J. X., SUN, X. J. & HUANG, F. D. 2013. Age-dependent alterations in the presynaptic active zone in a Drosophila model of Alzheimer's disease. *Neurobiol Dis,* 51**,** 161-7.

HUDSON, J. B., PODOS, S. D., KEITH, K., SIMPSON, S. L. & FERGUSON, E. L. 1998. The Drosophila Medea gene is required downstream of dpp and encodes a functional homolog of human Smad4. *Development,* 125**,** 1407-20.

IIJIMA, K., CHIANG, H. C., HEARN, S. A., HAKKER, I., GATT, A., SHENTON, C., GRANGER, L., LEUNG, A., IIJIMA-ANDO, K. & ZHONG, Y. 2008. Abeta42 mutants with different aggregation profiles induce distinct pathologies in Drosophila. *PLoS One,* 3**,** e1703.

IIJIMA, K., LIU, H. P., CHIANG, A. S., HEARN, S. A., KONSOLAKI, M. & ZHONG, Y. 2004. Dissecting the pathological effects of human Abeta40 and Abeta42 in Drosophila: a potential model for Alzheimer's disease. *Proc Natl Acad Sci U S A,* 101**,** 6623-8.

INESTROSA, N. C. & VARELA-NALLAR, L. 2014. Wnt signaling in the nervous system and in Alzheimer's disease. *Journal of Molecular Cell Biology,* 6**,** 64-74.

JOHNSON, L. N. & BARFORD, D. 1993. The effects of phosphorylation on the structure and function of proteins. *Annu Rev Biophys Biomol Struct,* 22**,** 199-232.

JORDAN-ALVAREZ, S., FOUQUET, W., SIGRIST, S. J. & ACEBES, A. 2012. Presynaptic PI3K activity triggers the formation of glutamate receptors at neuromuscular terminals of Drosophila. *J Cell Sci,* 125**,** 3621-9.

JURADO, S., BENOIST, M., LARIO, A., KNAFO, S., PETROK, C. N. & ESTEBAN, J. A. 2010. PTEN is recruited to the postsynaptic terminal for NMDA receptor-dependent long-term depression. *EMBO J,* 29**,** 2827-40.

KAMENETZ, F., TOMITA, T., HSIEH, H., SEABROOK, G., BORCHELT, D., IWATSUBO, T., SISODIA, S. & MALINOW, R. 2003. APP processing and synaptic function. *Neuron,* 37**,** 925-37.

KANG, M. J., HANSEN, T. J., MICKIEWICZ, M., KACZYNSKI, T. J., FYE, S. & GUNAWARDENA, S. 2014. Disruption of axonal transport perturbs bone morphogenetic protein (BMP)--signaling and contributes to synaptic abnormalities in two neurodegenerative diseases. *PLoS One,* 9**,** e104617.

KAYED, R. & GLABE, C. G. 2006. Conformation-dependent anti-amyloid oligomer antibodies. *Methods Enzymol,* 413**,** 326-44.

KESHISHIAN, H., BROADIE, K., CHIBA, A. & BATE, M. 1996. The drosophila neuromuscular junction: a model system for studying synaptic development and function. *Annu Rev Neurosci,* 19**,** 545-75.

KIDOKORO, Y. 2003. Roles of SNARE proteins and synaptotagmin I in synaptic transmission: studies at the Drosophila neuromuscular synapse. *Neurosignals,* 12**,** 13-30.

KNAFO, S. & ESTEBAN, J. A. 2012. Common pathways for growth and for plasticity. *Curr Opin Neurobiol,* 22**,** 405-11.

KNAFO, S., SANCHEZ-PUELLES, C., PALOMER, E., DELGADO, I., DRAFFIN, J. E., MINGO, J., WAHLE, T., KALEKA, K., MOU, L., PEREDA-PEREZ, I., KLOSI, E., FABER, E. B., CHAPMAN, H. M., LOZANO-MONTES, L., ORTEGA-MOLINA, A., ORDONEZ-GUTIERREZ, L., WANDOSELL, F., VINA, J., DOTTI, C. G., HALL, R. A., PULIDO, R., GERGES, N. Z., CHAN, A. M., SPALLER, M. R., SERRANO, M., VENERO, C. & ESTEBAN, J. A. 2016. PTEN recruitment controls synaptic and cognitive function in Alzheimer's models. *Nat Neurosci,* 19**,** 443-53.

KORZUS, E., ROSENFELD, M. G. & MAYFORD, M. 2004. CBP histone acetyltransferase activity is a critical component of memory consolidation. *Neuron,* 42**,** 961-72.

KUMAR, S., REZAEI-GHALEH, N., TERWEL, D., THAL, D. R., RICHARD, M., HOCH, M., MC DONALD, J. M., WULLNER, U., GLEBOV, K., HENEKA, M. T., WALSH, D. M., ZWECKSTETTER, M. & WALTER, J. 2011. Extracellular phosphorylation of the amyloid beta-peptide promotes formation of toxic aggregates during the pathogenesis of Alzheimer's disease. *EMBO J,* 30**,** 2255-65.

KUMAR, S., SINGH, S., HINZE, D., JOSTEN, M., SAHL, H. G., SIEPMANN, M. & WALTER, J. 2012. Phosphorylation of amyloid-beta peptide at serine 8 attenuates its clearance via insulin-degrading and angiotensin-converting enzymes. *J Biol Chem,* 287**,** 8641-51.

KUMMER, M. P. & HENEKA, M. T. 2014. Truncated and modified amyloid-beta species. *Alzheimers Res Ther,* 6**,** 28.

KUO, Y. M., BEACH, T. G., SUE, L. I., SCOTT, S., LAYNE, K. J., KOKJOHN, T. A., KALBACK, W. M., LUEHRS, D. C., VISHNIVETSKAYA, T. A., ABRAMOWSKI, D., STURCHLER-PIERRAT, C., STAUFENBIEL, M., WELLER, R. O. & ROHER, A. E. 2001. The evolution of A beta peptide burden in the APP23 transgenic mice: implications for A beta deposition in Alzheimer disease. *Mol Med,* 7**,** 609-18.

KUO, Y. M., EMMERLING, M. R., WOODS, A. S., COTTER, R. J. & ROHER, A. E. 1997. Isolation, chemical characterization, and quantitation of A beta 3-pyroglutamyl peptide from neuritic plaques and vascular amyloid deposits. *Biochem Biophys Res Commun,* 237**,** 188-91.

KWON, C. H., LUIKART, B. W., POWELL, C. M., ZHOU, J., MATHENY, S. A., ZHANG, W., LI, Y., BAKER, S. J. & PARADA, L. F. 2006. Pten regulates neuronal arborization and social interaction in mice. *Neuron,* 50**,** 377-88.

LAFERLA, F. M., GREEN, K. N. & ODDO, S. 2007. Intracellular amyloid-beta in Alzheimer's disease. *Nat Rev Neurosci,* 8**,** 499-509.

LAMBERT, J. C., GRENIER-BOLEY, B., HAROLD, D., ZELENIKA, D., CHOURAKI, V., KAMATANI, Y., SLEEGERS, K., IKRAM, M. A., HILTUNEN, M., REITZ, C., MATEO, I., FEULNER, T., BULLIDO, M., GALIMBERTI, D., CONCARI, L., ALVAREZ, V., SIMS, R., GERRISH, A., CHAPMAN, J., DENIZ-NARANJO, C., SOLFRIZZI, V., SORBI, S., AROSIO, B., SPALLETTA, G., SICILIANO, G., EPELBAUM, J., HANNEQUIN, D., DARTIGUES, J. F., TZOURIO, C., BERR, C., SCHRIJVERS, E. M., ROGERS, R., TOSTO, G., PASQUIER, F., BETTENS, K., VAN CAUWENBERGHE, C., FRATIGLIONI, L., GRAFF, C., DELEPINE, M., FERRI, R., REYNOLDS, C. A., LANNFELT, L., INGELSSON, M., PRINCE, J. A., CHILLOTTI, C., PILOTTO, A., SERIPA, D., BOLAND, A., MANCUSO, M., BOSSU, P., ANNONI, G., NACMIAS, B., BOSCO, P., PANZA, F., SANCHEZ-GARCIA, F., DEL ZOMPO, M., COTO, E., OWEN, M., O'DONOVAN, M., VALDIVIESO, F., CAFFARRA, P., SCARPINI, E., COMBARROS, O., BUEE, L., CAMPION, D., SOININEN, H., BRETELER, M., RIEMENSCHNEIDER, M., VAN BROECKHOVEN, C., ALPEROVITCH, A., LATHROP, M., TREGOUET, D. A., WILLIAMS, J. & AMOUYEL, P. 2013. Genome-wide haplotype association study identifies the FRMD4A gene as a risk locus for Alzheimer's disease. *Mol Psychiatry,* 18**,** 461-70.

LAMBERT, J. C., HEATH, S., EVEN, G., CAMPION, D., SLEEGERS, K., HILTUNEN, M., COMBARROS, O., ZELENIKA, D., BULLIDO, M. J., TAVERNIER, B., LETENNEUR, L., BETTENS, K., BERR, C., PASQUIER, F., FIEVET, N., BARBERGER-GATEAU, P., ENGELBORGHS, S., DE DEYN, P., MATEO, I., FRANCK, A., HELISALMI, S., PORCELLINI,

E., HANON, O., EUROPEAN ALZHEIMER'S DISEASE INITIATIVE, I., DE PANCORBO, M. M., LENDON, C., DUFOUIL, C., JAILLARD, C., LEVEILLARD, T., ALVAREZ, V., BOSCO, P., MANCUSO, M., PANZA, F., NACMIAS, B., BOSSU, P., PICCARDI, P., ANNONI, G., SERIPA, D., GALIMBERTI, D., HANNEQUIN, D., LICASTRO, F., SOININEN, H., RITCHIE, K., BLANCHE, H., DARTIGUES, J. F., TZOURIO, C., GUT, I., VAN BROECKHOVEN, C., ALPEROVITCH, A., LATHROP, M. & AMOUYEL, P. 2009. Genome-wide association study identifies variants at CLU and CR1 associated with Alzheimer's disease. *Nat Genet,* 41**,** 1094-9.

LAUREN, J., GIMBEL, D. A., NYGAARD, H. B., GILBERT, J. W. & STRITTMATTER, S. M. 2009. Cellular prion protein mediates impairment of synaptic plasticity by amyloid-beta oligomers. *Nature,* 457**,** 1128-32.

LEE, H. K., KUMAR, P., FU, Q., ROSEN, K. M. & QUERFURTH, H. W. 2009. The insulin/Akt signaling pathway is targeted by intracellular beta-amyloid. *Mol Biol Cell,* 20**,** 1533-44.

LEVENSON, J. M., O'RIORDAN, K. J., BROWN, K. D., TRINH, M. A., MOLFESE, D. L. & SWEATT, J. D. 2004. Regulation of histone acetylation during memory formation in the hippocampus. *J Biol Chem,* 279**,** 40545-59.

LLORENS-MARTIN, M., JURADO, J., HERNANDEZ, F. & AVILA, J. 2014. GSK-3beta, a pivotal kinase in Alzheimer disease. *Front Mol Neurosci,* 7**,** 46.

LONG, J. B. & VAN VACTOR, D. 2013. Embryonic and larval neural connectivity: progressive changes in synapse form and function at the neuromuscular junction mediated by cytoskeletal regulation. *Wiley Interdiscip Rev Dev Biol,* 2**,** 747-65.

LUCHTENBORG, A. M. & KATANAEV, V. L. 2014. Lack of evidence of the interaction of the Abeta peptide with the Wnt signaling cascade in Drosophila models of Alzheimer's disease. *Mol Brain,* 7**,** 81.

MAEHAMA, T. & DIXON, J. E. 1998. The tumor suppressor, PTEN/MMAC1, dephosphorylates the lipid second messenger, phosphatidylinositol 3,4,5-trisphosphate. *J Biol Chem,* 273**,** 13375-8.

MARTIN-PENA, A., ACEBES, A., RODRIGUEZ, J. R., SORRIBES, A., DE POLAVIEJA, G. G., FERNANDEZ-FUNEZ, P. & FERRUS, A. 2006. Age-independent synaptogenesis by phosphoinositide 3 kinase. *J Neurosci,* 26**,** 10199-208.

MCCABE, B. D., HOM, S., ABERLE, H., FETTER, R. D., MARQUES, G., HAERRY, T. E., WAN, H., O'CONNOR, M. B., GOODMAN, C. S. & HAGHIGHI, A. P. 2004. Highwire regulates presynaptic BMP signaling essential for synaptic growth. *Neuron,* 41**,** 891-905.

MCCABE, B. D., MARQUES, G., HAGHIGHI, A. P., FETTER, R. D., CROTTY, M. L., HAERRY, T. E., GOODMAN, C. S. & O'CONNOR, M. B. 2003. The BMP homolog Gbb provides a retrograde signal that regulates synaptic growth at the Drosophila neuromuscular junction. *Neuron,* 39**,** 241-54.

MELANI, A., TURCHI, D., VANNUCCHI, M. G., CIPRIANI, S., GIANFRIDDO, M. & PEDATA, F. 2005. ATP extracellular concentrations are increased in the rat striatum during in vivo ischemia. *Neurochem Int,* 47**,** 442-8.

MENON, S., DIBBLE, C. C., TALBOTT, G., HOXHAJ, G., VALVEZAN, A. J., TAKAHASHI, H., CANTLEY, L. C. & MANNING, B. D. 2014. Spatial control of the TSC complex integrates insulin and nutrient regulation of mTORC1 at the lysosome. *Cell,* 156**,** 771-85.

MHATRE, S. D., SATYASI, V., KILLEN, M., PADDOCK, B. E., MOIR, R. D., SAUNDERS, A. J. & MARENDA, D. R. 2014. Synaptic abnormalities in a Drosophila model of Alzheimer's disease. *Dis Model Mech,* 7**,** 373-85.

MILTON, N. G. 2001. Phosphorylation of amyloid-beta at the serine 26 residue by human cdc2 kinase. *Neuroreport,* 12**,** 3839-44.

MORENO, E., YAN, M. & BASLER, K. 2002. Evolution of TNF signaling mechanisms: JNK-dependent apoptosis triggered by Eiger, the Drosophila homolog of the TNF superfamily. *Curr Biol,* 12**,** 1263-8.

MORETH, J., MAVOUNGOU, C. & SCHINDOWSKI, K. 2013. Passive anti-amyloid immunotherapy in Alzheimer's disease: What are the most promising targets? *Immun Ageing,* 10**,** 18.

MURAKAMI, K., UNO, M., MASUDA, Y., SHIMIZU, T., SHIRASAWA, T. & IRIE, K. 2008. Isomerization and/or racemization at Asp23 of Abeta42 do not increase its aggregative ability, neurotoxicity, and radical productivity in vitro. *Biochem Biophys Res Commun,* 366**,** 745-51.

MURESU, R., BALDINI, A., GRESS, T., POSNER, J. B., FURNEAUX, H. M. & SINISCALCO, M. 1994. Mapping of the Gene Coding for a Paraneoplastic Encephalomyelitis Antigen (Hud) to Human-Chromosome Site-1p34. *Cytogenetics and Cell Genetics,* 65**,** 177-178.

MURPHY, M. P. & LEVINE, H., 3RD 2010. Alzheimer's disease and the amyloid-beta peptide. *J Alzheimers Dis,* 19**,** 311-23.

MURRAY, M. M., KRONE, M. G., BERNSTEIN, S. L., BAUMKETNER, A., CONDRON, M. M., LAZO, N. D., TEPLOW, D. B., WYTTENBACH, T., SHEA, J. E. & BOWERS, M. T. 2009. Amyloid beta-protein: experiment and theory on the 21-30 fragment. *J Phys Chem B,* 113**,** 6041-6.

MUSUMECI, G., SCIARRETTA, C., RODRIGUEZ-MORENO, A., AL BANCHAABOUCHI, M., NEGRETE-DIAZ, V., COSTANZI, M., BERNO, V., EGOROV, A. V., VON BOHLEN UND HALBACH, O., CESTARI, V., DELGADO-GARCIA, J. M. & MINICHIELLO, L. 2009. TrkB modulates fear learning and amygdalar synaptic plasticity by specific docking sites. *J Neurosci,* 29**,** 10131-43.

NI, J. Q., LIU, L. P., BINARI, R., HARDY, R., SHIM, H. S., CAVALLARO, A., BOOKER, M., PFEIFFER, B. D., MARKSTEIN, M., WANG, H., VILLALTA, C., LAVERTY, T. R., PERKINS, L. A. & PERRIMON, N. 2009. A Drosophila resource of transgenic RNAi lines for neurogenetics. *Genetics,* 182**,** 1089-100.

NIENHAUS, U., AEGERTER-WILMSEN, T. & AEGERTER, C. M. 2012. In-vivo imaging of the Drosophila wing imaginal disc over time: novel insights on growth and boundary formation. *PLoS One,* 7**,** e47594.

PALOP, J. J., CHIN, J., ROBERSON, E. D., WANG, J., THWIN, M. T., BIEN-LY, N., YOO, J., HO, K. O., YU, G. Q., KREITZER, A., FINKBEINER, S., NOEBELS, J. L. & MUCKE, L. 2007. Aberrant excitatory neuronal activity and compensatory remodeling of inhibitory hippocampal circuits in mouse models of Alzheimer's disease. *Neuron,* 55**,** 697-711.

PALOP, J. J. & MUCKE, L. 2010. Amyloid-. 13**,** 812-818.

PARRISH, J. Z., XU, P., KIM, C. C., JAN, L. Y. & JAN, Y. N. 2009. The microRNA bantam functions in epithelial cells to regulate scaling growth of dendrite arbors in drosophila sensory neurons. *Neuron,* 63**,** 788-802.

PHAM, E., CREWS, L., UBHI, K., HANSEN, L., ADAME, A., CARTIER, A., SALMON, D., GALASKO, D., MICHAEL, S., SAVAS, J. N., YATES, J. R., GLABE, C. & MASLIAH, E. 2010. Progressive accumulation of amyloid-beta oligomers in Alzheimer's disease and in amyloid precursor protein transgenic mice is accompanied by selective alterations in synaptic scaffold proteins. *FEBS J,* 277**,** 3051-67.

REDEGELD, F. A., CALDWELL, C. C. & SITKOVSKY, M. V. 1999. Ecto-protein kinases: ecto-domain phosphorylation as a novel target for pharmacological manipulation? *Trends Pharmacol Sci,* 20**,** 453-9.

REZAEI-GHALEH, N., AMININASAB, M., GILLER, K., KUMAR, S., STUNDL, A., SCHNEIDER, A., BECKER, S., WALTER, J. & ZWECKSTETTER, M. 2014. Turn plasticity distinguishes different modes of amyloid-beta aggregation. *J Am Chem Soc,* 136**,** 4913-9.

RINCON-LIMAS, D. E., JENSEN, K. & FERNANDEZ-FUNEZ, P. 2012. Drosophila models of proteinopathies: the little fly that could. *Curr Pharm Des,* 18**,** 1108-22.

ROBINOW, S. & WHITE, K. 1988. The locus elav of Drosophila melanogaster is expressed in neurons at all developmental stages. *Dev Biol,* 126**,** 294-303.

ROBINOW, S. & WHITE, K. 1991. Characterization and spatial distribution of the ELAV protein during Drosophila melanogaster development. *J Neurobiol,* 22**,** 443-61.

ROGAEVA, E., MENG, Y., LEE, J. H., GU, Y., KAWARAI, T., ZOU, F., KATAYAMA, T., BALDWIN, C. T., CHENG, R., HASEGAWA, H., CHEN, F., SHIBATA, N., LUNETTA, K. L., PARDOSSI-PIQUARD, R., BOHM, C., WAKUTANI, Y., CUPPLES, L. A., CUENCO, K. T., GREEN, R. C., PINESSI, L., RAINERO, I., SORBI, S., BRUNI, A., DUARA, R., FRIEDLAND, R. P., INZELBERG, R., HAMPE, W., BUJO, H., SONG, Y. Q., ANDERSEN, O. M., WILLNOW, T. E., GRAFF-RADFORD, N., PETERSEN, R. C., DICKSON, D., DER, S. D., FRASER, P. E., SCHMITT-ULMS, G., YOUNKIN, S., MAYEUX, R., FARRER, L. A. & ST GEORGE-HYSLOP, P. 2007. The neuronal sortilin-related receptor SORL1 is genetically associated with Alzheimer disease. *Nat Genet,* 39**,** 168-77.

ROLLS, M. M., SATOH, D., CLYNE, P. J., HENNER, A. L., UEMURA, T. & DOE, C. Q. 2007. Polarity and intracellular compartmentalization of Drosophila neurons. *Neural Dev,* 2**,** 7.

ROSI, M. C., LUCCARINI, I., GROSSI, C., FIORENTINI, A., SPILLANTINI, M. G., PRISCO, A., SCALI, C., GIANFRIDDO, M., CARICASOLE, A., TERSTAPPEN, G. C. & CASAMENTI, F. 2010. Increased Dickkopf-1 expression in transgenic mouse models of neurodegenerative disease. *J Neurochem,* 112**,** 1539-51.

ROYCHAUDHURI, R., LOMAKIN, A., BERNSTEIN, S., ZHENG, X., CONDRON, M. M., BENEDEK, G. B., BOWERS, M. & TEPLOW, D. B. 2014. Gly25-Ser26 amyloid beta-protein structural isomorphs produce distinct Abeta42 conformational dynamics and assembly characteristics. *J Mol Biol,* 426**,** 2422-41.

RUGGERO, D. & SONENBERG, N. 2005. The Akt of translational control. *Oncogene,* 24**,** 7426-34.

SANYAL, S. 2009. Genomic mapping and expression patterns of C380, OK6 and D42 enhancer trap lines in the larval nervous system of Drosophila. *Gene Expr Patterns,* 9**,** 371-80.

SCHELTENS, P., BLENNOW, K., BRETELER, M. M., DE STROOPER, B., FRISONI, G. B., SALLOWAY, S. & VAN DER FLIER, W. M. 2016. Alzheimer's disease. *Lancet*.

SELKOE, D. J. & HARDY, J. 2015. The amyloid hypothesis of Alzheimer’s disease at 25 years. *EMBO Molecular Medicine*.

SHALTIEL, S., SCHVARTZ, I., KORC-GRODZICKI, B. & KREIZMAN, T. 1993. Evidence for an extra-cellular function for protein kinase A. *Mol Cell Biochem,* 127-128**,** 283-91.

SHIMIZU, T., WATANABE, A., OGAWARA, M., MORI, H. & SHIRASAWA, T. 2000. Isoaspartate formation and neurodegeneration in Alzheimer's disease. *Arch Biochem Biophys,* 381**,** 225-34.

SHOJI, M., GOLDE, T. E., GHISO, J., CHEUNG, T. T., ESTUS, S., SHAFFER, L. M., CAI, X. D., MCKAY, D. M., TINTNER, R., FRANGIONE, B. & ET AL. 1992. Production of the Alzheimer amyloid beta protein by normal proteolytic processing. *Science,* 258**,** 126-9.

SOFOLA, O., KERR, F., ROGERS, I., KILLICK, R., AUGUSTIN, H., GANDY, C., ALLEN, M. J., HARDY, J., LOVESTONE, S. & PARTRIDGE, L. 2010. Inhibition of GSK-3 ameliorates Abeta pathology in an adult-onset Drosophila model of Alzheimer's disease. *PLoS Genet,* 6**,** e1001087.

SOFOLA-ADESAKIN, O., CASTILLO-QUAN, J. I., RALLIS, C., TAIN, L. S., BJEDOV, I., ROGERS, I., LI, L., MARTINEZ, P., KHERICHA, M., CABECINHA, M., BAHLER, J. & PARTRIDGE, L. 2014. Lithium suppresses Abeta pathology by inhibiting translation in an adult Drosophila model of Alzheimer's disease. *Front Aging Neurosci,* 6**,** 190.

SOLDANO, A., OKRAY, Z., JANOVSKA, P., TMEJOVA, K., REYNAUD, E., CLAEYS, A., YAN, J., ATAK, Z. K., DE STROOPER, B., DURA, J. M., BRYJA, V. & HASSAN, B. A. 2013. The Drosophila homologue of the amyloid precursor protein is a conserved modulator of Wnt PCP signaling. *PLoS Biol,* 11**,** e1001562.

STEFANI, M. 2010. Biochemical and biophysical features of both oligomer/fibril and cell membrane in amyloid cytotoxicity. *FEBS J,* 277**,** 4602-13.

SUAREZ-CALVET, M., KLEINBERGER, G., ARAQUE CABALLERO, M. A., BRENDEL, M., ROMINGER, A., ALCOLEA, D., FORTEA, J., LLEO, A., BLESA, R., GISPERT, J. D., SANCHEZ-VALLE, R., ANTONELL, A., RAMI, L., MOLINUEVO, J. L., BROSSERON, F., TRASCHUTZ, A., HENEKA, M. T., STRUYFS, H., ENGELBORGHS, S., SLEEGERS, K., VAN BROECKHOVEN, C., ZETTERBERG, H., NELLGARD, B., BLENNOW, K., CRISPIN, A., EWERS, M. & HAASS, C. 2016. sTREM2 cerebrospinal fluid levels are a potential biomarker for microglia activity in early-stage Alzheimer's disease and associate with neuronal injury markers. *EMBO Mol Med,* 8**,** 466-76.

SUDHOF, T. C. 2012. The presynaptic active zone. *Neuron,* 75**,** 11-25.

TEICH, A. F., NICHOLLS, R. E., PUZZO, D., FIORITO, J., PURGATORIO, R., FA, M. & ARANCIO, O. 2015. Synaptic therapy in Alzheimer's disease: a CREB-centric approach. *Neurotherapeutics,* 12**,** 29-41.

TORROJA, L., CHU, H., KOTOVSKY, I. & WHITE, K. 1999a. Neuronal overexpression of APPL, the Drosophila homologue of the amyloid precursor protein (APP), disrupts axonal transport. *Curr Biol,* 9**,** 489-92.

TORROJA, L., PACKARD, M., GORCZYCA, M., WHITE, K. & BUDNIK, V. 1999b. The Drosophila beta-amyloid precursor protein homolog promotes synapse differentiation at the neuromuscular junction. *J Neurosci,* 19**,** 7793-803.

TURNER, A. J., FISK, L. & NALIVAEVA, N. N. 2004. Targeting amyloid-degrading enzymes as therapeutic strategies in neurodegeneration. *Ann N Y Acad Sci,* 1035**,** 1-20.

UGUR, B., CHEN, K. & BELLEN, H. J. 2016. Drosophila tools and assays for the study of human diseases. *Dis Model Mech,* 9**,** 235-44.

VAN TINE, B. A., KNOPS, J. F., BUTLER, A., DELOUKAS, P., SHAW, G. M. & KING, P. H. 1998. Localization of HuC (ELAVL3) to chromosome 19p13.2 by fluorescence in situ hybridization utilizing a novel tyramide labeling technique. *Genomics,* 53**,** 296-299.

VARGAS, L. M., LEAL, N., ESTRADA, L. D., GONZALEZ, A., SERRANO, F., ARAYA, K., GYSLING, K., INESTROSA, N. C., PASQUALE, E. B. & ALVAREZ, A. R. 2014. EphA4 activation of c-Abl mediates synaptic loss and LTP blockade caused by amyloid-beta oligomers. *PLoS One,* 9**,** e92309.

WAGNER, N., LAUGKS, U., HECKMANN, M., ASAN, E. & NEUSER, K. 2015. Aging Drosophila melanogaster display altered pre- and postsynaptic ultrastructure at adult neuromuscular junctions. *J Comp Neurol,* 523**,** 2457-75.

WALSH, D. M., KLYUBIN, I., FADEEVA, J. V., CULLEN, W. K., ANWYL, R., WOLFE, M. S., ROWAN, M. J. & SELKOE, D. J. 2002. Naturally secreted oligomers of amyloid beta protein potently inhibit hippocampal long-term potentiation in vivo. *Nature,* 416**,** 535-9.

WALTER, J., KINZEL, V. & KUBLER, D. 1994. Evidence for CKI and CKII at the cell surface. *Cell Mol Biol Res,* 40**,** 473-80.

WANG, H. Y., LEE, D. H., D'ANDREA, M. R., PETERSON, P. A., SHANK, R. P. & REITZ, A. B. 2000. beta-Amyloid(1-42) binds to alpha7 nicotinic acetylcholine receptor with high affinity. Implications for Alzheimer's disease pathology. *J Biol Chem,* 275**,** 5626-32.

WASCO, W., GURUBHAGAVATULA, S., PARADIS, M. D., ROMANO, D. M., SISODIA, S. S., HYMAN, B. T., NEVE, R. L. & TANZI, R. E. 1993. Isolation and characterization of APLP2 encoding a homologue of the Alzheimer's associated amyloid beta protein precursor. *Nat Genet,* 5**,** 95-100.

WEAVER, C., LEIDEL, C., SZPANKOWSKI, L., FARLEY, N. M., SHUBEITA, G. T. & GOLDSTEIN, L. S. 2013. Endogenous GSK-3/shaggy regulates bidirectional axonal transport of the amyloid precursor protein. *Traffic,* 14**,** 295-308.

WIRTHS, O., MULTHAUP, G. & BAYER, T. A. 2004. A modified beta-amyloid hypothesis: intraneuronal accumulation of the beta-amyloid peptide--the first step of a fatal cascade. *J Neurochem,* 91**,** 513-20.

WISNIEWSKI, T. & SIGURDSSON, E. M. 2010. Murine models of Alzheimer's disease and their use in developing immunotherapies. *Biochim Biophys Acta,* 1802**,** 847-59.

XU, S., LIU, G., BAO, X., WU, J., LI, S., ZHENG, B., ANWYL, R. & WANG, Q. 2014. Rosiglitazone prevents amyloid-beta oligomer-induced impairment of synapse formation and plasticity via increasing dendrite and spine mitochondrial number. *J Alzheimers Dis,* 39**,** 239-51.

YAAR, M., ZHAI, S., PILCH, P. F., DOYLE, S. M., EISENHAUER, P. B., FINE, R. E. & GILCHREST, B. A. 1997. Binding of beta-amyloid to the p75 neurotrophin receptor induces apoptosis. A possible mechanism for Alzheimer's disease. *J Clin Invest,* 100**,** 2333-40.

ZHANG, Z., HARTMANN, H., DO, V. M., ABRAMOWSKI, D., STURCHLER-PIERRAT, C., STAUFENBIEL, M., SOMMER, B., VAN DE WETERING, M., CLEVERS, H., SAFTIG, P., DE STROOPER, B., HE, X. & YANKNER, B. A. 1998. Destabilization of beta-catenin by mutations in presenilin-1 potentiates neuronal apoptosis. *Nature,* 395**,** 698-702.

ZHAO, X. L., WANG, W. A., TAN, J. X., HUANG, J. K., ZHANG, X., ZHANG, B. Z., WANG, Y. H., YANGCHENG, H. Y., ZHU, H. L., SUN, X. J. & HUANG, F. D. 2010. Expression of beta-

amyloid induced age-dependent presynaptic and axonal changes in Drosophila. *J Neurosci,* 30**,** 1512-22.

ZHAO, Z., SAGARE, A. P., MA, Q., HALLIDAY, M. R., KONG, P., KISLER, K., WINKLER, E. A., RAMANATHAN, A., KANEKIYO, T., BU, G., OWENS, N. C., REGE, S. V., SI, G., AHUJA, A., ZHU, D., MILLER, C. A., SCHNEIDER, J. A., MAEDA, M., MAEDA, T., SUGAWARA, T., ICHIDA, J. K. & ZLOKOVIC, B. V. 2015. Central role for PICALM in amyloid-beta blood-brain barrier transcytosis and clearance. *Nat Neurosci,* 18**,** 978-87.

FIGURE LEGENDS

Fig. I1 Hypothetical model for the temporal progression of AD markers. Schematic graph representing the abnormal progression of AD biomarkers. Biomarkers start to abnormally change before they reach the detection threshold (black horizontal line), as it is denoted by the gray area in the graph. Aβ levels are the first measures to be detected (red and purple arrows), followed by tau (light blue arrow), FDG PET and MRI (dark blue arrow) and cognitive impairment (green arrow). Light green filled area represents the range of cognitive responses, which depends on each individual's risk profile. Extracted from Hardy and Selkoe 2016.

Fig. I2 Sequence of events proposed in Aβ cascade for AD pathology. Both inherited and not-inherited forms of AD converge in the accumulation and oligomerization of Aβ species, which induce the progression of the rest of events to eventually result the cognitive and memory impairment that AD patients manifest. This hypothesis proposes that Aβ assemblies are the leading cause of AD, as they directly induce early synaptic loss. (Adapted from Hardy and Selkoe 2002; Hardy and Selkoe 2016)

Fig. I3 APP proteolytic processing. Schematic cartoon representing the amyloidogenic and non-amyloidogenic processing that the full-length APP can suffer. In the amyloidogenic pathway (right) β and γ secretases sequentially cut APP generating the resulting Aβ peptide (orange fragment) and the AICD fragment (purple). In the non-amyloidogenic pathway (left) a different cleavage is accomplished by the α-secretase first, and thus, the resulting fragment, after being processed by the γ-secretase, different fragments are released, p3 (orange) and AICD (purple). (Adapted from Nicolas and Hassan 2014).

Fig. I4 Aβ aggregates. Schematic cartoon representing the different Aβ assemblies that can be generated upon β-amyloid aggregation. APP full-length protein is represented in purple, with the Aβ fragment in orange. Arrows indicate the cleavage elicited by β and γ secretases. The spectrum of Aβ species range from soluble monomers to insoluble fibrils and are known to vary from less toxic assemblies (green) to more toxic aggregates (orange).

Fig. I5 Aβ effects in synaptic transmission. Schematic representation summarizing the hypothetical sequential effects of Aβ in presynaptic and postsynaptic regulation. Aβ abnormally low and high levels impair synaptic activity, but intermediate levels enhance synaptic activity (a). In particular, intermediate Aβ levels affect presynaptic and post-synaptic terminals (b), but high Aβ levels regulate only postsynaptic functions (c). (Palop and Mucke 2010).

Fig. I6 APP structure and domains across species. Schematic representation of APP domain structure in *Homo sapiens*, *Mus musculus*, *Dario rerio*, *Caenorhabditis elegans* and *Drosophila melanogaster*. The following domains are represented: Heparin-binding domain (HBD), copper-binding domain (CuBD), acidic domain (Ac), Kunitz protease inhibitor domain (KPI), E2 domain (E2) containing a Zinc binding site in APLP1 (Mayer et al,

2014) and known to bind heparin-sulphate proteoglycans, Aβ sequence (Aβ) and a specific domain conserved across species that serves as a signal for clathrin-mediated endocytosis and binding site for cytosolic adaptor proteins (YENPTY).

Fig. I7 Location and structure of *Drosophila* neuromuscular active zone. Schematic cartoon representing the pre-synaptic and post-synaptic sides of a synapse, and in particular, active zones ultrastructure as revealed by high-resolution LM (Liu et al 2011) (adapted from Südhof 2012).

Fig. M1 Gal4/UAS system for directed gene expression. Schematic representation of the Gal4/UA system (St Johnston 2002).

Fig. M2 Gal80^{TS} repressor system. Scheme representing the termosensitive Gal4 repressor system Gal80^{TS} system (McGuire et al 2003).

Fig. M3 G-TRACE analysis system. Schematic cartoon representing the molecular mechanism of the G-TRACE (Gal4 Technique for Real-time And Clonal Expression) (Evans et al, 2009).

Fig. R1 PI3K activation prevents Aβ42 induced synapse loss. (A-D'') Representative confocal image examples of Bruchpilot immunostainings visualizing adult VLM NMJs expressing UAS-lacZ (control), UAS-PI3K^{caax}, UAS-Aβ42(2x), and UAS-PI3K^{CAAX}/UAS-Aβ42(2x) constructs at 7 (A-D), 15 (A'-D') and 25 days of expression (A''-D'') with *elav*^{c155}-Gal4/TubGal80^{TS}. **(E)** Quantification of synaptic area representing normalized Bruchpilot positive signal detected in the immunostainings of the different genotypes and time-points shown in A-D''. Results are represented in dot-blot diagrams showing all measured and normalized values. Bars represent mean and SDM. Statistical t-test results are indicated with *** p<0,001, ** p< 0,01 and * p<0,05 for control group comparisons, and ### p<0,001, ## p<0,01 and # p<0,05 for Aβ42 group comparisons. When no statistical significance is found p value is indicated. Scale bar is 20μm.

Fig. R2 No transcriptional changes are found in any of the studied genotypes. Histograms plotting mRNA levels of *bruchpilot* **(A)**, l*iprin* **(B)** and *synaptobrevin* **(C)** measured by quantitative RT-PCR in 15 days-old adult brains of the indicated genotypes expressed with *elav*^{c155}-Gal4/TubGal80^{ts}. Results are represented as fold induction with respect to UAS-lacZ (control) group (red dotted line). Error bars represent SDM. Comparisons between groups correspond to t-test analysis.

Fig. R3 PI3K prevents Aβ42-induced microtubule dynamics deficits. (A) Schematic cartoon depicting microtubule growth and shrinking processes noting the presences of EB1 protein at the plus-end of a growing microtubule. **(B-E)** Still images of live imaging

recordings for EB1-GFP in ddA sensory neurons of third instar larvae expressing UAS-lacZ (control), UAS-PI3K^{CAAX}, UAS-Aβ42(2x), and UAS-PI3K^{CAAX}/UAS-Aβ42(2x) with *elav*^{c155}-Gal4 driver. **(F-I)** Dot-blot diagrams showing EB1-GFP comets quantification of track speed (F), track length (G), track duration (H), and track density (I). Normalized values and SDM bars are represented and statistical t-test analysis is shown with *** p<0,001, ** p< 0,01 and * p<0,05 for control group comparisons, and ### p<0,001, ## p<0,01 and # p<0,05 for Aβ42 group comparisons. When no statistical significance is found p value is indicated. Scale bar is 50µm.

Fig. R4 Aβ42-induced locomotion activity reduction is delayed by PI3K overexpression. (A) Schematic cartoon representing the three fly populations considered in the locomotion analysis. **(B-E)** Histograms showing standardized values of the number of flies climbing to the top of the tube (blue), climbing the tube but not reaching the 4cm line (orange), and staying at the bottom of the tube (black). UAS-lacZ (control) (B,F,G), UAS-PI3K^{CAAX} (C,H,I), UAS-Aβ42(2x) (D,J,K), and UAS-PI3K^{CAAX}/UAS-Aβ42(2x) (E,L,M) expression with *elav*^{c155}-Gal4/TubGal80^{TS} respectively corresponds to the indicated genotypes. **(F-M)** Pie chart diagrams representing detailed percent values at 15 days (F,H,J,L) and 20 days (G,I,K,M).

Fig. R5 PI3K expression increases lifespan of Aβ42 flies. (A-E) Survival curves for the following genotypes: PI3K (A,E); Aβ42 (B,D,E); and PI3K/Aβ42 (C,D,E) compared to lacZ (control) genotype (black lines in A-C), or compared to Aβ42 genotype (D) expressing the corresponding UAS constructs with *elav*^{c155}-Gal4/TubGal80^{TS}. **(E)** Survival curve representing survival data in all genotypes. Statistical analysis with Mantel-Cox test is shown as **** p<0,0001.

Fig. R6 PI3K activation in human neurons prevents the cell survival reduction induced by Aβ42. HTSY-5Y cells differentiated (retinoic acid 10µM) and treated with increasing concentrations of Aβ42 oligomers (18µg/ml, 36µg/ml and 72µg/ml) for 48h, and PTD4-PI3KAc peptide (50µg/ml) at different time-points: 24 hours before Aβ42 oligomers (pretreatment), at the same time that Aβ42 oligomers (co-treatment), and 24 hours after Aβ42 oligomers (post-treatment). Data from Cell Titer Glo luminescence is shown as percent viability and compared to control values of non-treated cells (red-dotted line). Error bars indicate SDM. Statistical significance is represented from t-test analysis with *** p<0,001, ** p< 0,01 and * p<0,05.

Fig. R7 Synaptogenic proteins, but not canonical PI3K effectors, prevent Aβ42-induced synapse loss. (A-F) Representative confocal image examples of Bruchpilot immunostainings visualizing adult VLM NMJs expressing UAS-lacZ (control) (A), UAS-mTOR (B), UAS-Medea$_{RNAi}$ (C), UAS-Aβ42(2x) (D), UAS-mTOR/UAS-Aβ42(2x) (E), and UAS-Medea$_{RNAi}$/ UAS-Aβ42(2x) (F) constructs with *elav*^{c155}-Gal4/TubGal80^{TS} at 15 days. **(G)** Quantification of synaptic area representing normalized Bruchpilot positive signal detected in the immunostainings of the different genotypes in A-F. Results are represented in dot-blot diagrams showing all measured and normalized values. Bars represent mean and SDM. Statistical t-test results are indicated with *** p<0,001, ** p< 0,01 and * p<0,05 for control group comparisons, and ### p<0,001, ## p<0,01 and # p<0,05 for Aβ42 group comparisons. When no statistical significance is found p value is indicated. Scale bar is 20µm.

Fig. R8 Aβ42-induced locomotor decline is prevented by Medea knockdown. (A) Schematic cartoon representing the three fly populations considered in the locomotion analysis. **(B-F)** Histograms showing standardized values of the number of flies climbing to the top of the tube (blue), climbing the tube but not reaching the 4cm line (orange), and staying at the bottom of the tube (black). Corresponding genotypes are: UAS-lacZ (control) (B,G,H), UAS-mTOR (C,I,J), UAS-mTOR/UAS-Aβ42(2x) (D,K), UAS-Medea$_{RNAi}$ (E,L,M), and UAS-Medea$_{RNAi}$/ UAS-Aβ42(2x) (F,N,O) constructs expressed with *elav*^{c155}-Gal4/TubGal80^{TS}. **(G-O)** Pie chart diagrams representing detailed percent values at 15 days (G,I,K,L,N) and 20 days (H,J,M,O).

Fig. R9 Medea downexpression blocks the Aβ42-induced lifespan reduction. (A-G) Survival curves for the following genotypes: UAS-mTOR (A,G); UAS-Medea$_{RNAi}$ (C,G), UAS-Aβ42(2x) (E,F,G); UAS-mTOR/UAS-Aβ42(2x) (B,E,G), and UAS-Medea$_{RNAi}$/ UAS-Aβ42(2x) (D,F,G); compared to UAS-lacZ (control) genotype (black lines in A-D), or compared to Aβ42 genotype (E-F). Constructs are expressed with *elav*^{c155}-Gal4/TubGal80^{TS} driver. **(G)** Survival curve representing survival data in all genotypes. Statistical analysis with Mantel-Cox test is shown as **** p<0,0001.

Fig. R10 PI3K activation increases Aβ42 levels without affecting transcription. (A-D) Representative confocal image examples of Aβ (white) immunostainings visualizing adult brains expressing UAS-lacZ (control) (A), UAS-PI3K^{caax} (B), UAS-Aβ42(2x) (C), and UAS-PI3K^{CAAX}/UAS-Aβ42(2x) (D) constructs at 15 with *elav*^{c155}-Gal4/TubGal80^{TS}. **(E)** Representative immunoblot indicating Aβ levels in control, Aβ42 and PI3K/Aβ42 adult heads corresponding to the same time-point and genotypes used for immunostainings (A-D). Histogram represents mean Aβ levels quantified and normalized to tubulin of three independent Western-blots. Error bars indicate SDM. **(F)** Histograms plotting mRNA levels of Aβ measured by quantitative RT-PCR in 15 days-old adult brains of the indicated genotypes expressed with *elav*^{c155}-Gal4/TubGal80^{ts}. Results are represented as fold induction with respect to Aβ42 group. Error bars represent SDM. Comparisons between groups correspond to t-test analysis.

Fig. R11 PI3K overexpression increases Aβ42 insoluble fraction. (A) Schematic cartoon showing the different Aβ conformers generated upon β and γ secretases processing of APP. Aggregates range from soluble to insoluble and differ in toxicity from less toxic species (green) to more toxic assemblies (orange). **(B-C')** Representative confocal images of thioflavin stainings visualizing 7 days (B,C) and 15 days (B', C') adult brains of the following genotypes: UAS-Aβ42(2x) (B-B'), and UAS-PI3K^{CAAX}/UAS-Aβ42(2x) (C,C') with *elav*^{c155}-Gal4/TubGal80^{TS} driver. **(D)** Histograms representing thioflavin staining quantification. Data are shown as mean Aβ levels normalized with respect to Aβ42 group. Error bars represent SDM. Comparisons between groups correspond to t-test analysis. * p<0,05. **(E)** Representative immunoblot indicating insoluble Aβ levels in control, PI3K, Aβ42 and PI3K/Aβ42 adult heads of 15 days-old flies. Histogram represents mean Aβ levels quantified and normalized to tubulin of three independent Western-blots. Error bars indicate SDM.

Fig. R12 PI3K-induced Aβ42 aggregation changes are reproduced in human neurons. (A) Schematic cartoon representing the experimental design in HT-SY5Y cells differentiated (retinoic acid 10μM) and treated with Aβ42 oligomers (36μg/ml) and PTD4-PI3KAc peptide

(50µg/ml) for 48h. **(B-D)** Histograms representing percent values of number of deposits (B), total deposit area (C) and deposit size distribution (D) of PI3K/Aβ42 and Aβ42 treated cells. Statistical t-test results are indicated with * p<0,05. **(E-H')** Representative confocal images showing Aβ (green) and DAPI (magenta) immunostainings. Merged (E-H) and Aβ signal (E'-H') images represent Aβ deposits for the indicated treatments.

Fig. R13 PI3K-induced changes in Aβ42 aggregation can be reproduced outside of cells. (A) Schematic cartoon representing the experimental design in HT-SY5Y cells differentiated (retinoic acid 10µM) and treated with Aβ42 oligomers (36µg/ml) and PTD4-PI3KAc peptide (50µg/ml) at different time-points. **(B-E)** Histograms representing percent values of number of deposits (B), total deposit area (C), number of deposits/ deposit area ratio (D), and deposit size distribution (E) of Aβ42 and PI3K/Aβ42 treated cells.

Fig. R14 pSer-Aβ42 increases following PI3K overexpression. (A) Scheme representing Aβ42 sequence and the Net-Phos predicted residues for potential phosphorylations. **(B-E')** Representative confocal images of p-serine (green) and DAPI (magenta) immunostainings visualizing 15 days-old adult brains of the following genotypes: UAS-lacZ (control) (B,B'), UAS-PI3K^{caax} (C,C'), UAS-Aβ42(2x) (D,D'), and UAS-PI3K^{CAAX}/UAS-Aβ42(2x) (E,E') constructs with *elav*^{c155}-Gal4/TubGal80^{TS} driver. **(F-I')** Representative confocal images of p-tyrosine (green) and DAPI (magenta) immunostainings visualizing 15 days-old adult brains of the following genotypes: UAS-lacZ (control) (F,F'), UAS-PI3K^{caax} (G,G'), UAS-Aβ42(2x) (H,H'), and UAS-PI3K^{CAAX}/UAS-Aβ42(2x) (I,I') constructs with *elav*^{c155}-Gal4/TubGal80^{TS} driver. Scale bar is 10µm.

Fig. R15 PI3K specifically triggers Ser26-Aβ42 phosphorylation. (A-B''') Representative confocal images of p.Ser26-Aβ42 (green), p.Ser8-Aβ42 (red) and DAPI (magenta) immunostainings visualizing 15 days-old adult brains of the following genotypes: UAS-UAS-Aβ42(2x) (A-A'''), and UAS-PI3K^{CAAX}/UAS-Aβ42(2x) (B-B''') constructs with *elav*^{c155}-Gal4/TubGal80^{TS} driver. (A´-A''', B-B''') show magnified images for both genotypes Scale bar is 50µm in (B) and 10µm in (B').

Fig. R16 Aβ42-induced inflated abdomen phenotype is prevented by PI3K overexpression. (A) Representative images of 15 days-old adult flies expressing the following UAS constructs: UAS-lacZ (control), UAS-Aβ42(2x), UAS-PI3K^{CAAX} and UAS-PI3K^{CAAX}/UAS-Aβ42(2x) with *elav*^{c155}-Gal4/TubGal80^{TS} driver. (B) Lateral views of Aβ42 and PI3K/Aβ42 genotypes. (C) Lateral views of head and proboscis of Aβ42 and PI3K/Aβ42 genotypes

Fig. R17 The nervous system enhancer *elav* is transiently active in epithelial cells of the wing disc. (A-B') Representative images of G-TRACE pattern from *elav* enhancer in larval brains (A,A') and wing discs (B,B'). **(C-D')** Still images of G-TRACE pattern from early developmental wing disc stages of first instar (C,C') and second instar (D,D') larvae**. (E-I)** Representative images of G-TRACE pattern of third instar larvae wing discs of *elav*-Gal4 in the third chromosome (E-F) in particular left (E) and right (F); and *elav*-Gal4 in the second chromosome (H-I) in particular left (H and right (I). **(G)** Overlapped images of GFP-positive cells from left (red) and right (green) wing discs of *elav*-Gal4 in the third chromosome. **(J)** Quantification (n=5) of G-TRACE pattern of *elav* enhancer comparing two different *elav*-Gal4 insertions, chromosome III (E-F) and chromosome II (H-I). **(K-L')** Representative

confocal images of elav G-TRACE pattern (K,L) and Elav immunostaining (K',L') in larval brain (K,K') and in wing discs (L,L'). Statistical t-test is represented with *p<0,05. Scale bar is 50μm.

Fig. R18 *Toll-6* enhancer (D42-Gal4) is transiently activated in wing imaginal discs during the first 12h after egg-laying. (**A)** Schematic representation of experimental design. Crosses were set and maintained 24 hours at 25°C. Then, first instar larvae were placed at 17°C (expression system OFF) or at 29°C (expression system ON) for the indicated time points: Always at 17°C "OFF", 48h, 24h or 12h at 17°C or always at 29°C "ON". **(B-H)** Representative images of temporal expression experiments in *D42-Gal4>G-TRACE>elav-Gal80^{TS}* brain (B,C)) and wing discs (D-H) maintained at 17°C "OFF" (Gal4 silenced), 48h, 24h or 12h OFF or maintained at 29°C "ON" (Gal4 active). (**I**) Quantification (n=5) of GFP-positive cells per time point. Statistical t-test analysis is represented with * p<0,05.

Fig. R19 *Toll-6* gene product is not necessary for wing disc development. (A-F) Representative images of Caspase 3 activation (green) (C3) and Wingless expression (red) and DAPI (blue) immunostainings in wild type (A-B), D42-Gal4>Toll6$_{RNAi}$ (C-D) and *D42-Gal4>Bsk* (E-F) genotypes. **(G-I)** Representative images of resulting adult wings in wild type (G), D42-Gal4>Toll6$_{RNAi}$ (H), and *D42-Gal4>Bsk* (I) genotypes.

Fig. R20 Adult wing defects in Aβ42 flies are restored by PI3K overexpression. Representative images of adult fly wings of the following genotypes: UAS-lacZ (control), UAS-PI3K^{CAAX}, UAS-Aβ42(2x) and UAS-PI3K^{CAAX}/UAS-Aβ42(2x) with D42-Gal4 driver.

Fig. R21 PI3K overexpression reduces Aβ42-induced apoptosis in epithelial cells of the wing disc. (A-D') Representative confocal images of caspase-3 (A'-B') and phospho-histone-3 (C'-D') and DAPI (magenta) immunostainings from third instar larval wing discs expressing UAS-Aβ42(2x) and UAS-PI3K^{CAAX}/Aβ42(2x) with *engrailed*-Gal4/UAS-GFPnls driver that expresses GFP in the affected nuclei (green) (A-B,C-D).

Fig. R22 PI3K overexpression restores Wnt signaling impairment caused by Aβ42 in epithelial cells of the wing disc. (A-D') Representative confocal images of wingless (A'-B') and armadillo (C'-D') and DAPI (magenta) immunostainings from third instar larval wing discs expressing UAS-Aβ42(2x) and UAS-PI3K^{CAAX}/Aβ42(2x) with *engrailed*-Gal4/UAS-GFPnls driver, that expresses GFP in the affected nuclei (green) (A-B,C-D).

Fig. D1 APP described mutations in Aβ region. Aβ aminoacidic sequence representation showing the sites for β and γ secretase cleavage (red arrows). Mutations in APP inside the Aβ region indicate changes that lead to an increase in Aβ production (blue), modify Aβ biophysical characteristics (black), or alter Aβ spectrum (green) (Benilova et al, 2012).

FIGURES

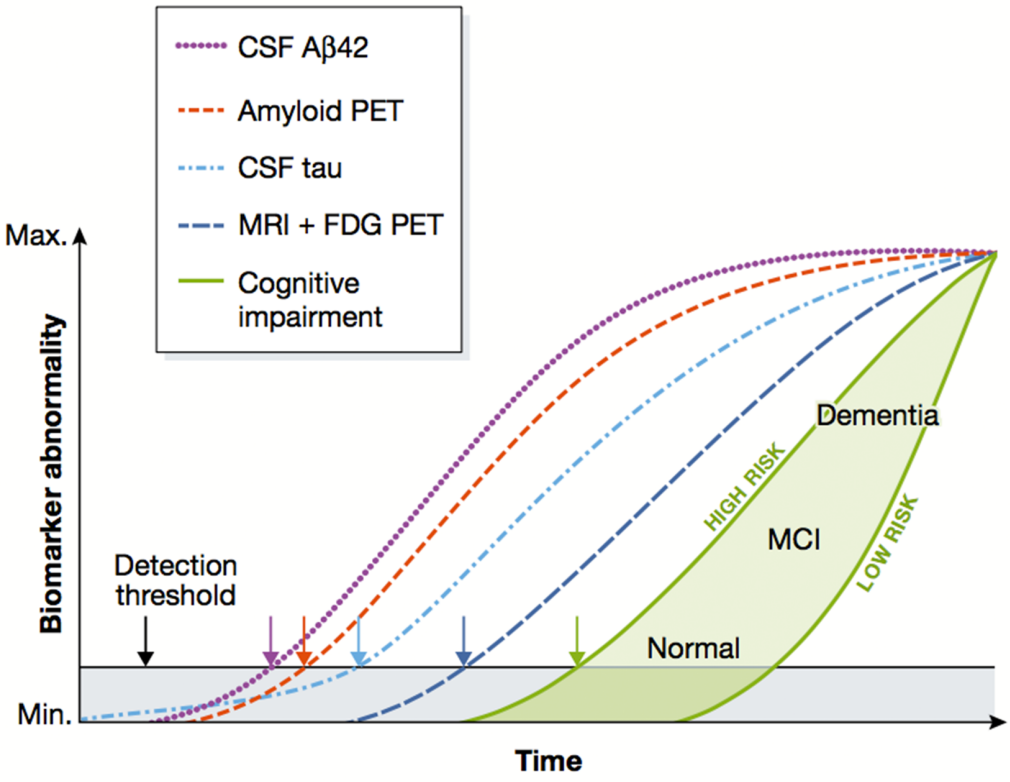
CSF Aβ42
Amyloid PET
CSF tau
MRI + FDG PET
Cognitive impairment
Max.
Min.
Biomarker abnormality
Detection threshold
Normal
MCI
Dementia
HIGH RISK
LOW RISK
Time

Fig. I1

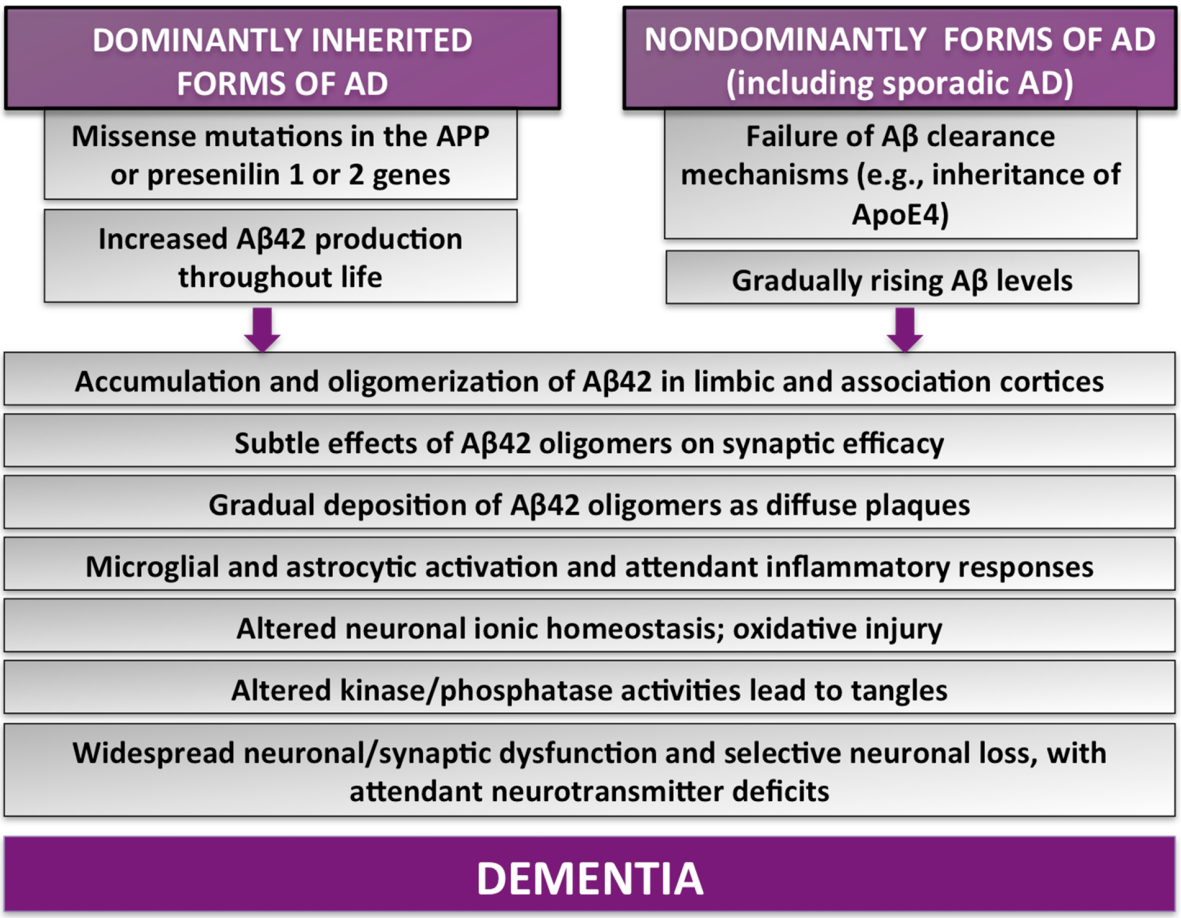
DOMINANTLY INHERITED FORMS OF AD
Missense mutations in the APP or presenilin 1 or 2 genes
Increased Aβ42 production throughout life
NONDOMINANTLY FORMS OF AD (including sporadic AD)
Failure of Aβ clearance mechanisms (e.g., inheritance of ApoE4)
Gradually rising Aβ levels
Accumulation and oligomerization of Aβ42 in limbic and association cortices
Subtle effects of Aβ42 oligomers on synaptic efficacy
Gradual deposition of Aβ42 oligomers as diffuse plaques
Microglial and astrocytic activation and attendant inflammatory responses
Altered neuronal ionic homeostasis; oxidative injury
Altered kinase/phosphatase activities lead to tangles
Widespread neuronal/synaptic dysfunction and selective neuronal loss, with attendant neurotransmitter deficits
DEMENTIA

Fig. I2

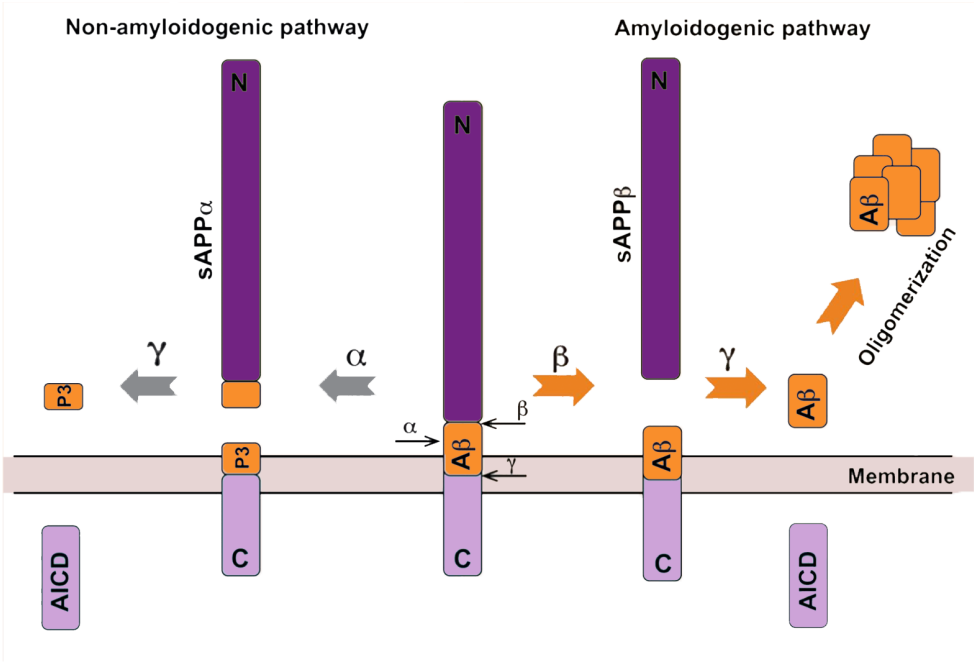
Non-amyloidogenic pathway
Amyloidogenic pathway
N
sAPPα
N
sAPPβ
N
Aβ
Oligomerization
γ
α
β
γ
P3
α
β
Aβ
Aβ
Aβ
γ
Membrane
P3
C
C
C
AICD
AICD

Fig. I3

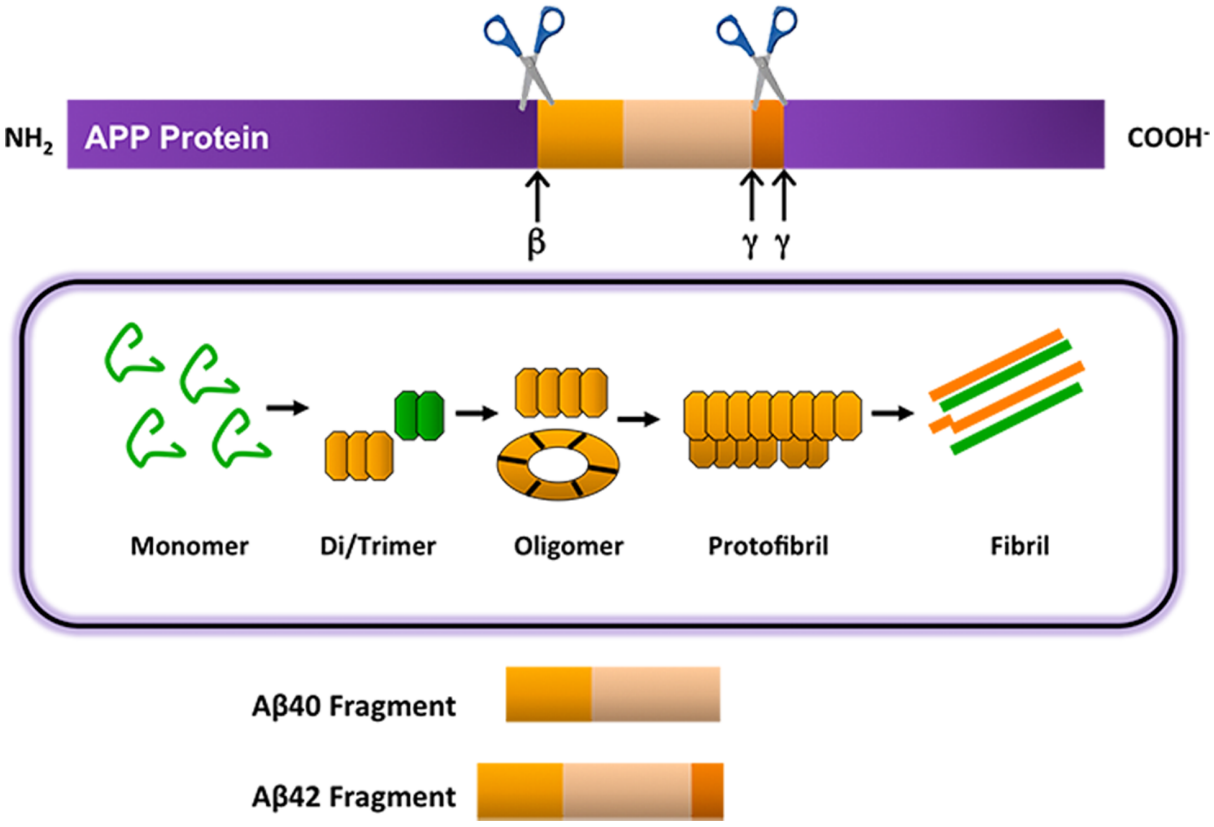
NH2
APP Protein
COOH-
β
γ γ
Monomer
Di/Trimer
Oligomer
Protofibril
Fibril
Aβ40 Fragment
Aβ42 Fragment

Fig. I4

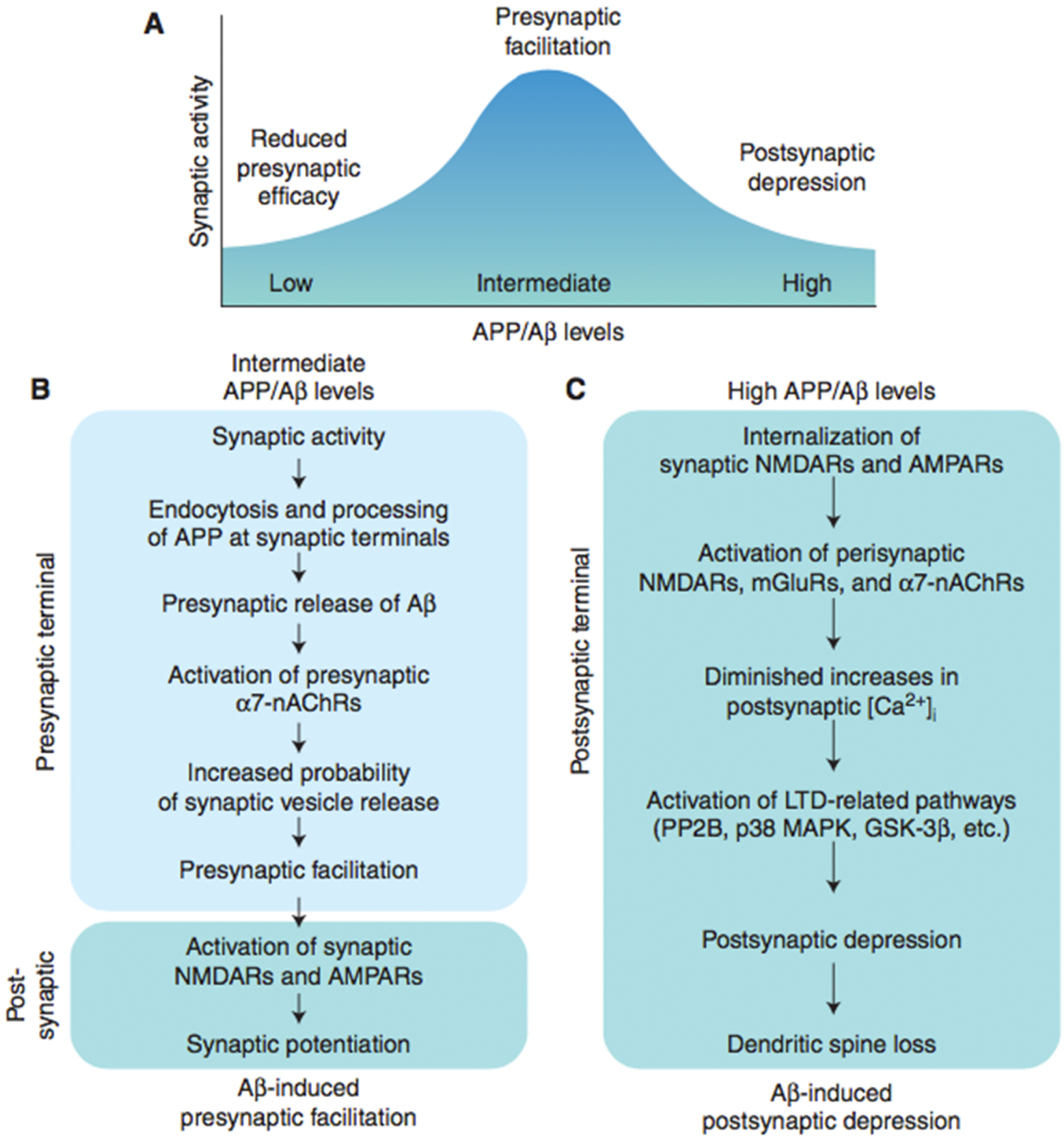
A
Presynaptic facilitation
Synaptic activity
Reduced presynaptic efficacy
Postsynaptic depression
Low
Intermediate
High
APP/Aβ levels
B
Intermediate APP/Aβ levels
Presynaptic terminal
Synaptic activity
Endocytosis and processing of APP at synaptic terminals
Presynaptic release of Aβ
Activation of presynaptic α7-nAChRs
Increased probability of synaptic vesicle release
Presynaptic facilitation
Post-synaptic
Activation of synaptic NMDARs and AMPARs
Synaptic potentiation
Aβ-induced presynaptic facilitation
C
High APP/Aβ levels
Postsynaptic terminal
Internalization of synaptic NMDARs and AMPARs
Activation of perisynaptic NMDARs, mGluRs, and α7-nAChRs
Diminished increases in postsynaptic $[Ca^{2+}]_i$
Activation of LTD-related pathways (PP2B, p38 MAPK, GSK-3β, etc.)
Postsynaptic depression
Dendritic spine loss
Aβ-induced postsynaptic depression

Fig. I5

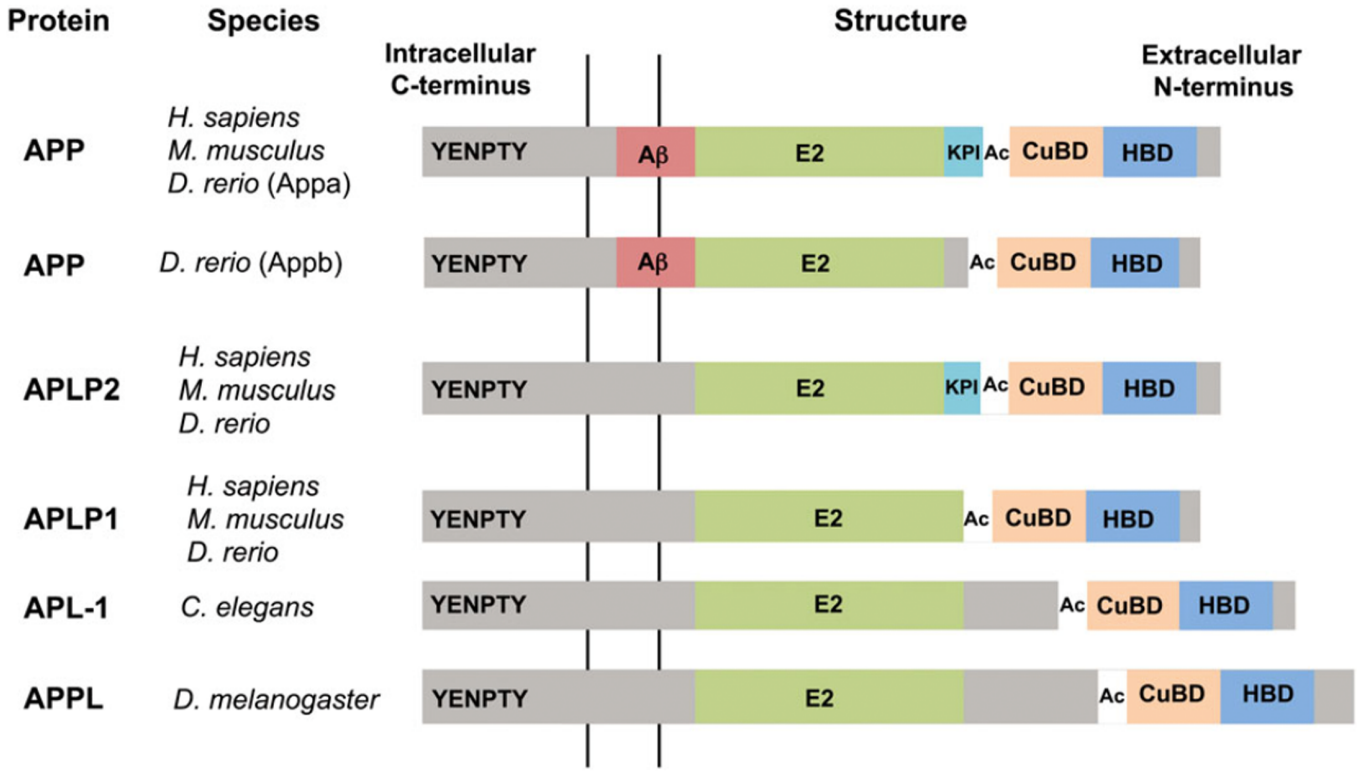
Protein
Species
Structure
Intracellular
C-terminus
Extracellular
N-terminus
APP
H. sapiens
M. musculus
D. rerio (Appa)
APP
D. rerio (Appb)
APLP2
H. sapiens
M. musculus
D. rerio
APLP1
H. sapiens
M. musculus
D. rerio
APL-1
C. elegans
APPL
D. melanogaster
YENPTY
Aβ
E2
KPI
Ac
CuBD
HBD

Fig. I6

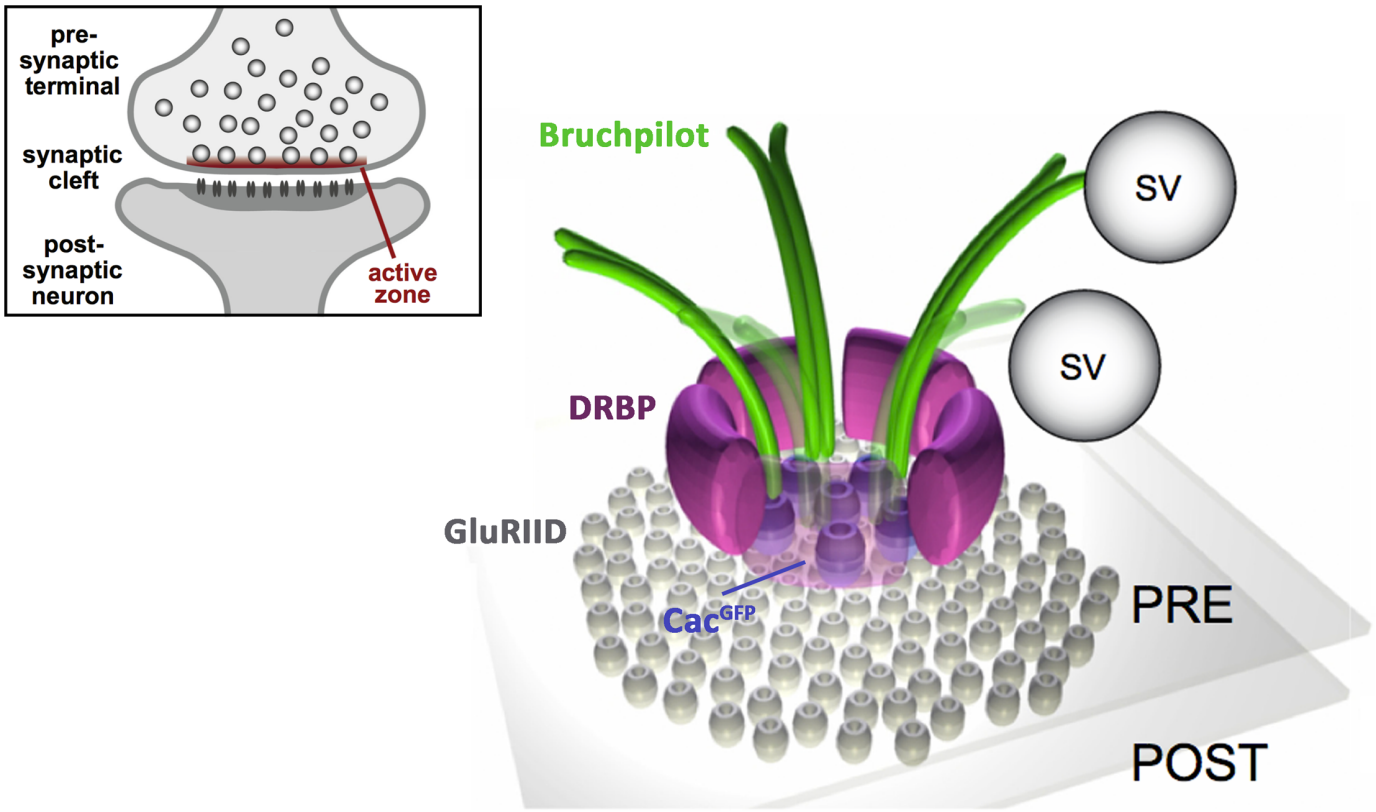
pre-
synaptic
terminal
synaptic
cleft
post-
synaptic
neuron
active
zone
Bruchpilot
SV
SV
DRBP
GluRIID
Cac^GFP
PRE
POST

Fig. I7

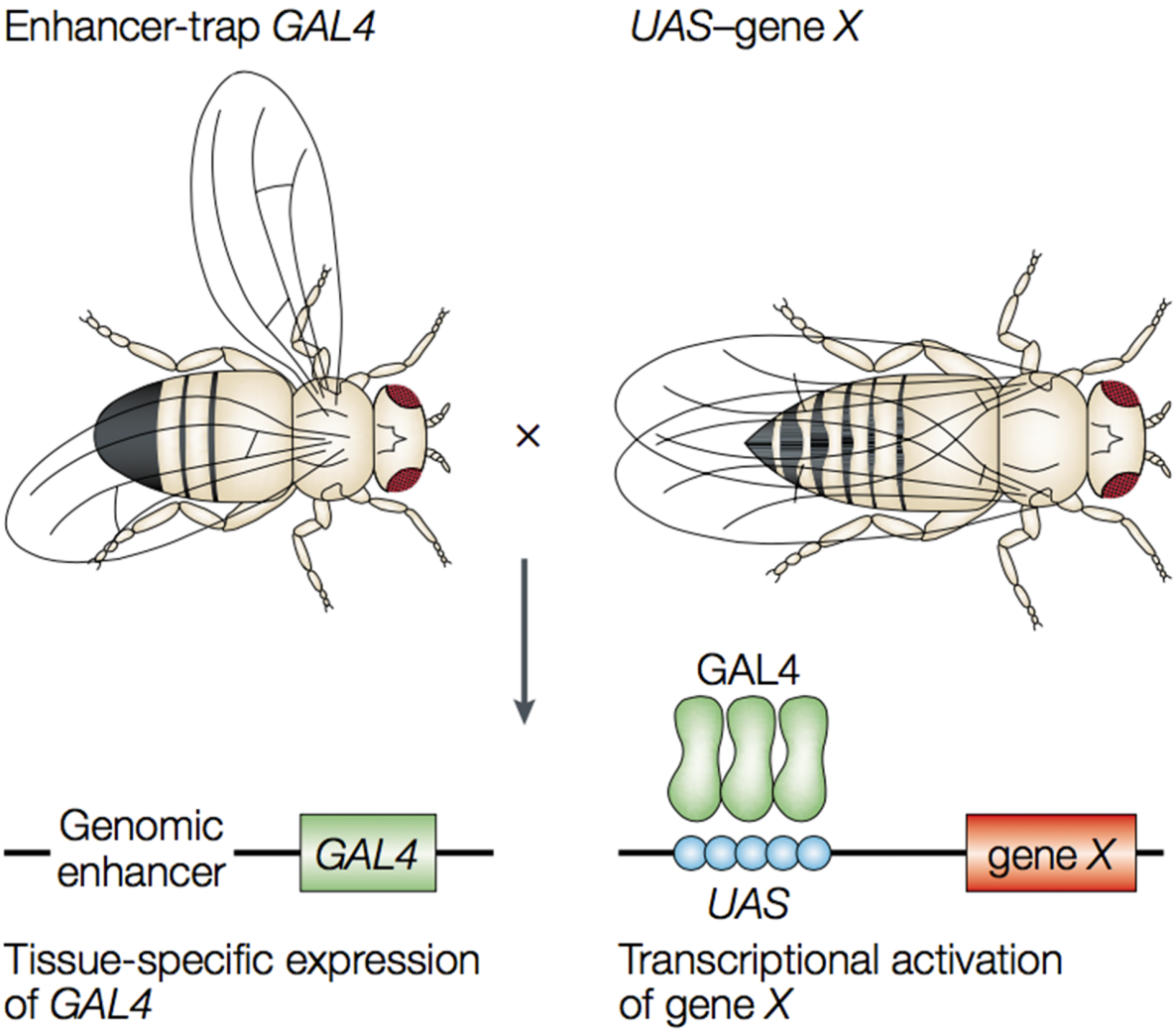
Enhancer-trap GAL4
UAS–gene X
×
GAL4
Genomic enhancer
GAL4
UAS
gene X
Tissue-specific expression of GAL4
Transcriptional activation of gene X

Fig. M1

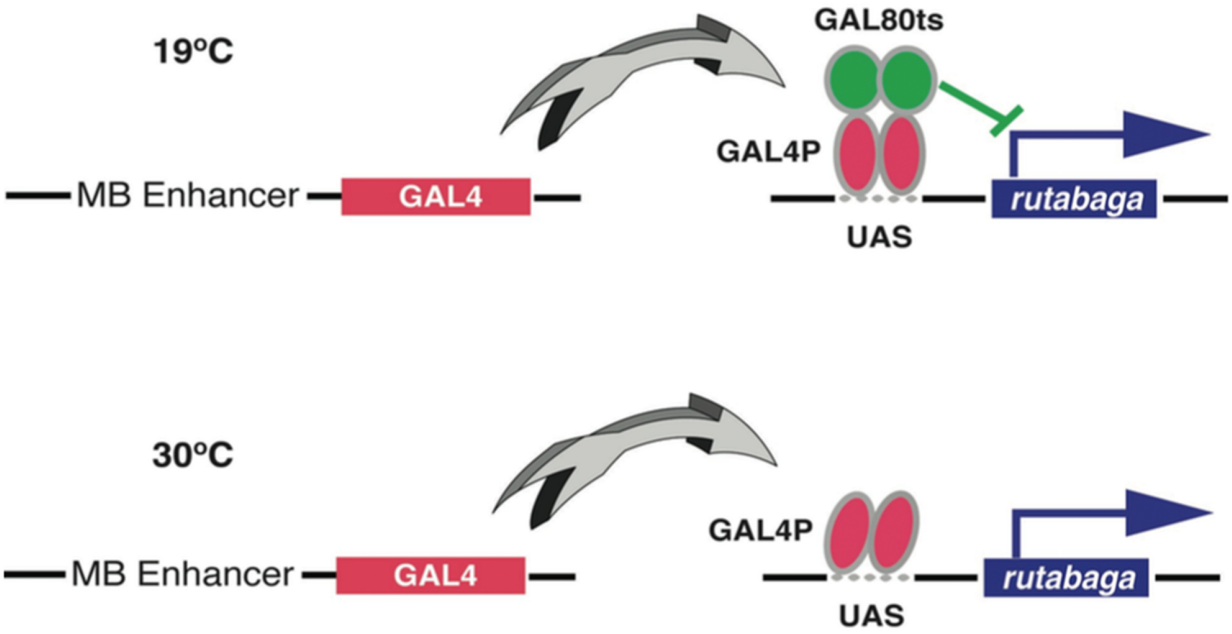
19°C
GAL80ts
GAL4P
MB Enhancer
GAL4
rutabaga
UAS
30°C
GAL4P
MB Enhancer
GAL4
rutabaga
UAS

Fig. M2

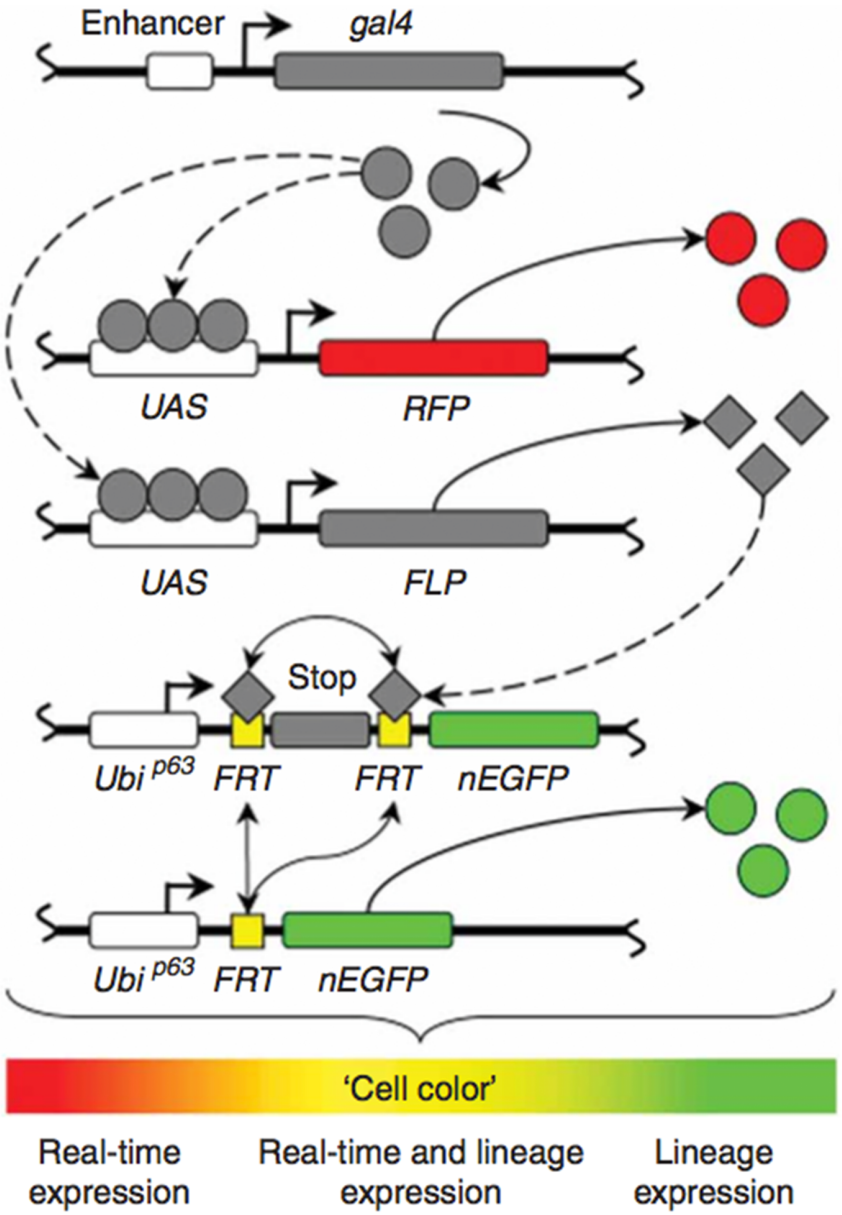
Enhancer
gal4
UAS
RFP
UAS
FLP
Stop
Ubi p63
FRT
FRT
nEGFP
Ubi p63
FRT
nEGFP
'Cell color'
Real-time expression
Real-time and lineage expression
Lineage expression

Fig. M3

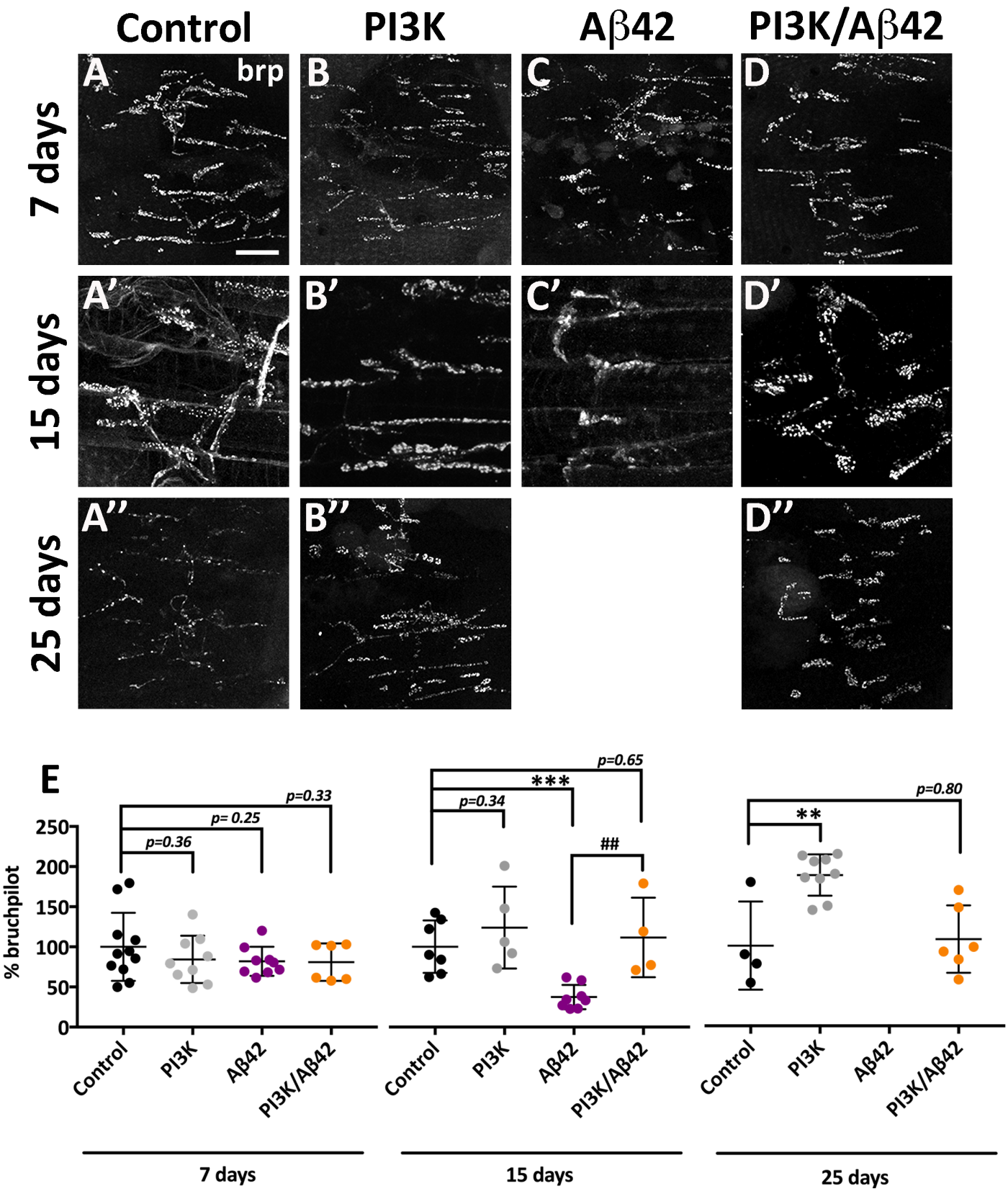
Control
PI3K
Aβ42
PI3K/Aβ42
7 days
15 days
25 days
A
brp
B
C
D
A'
B'
C'
D'
A''
B''
D''
E
% bruchpilot
p=0.33
p= 0.25
p=0.36
p=0.65
***
p=0.34
##
p=0.80
**
Control
PI3K
Aβ42
PI3K/Aβ42
7 days
15 days
25 days

Fig. R1

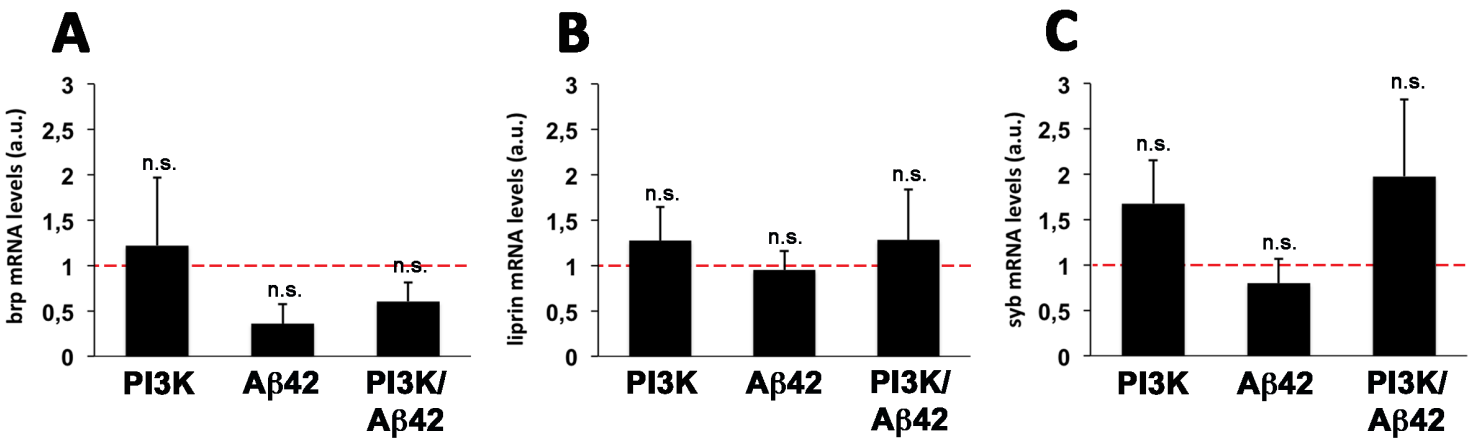
A
B
C
brp mRNA levels (a.u.)
liprin mRNA levels (a.u.)
syb mRNA levels (a.u.)
3
2,5
2
1,5
1
0,5
0
n.s.
PI3K
Aβ42
PI3K/
Aβ42

Fig. R2

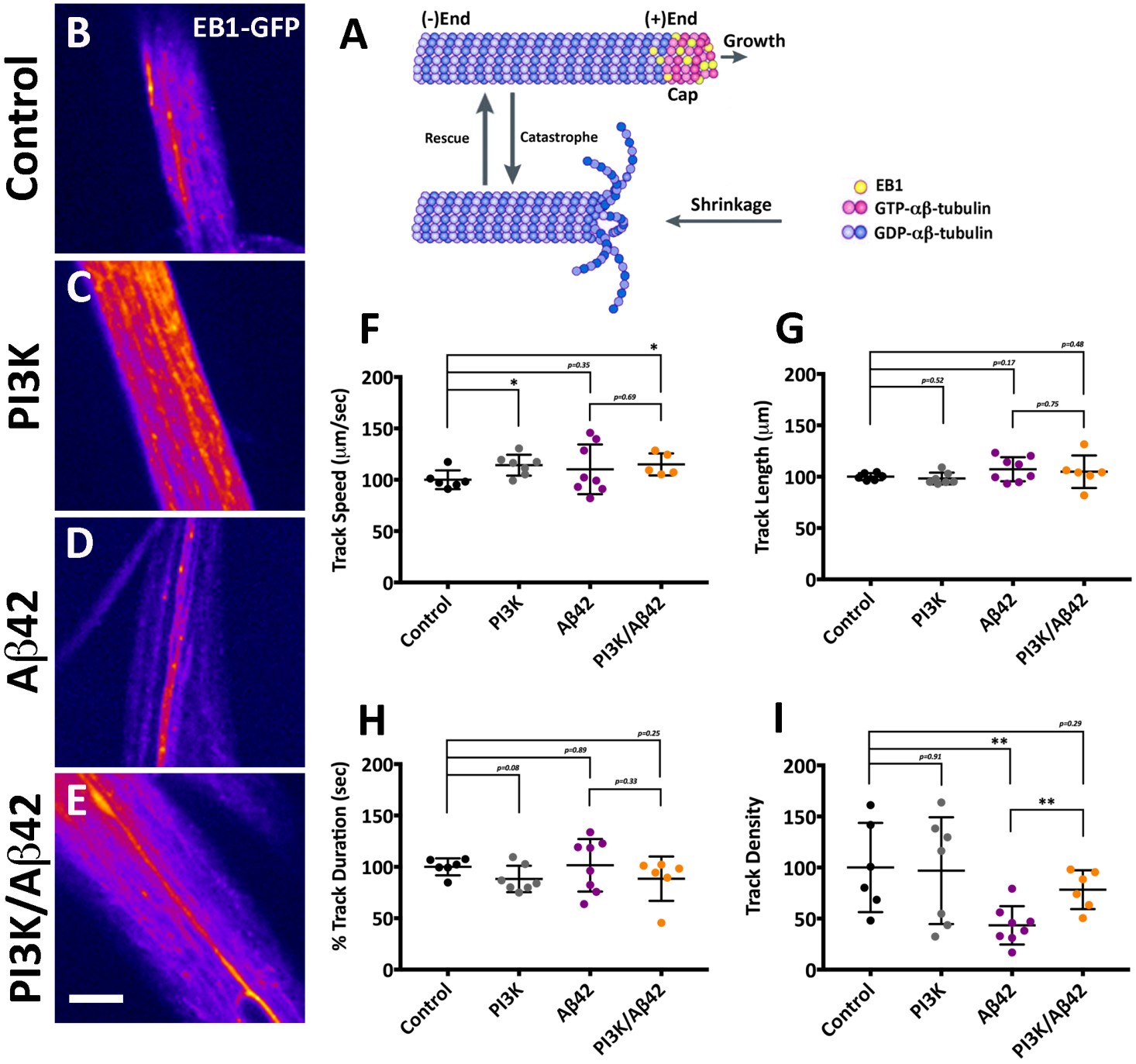
Control
PI3K
Aβ42
PI3K/Aβ42
B
EB1-GFP
C
D
E
A
(-)End
(+)End
Growth
Cap
Rescue
Catastrophe
Shrinkage
EB1
GTP-αβ-tubulin
GDP-αβ-tubulin
F
Track Speed (μm/sec)
G
Track Length (μm)
H
% Track Duration (sec)
I
Track Density
Control
PI3K
Aβ42
PI3K/Aβ42

Fig. R3

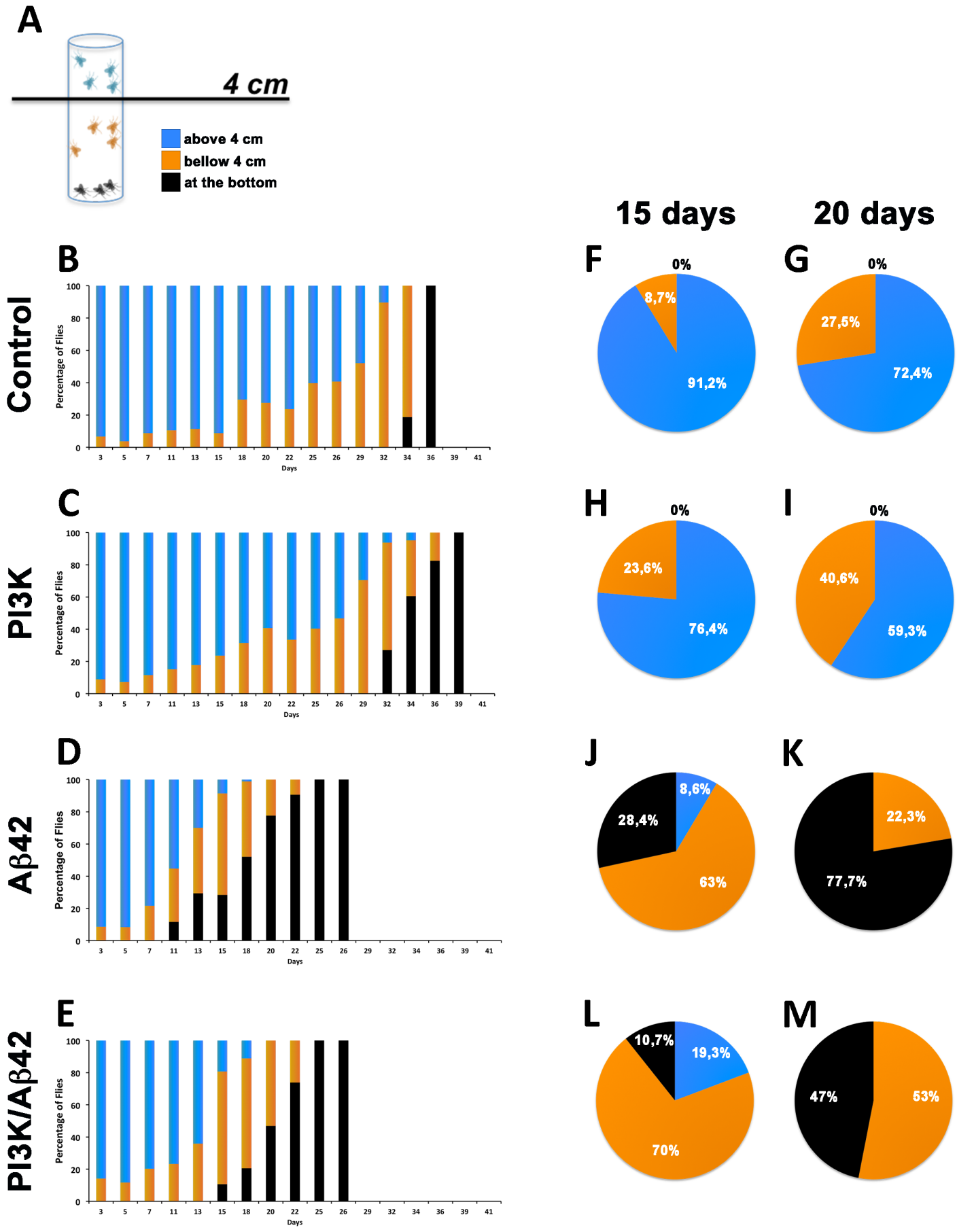
A
4 cm
above 4 cm
bellow 4 cm
at the bottom
15 days
20 days
Control
PI3K
Aβ42
PI3K/Aβ42
B
C
D
E
F
G
H
I
J
K
L
M
Percentage of Flies
Days
0%
8,7%
91,2%
27,5%
72,4%
23,6%
76,4%
40,6%
59,3%
8,6%
28,4%
63%
22,3%
77,7%
10,7%
19,3%
70%
47%
53%

Fig. R4

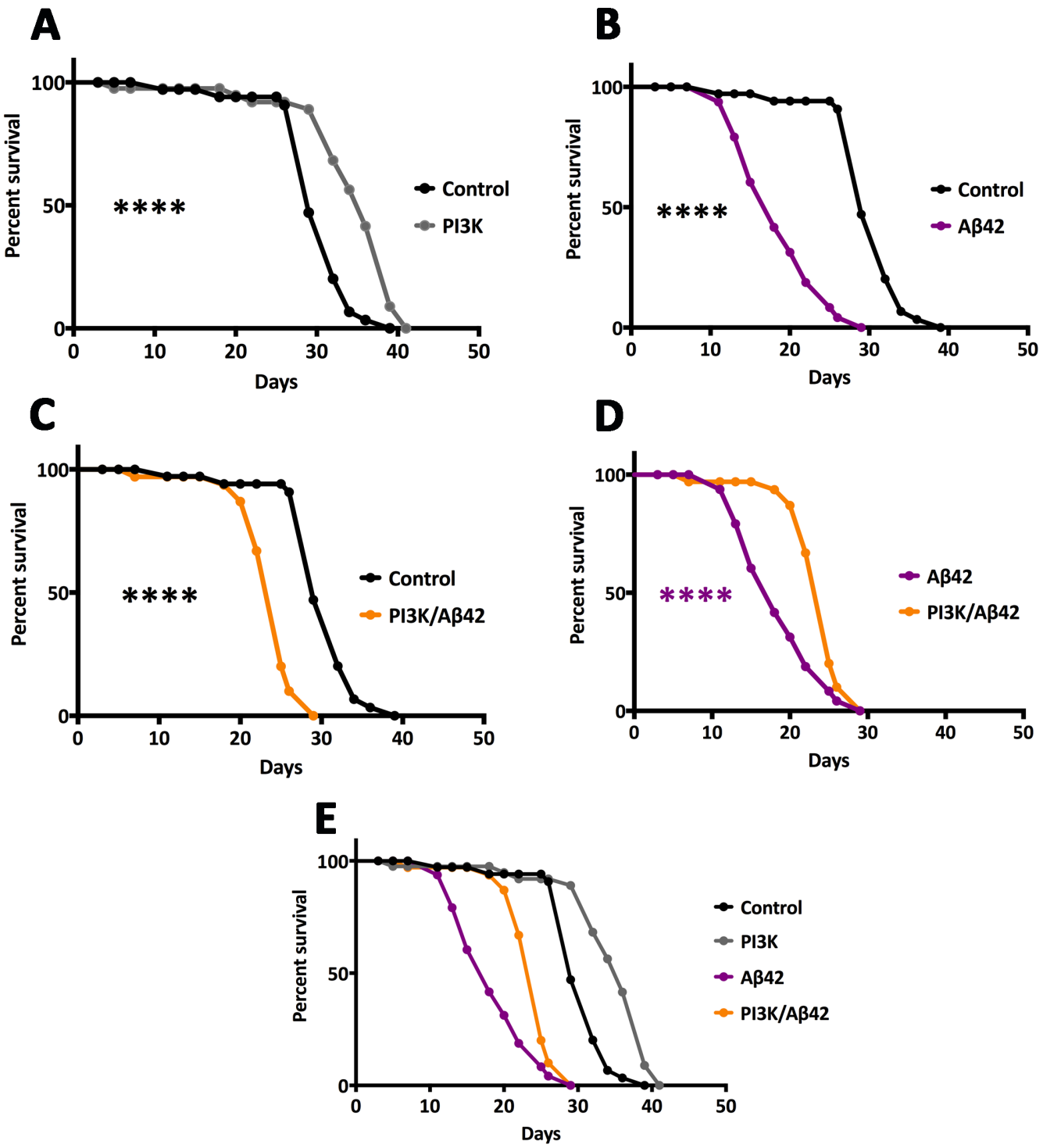
A
Percent survival
100
50
0
****
Control
PI3K
0
10
20
30
40
50
Days
B
Percent survival
100
50
0
****
Control
Aβ42
0
10
20
30
40
50
Days
C
Percent survival
100
50
0
****
Control
PI3K/Aβ42
0
10
20
30
40
50
Days
D
Percent survival
100
50
0
****
Aβ42
PI3K/Aβ42
0
10
20
30
40
50
Days
E
Percent survival
100
50
0
Control
PI3K
Aβ42
PI3K/Aβ42
0
10
20
30
40
50
Days

Fig. R5

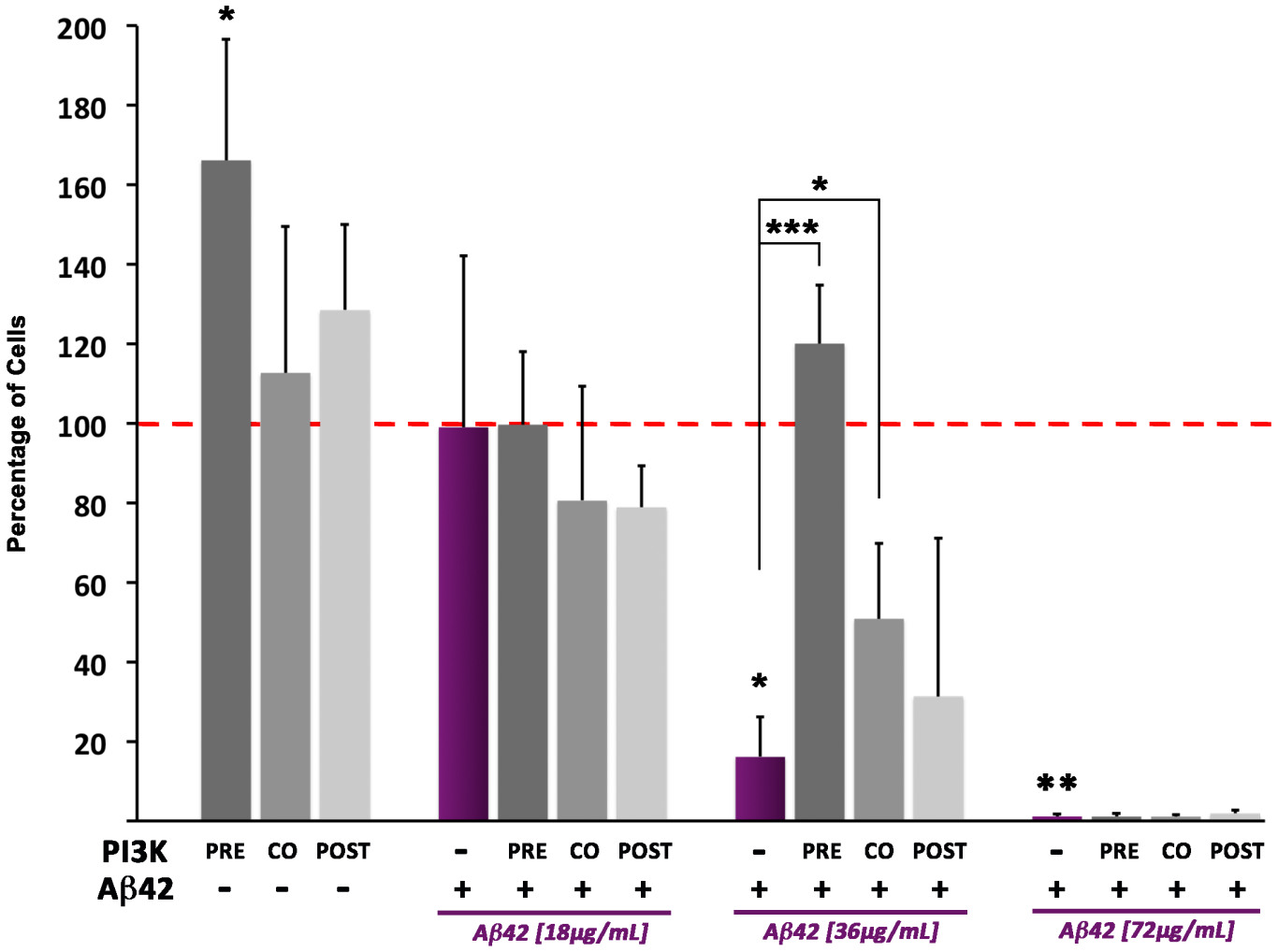
Percentage of Cells
200
180
160
140
120
100
80
60
40
20
*
*
***
*
**
PI3K PRE CO POST - PRE CO POST - PRE CO POST - PRE CO POST
Aβ42 - - - + + + + + + + + + + + + +
Aβ42 [18μg/mL]
Aβ42 [36μg/mL]
Aβ42 [72μg/mL]

Fig. R6

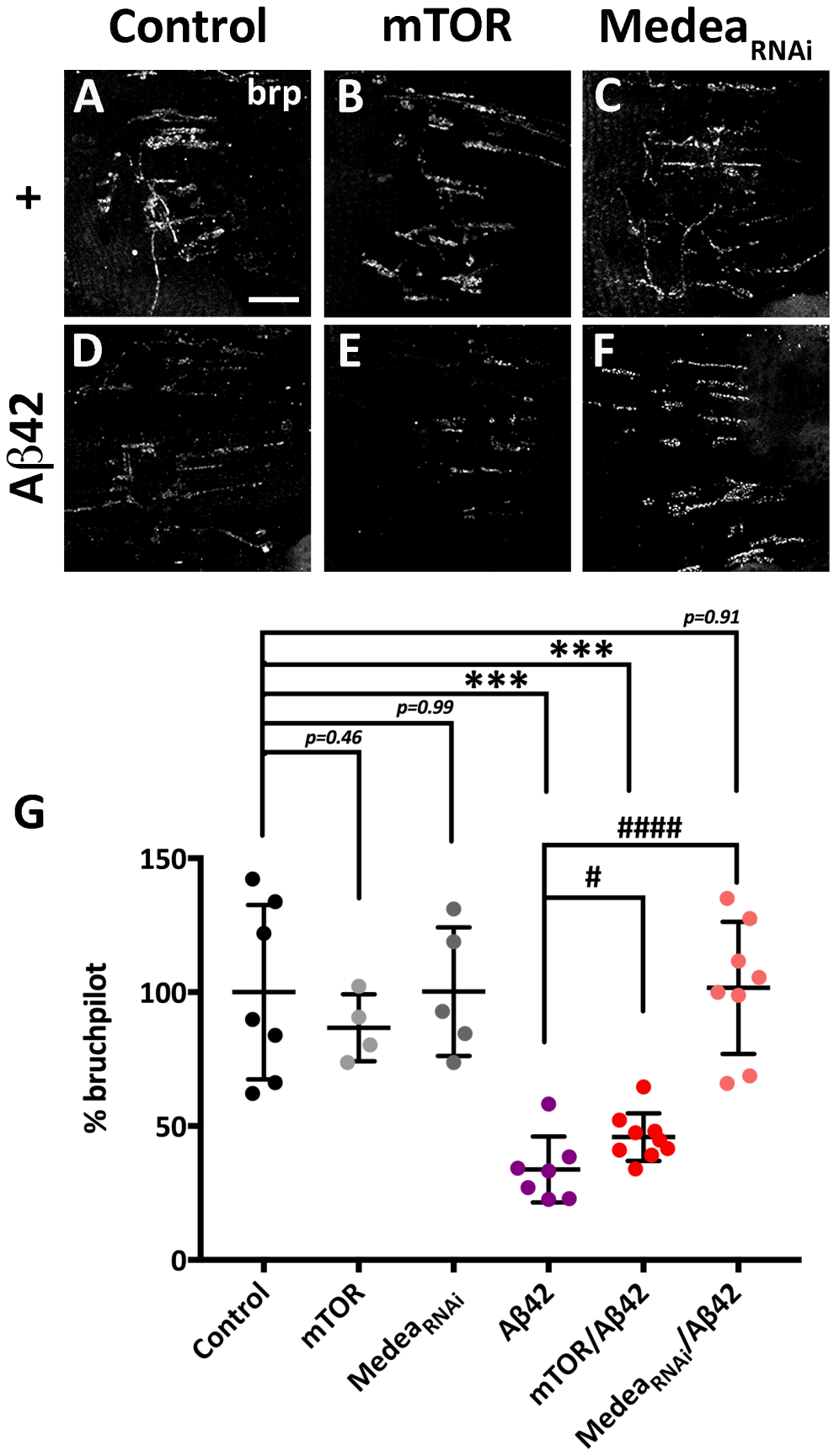
Control
mTOR
Medea RNAi
A
brp
B
C
+
D
E
F
Aβ42
G
p=0.91
***
***
p=0.99
p=0.46
####
#
150
100
50
0
% bruchpilot
Control
mTOR
Medea RNAi
Aβ42
mTOR/Aβ42
Medea RNAi/Aβ42

Fig. R7

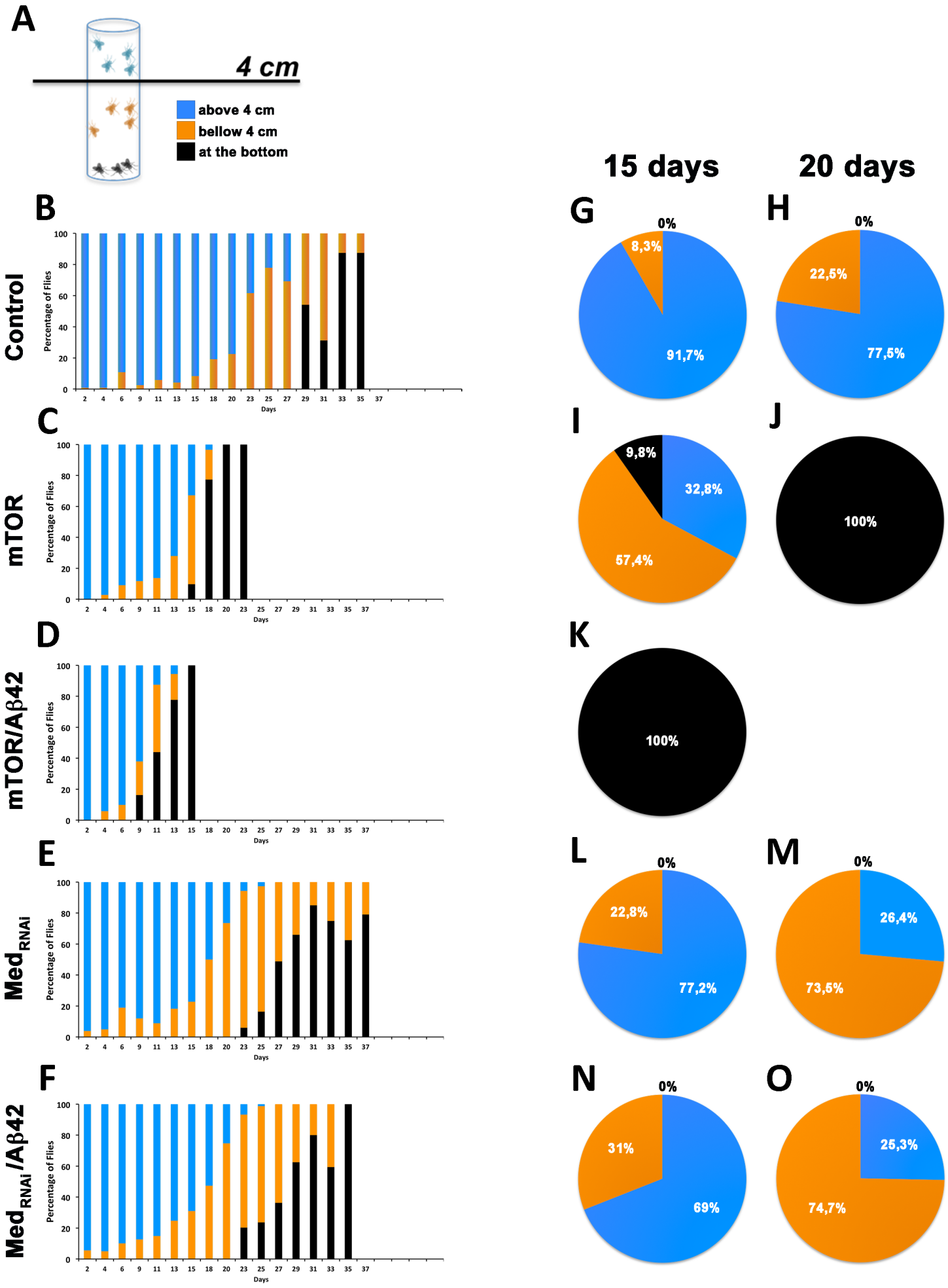
A
4 cm
above 4 cm
bellow 4 cm
at the bottom
15 days
20 days
B
Control
C
mTOR
D
mTOR/Aβ42
E
Med RNAi
F
Med RNAi /Aβ42
Percentage of Flies
Days
G
0%
8,3%
91,7%
H
0%
22,5%
77,5%
I
9,8%
32,8%
57,4%
J
100%
K
100%
L
0%
22,8%
77,2%
M
0%
26,4%
73,5%
N
0%
31%
69%
O
0%
25,3%
74,7%

Fig. R8

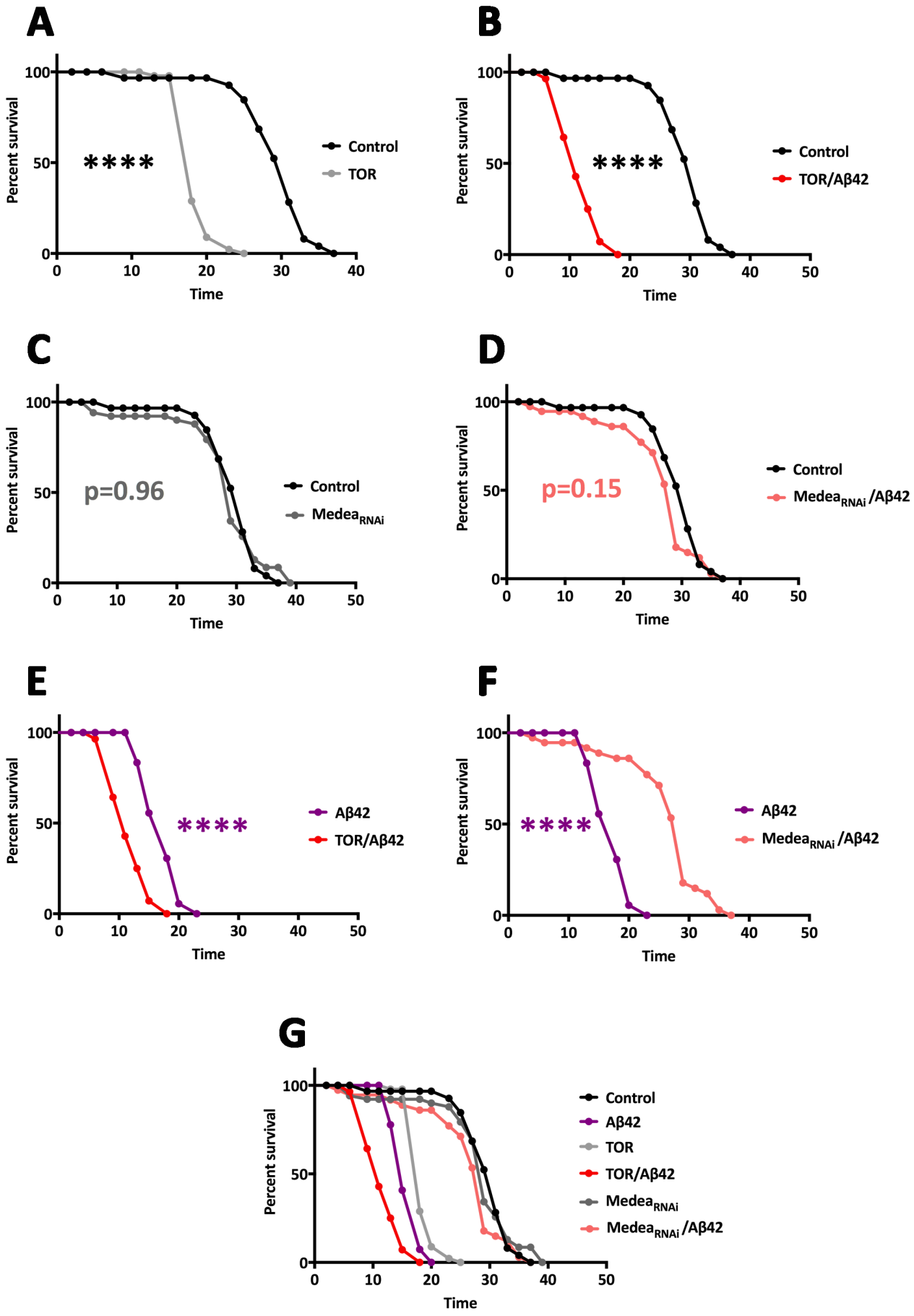
A
Percent survival
Time
****
Control
TOR
B
Percent survival
Time
****
Control
TOR/Aβ42
C
Percent survival
Time
p=0.96
Control
Medea RNAi
D
Percent survival
Time
p=0.15
Control
Medea RNAi /Aβ42
E
Percent survival
Time
****
Aβ42
TOR/Aβ42
F
Percent survival
Time
****
Aβ42
Medea RNAi /Aβ42
G
Percent survival
Time
Control
Aβ42
TOR
TOR/Aβ42
Medea RNAi
Medea RNAi /Aβ42

Fig. R9

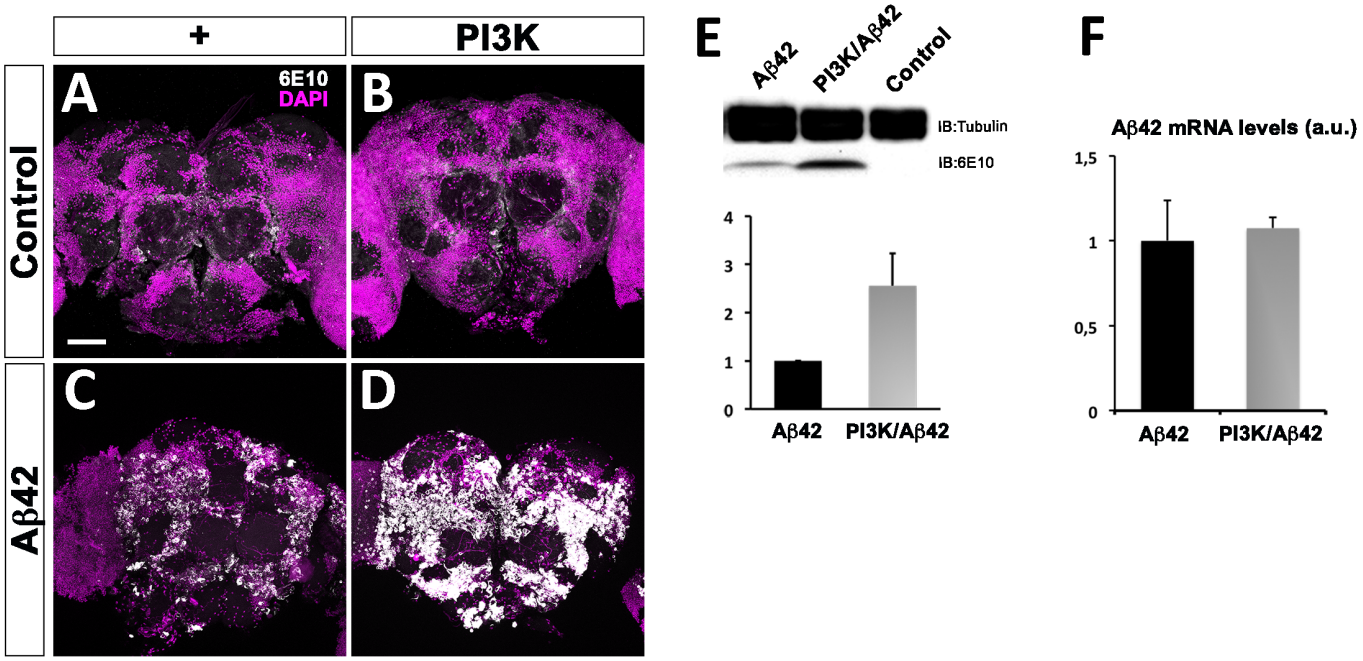
+
PI3K
Control
Aβ42
A
6E10
DAPI
B
C
D
E
Aβ42
PI3K/Aβ42
Control
IB:Tubulin
IB:6E10
4
3
2
1
0
Aβ42
PI3K/Aβ42
F
Aβ42 mRNA levels (a.u.)
1,5
1
0,5
0
Aβ42
PI3K/Aβ42

Fig. R10

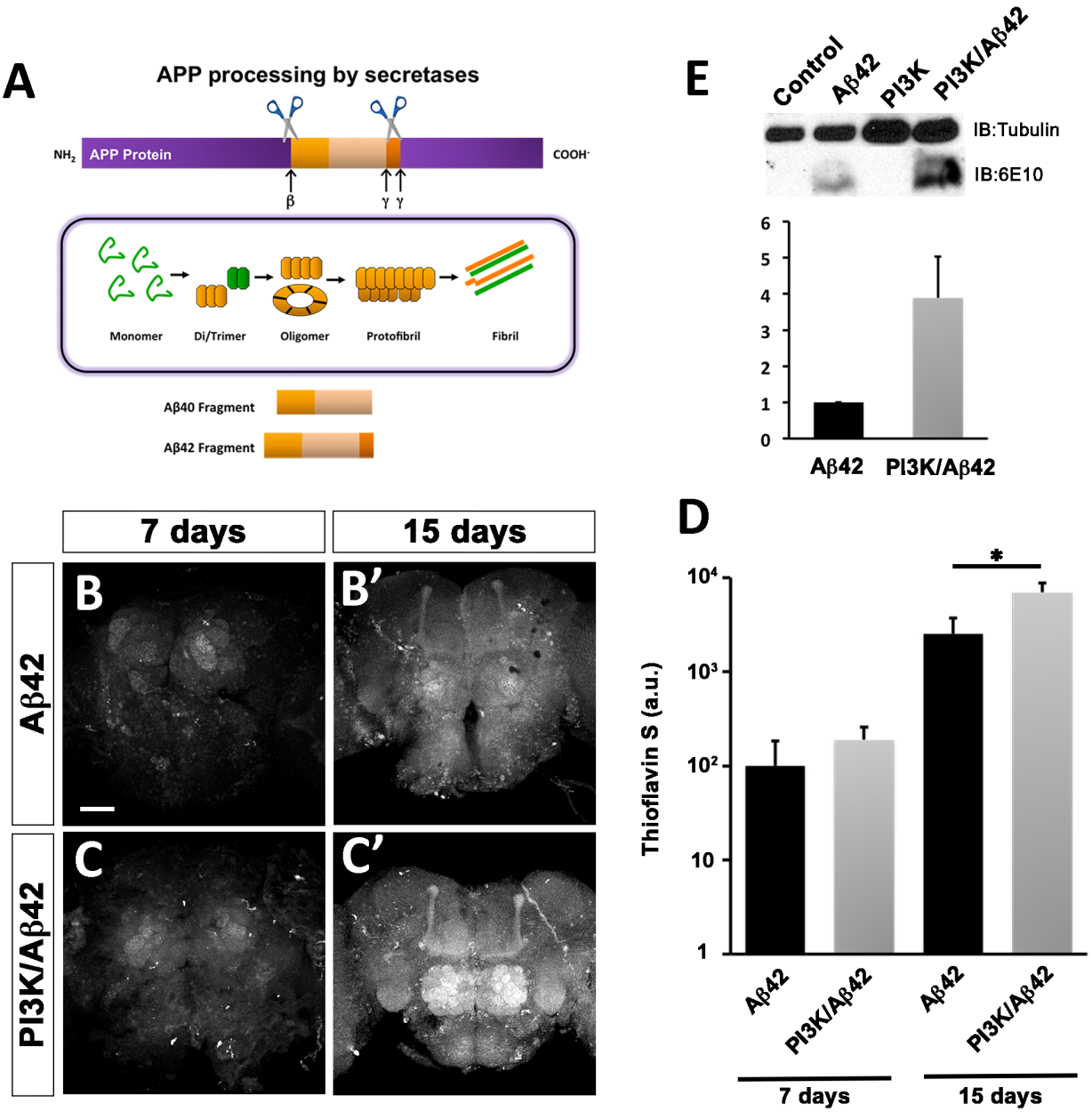
A
APP processing by secretases
NH2
APP Protein
COOH
β
γ γ
Monomer
Di/Trimer
Oligomer
Protofibril
Fibril
Aβ40 Fragment
Aβ42 Fragment
E
Control
Aβ42
PI3K
PI3K/Aβ42
IB:Tubulin
IB:6E10
6
5
4
3
2
1
0
Aβ42
PI3K/Aβ42
7 days
15 days
Aβ42
PI3K/Aβ42
B
B'
C
C'
D
Thioflavin S (a.u.)
10⁴
10³
10²
10
1
*
Aβ42
PI3K/Aβ42
Aβ42
PI3K/Aβ42
7 days
15 days

Fig. R11

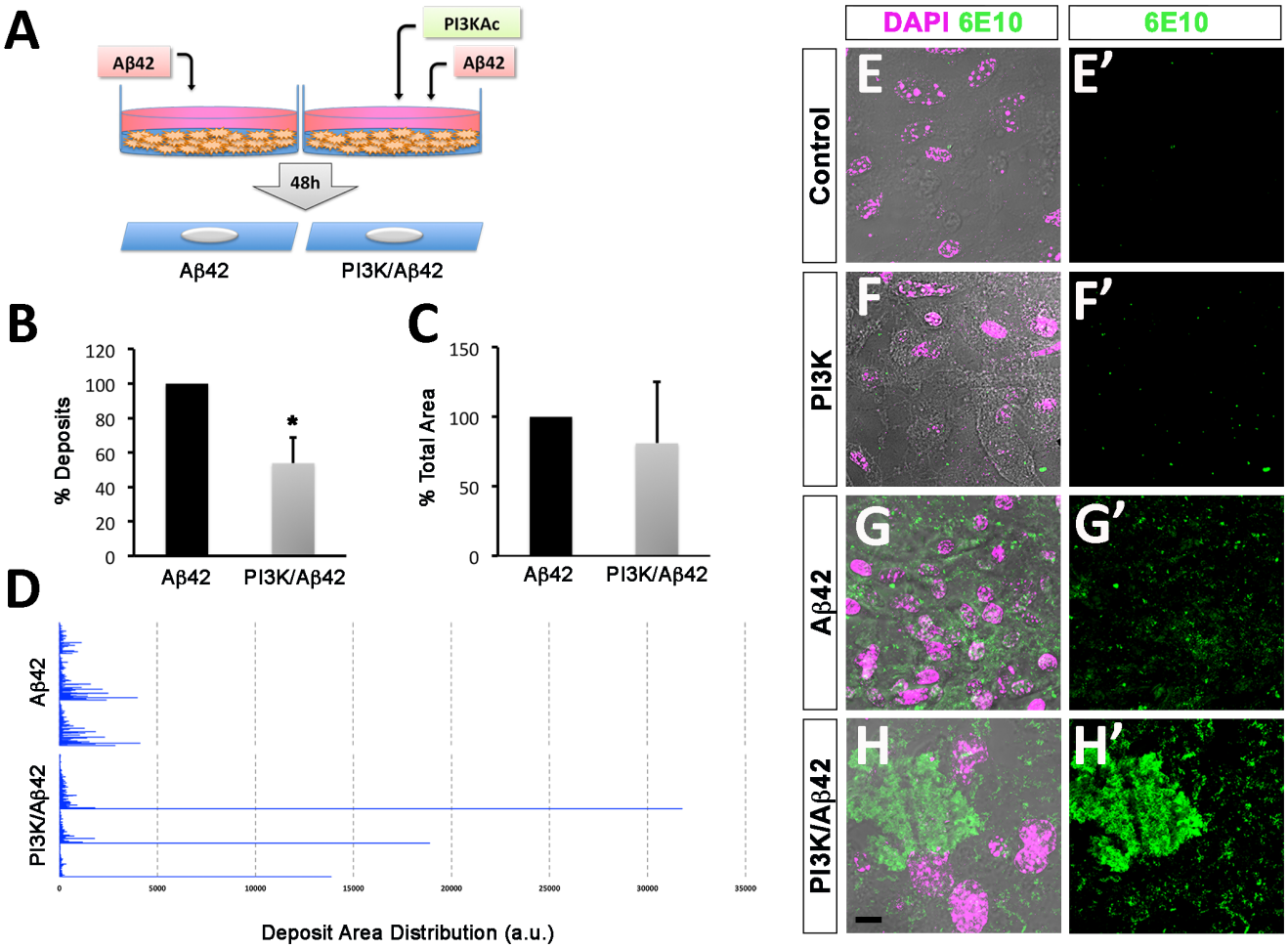
A
Aβ42
PI3KAc
Aβ42
48h
Aβ42
PI3K/Aβ42
B
% Deposits
120
100
80
60
40
20
0
*
Aβ42
PI3K/Aβ42
C
% Total Area
150
100
50
0
Aβ42
PI3K/Aβ42
D
Aβ42
PI3K/Aβ42
0
5000
10000
15000
20000
25000
30000
35000
Deposit Area Distribution (a.u.)
DAPI 6E10
6E10
Control
PI3K
Aβ42
PI3K/Aβ42
E
E'
F
F'
G
G'
H
H'

Fig. R12

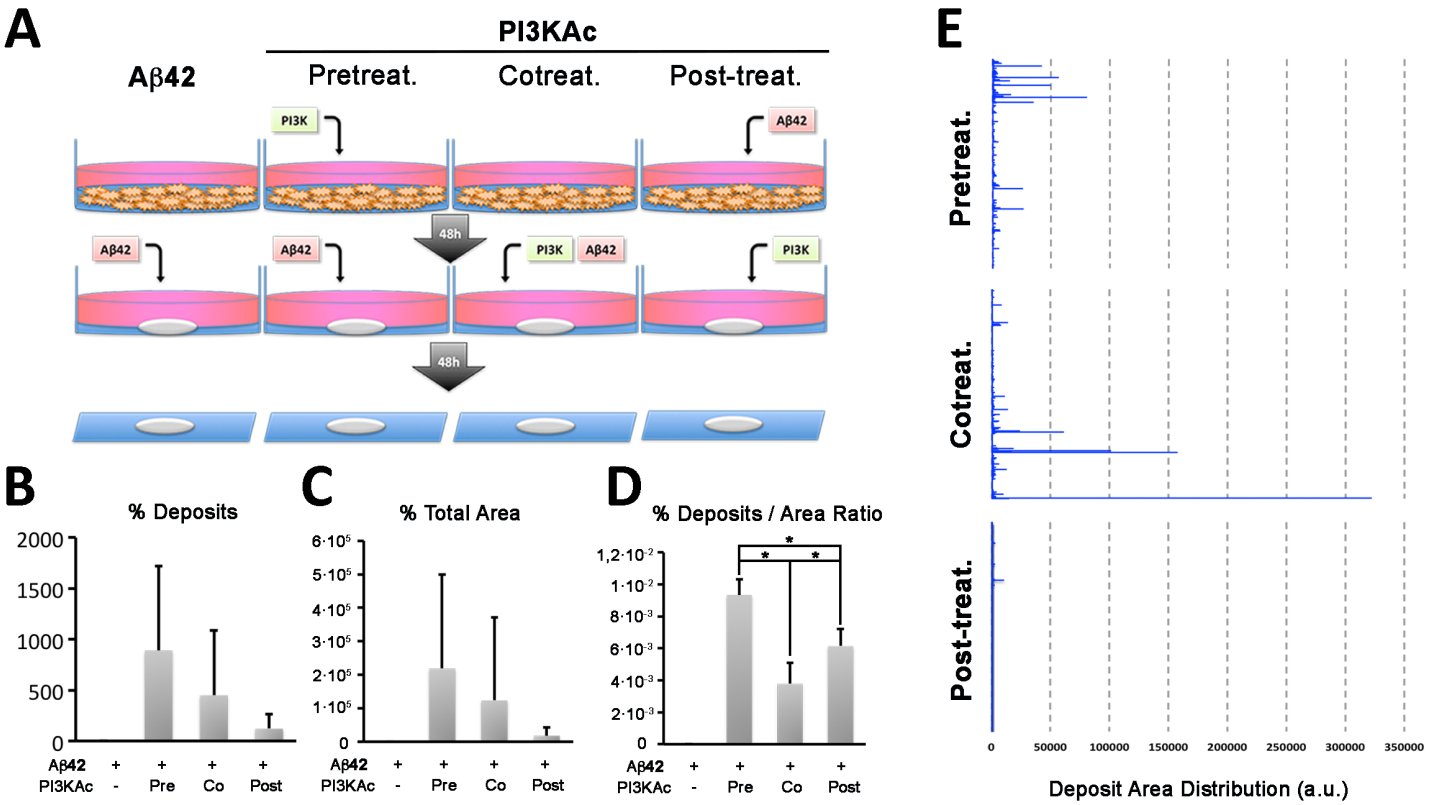
A
PI3KAc
Aβ42
Pretreat.
Cotreat.
Post-treat.
PI3K
Aβ42
48h
48h
B
% Deposits
2000
1500
1000
500
0
Aβ42 + + + +
PI3KAc - Pre Co Post
C
% Total Area
6·10⁵
5·10⁵
4·10⁵
3·10⁵
2·10⁵
1·10⁵
0
Aβ42 + + + +
PI3KAc - Pre Co Post
D
% Deposits / Area Ratio
1,2·10⁻²
1·10⁻²
8·10⁻³
6·10⁻³
4·10⁻³
2·10⁻³
0
*
*
*
Aβ42 + + + +
PI3KAc - Pre Co Post
E
Pretreat.
Cotreat.
Post-treat.
0
50000
100000
150000
200000
250000
300000
350000
Deposit Area Distribution (a.u.)

Fig. R13

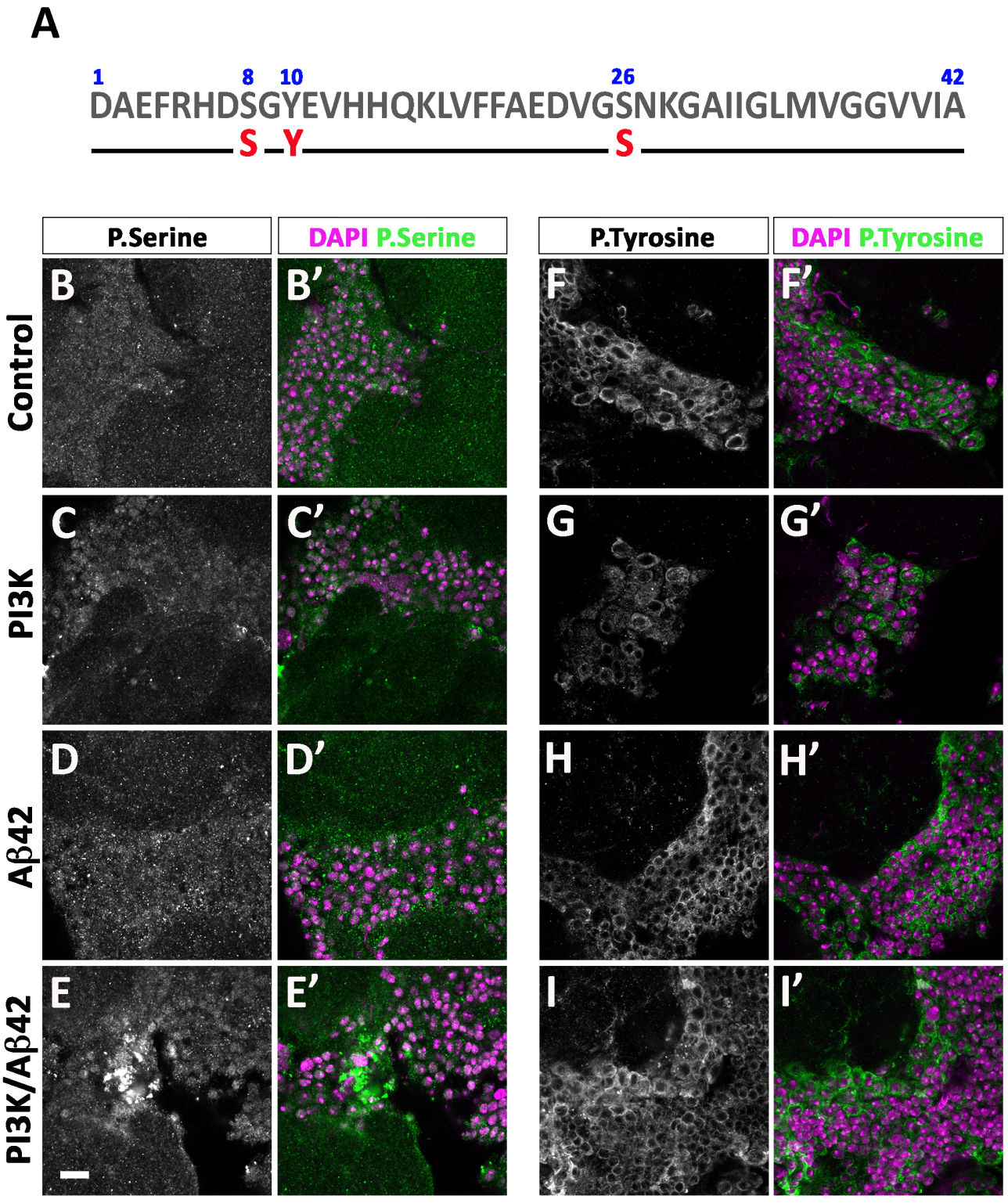
A
1
8
10
26
42
DAEFRHDSGYEVHHQKLVFFAEDVGSNKGAIIGLMVGGVVIA
S
Y
S
P.Serine
DAPI P.Serine
P.Tyrosine
DAPI P.Tyrosine
Control
PI3K
Aβ42
PI3K/Aβ42
B
B'
C
C'
D
D'
E
E'
F
F'
G
G'
H
H'
I
I'

Fig. R14

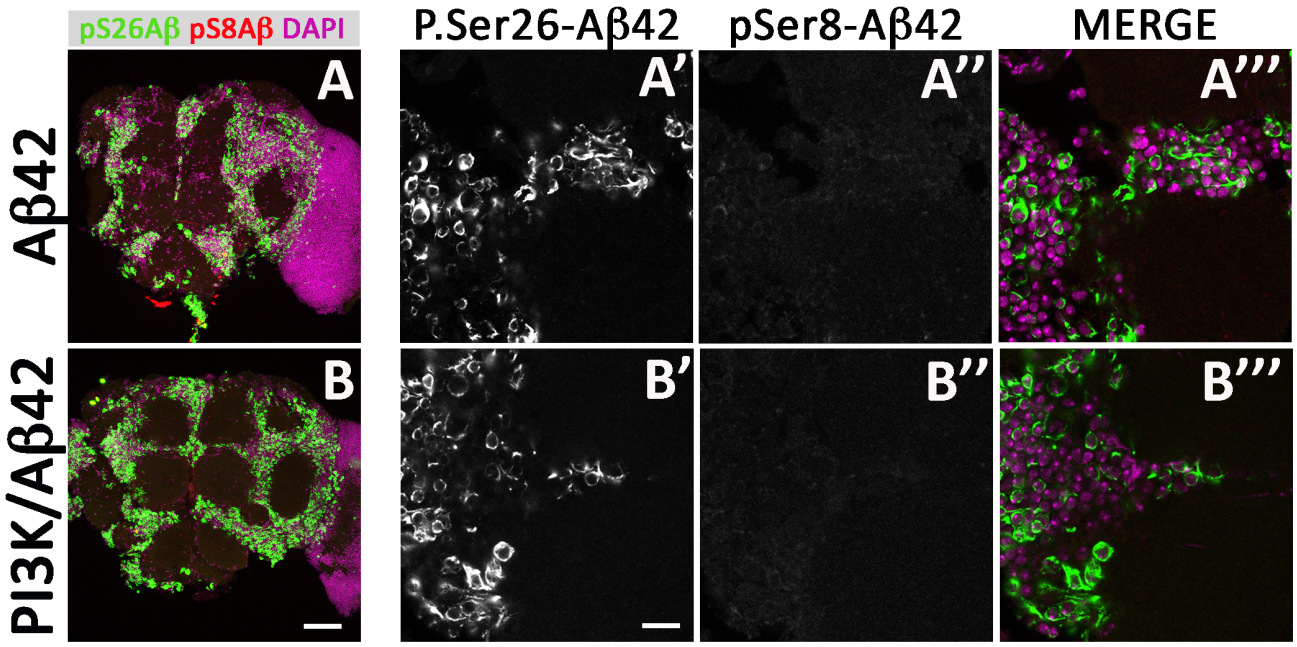
pS26Aβ pS8Aβ DAPI
P.Ser26-Aβ42
pSer8-Aβ42
MERGE
Aβ42
PI3K/Aβ42
A
A'
A''
A'''
B
B'
B''
B'''

Fig. R15

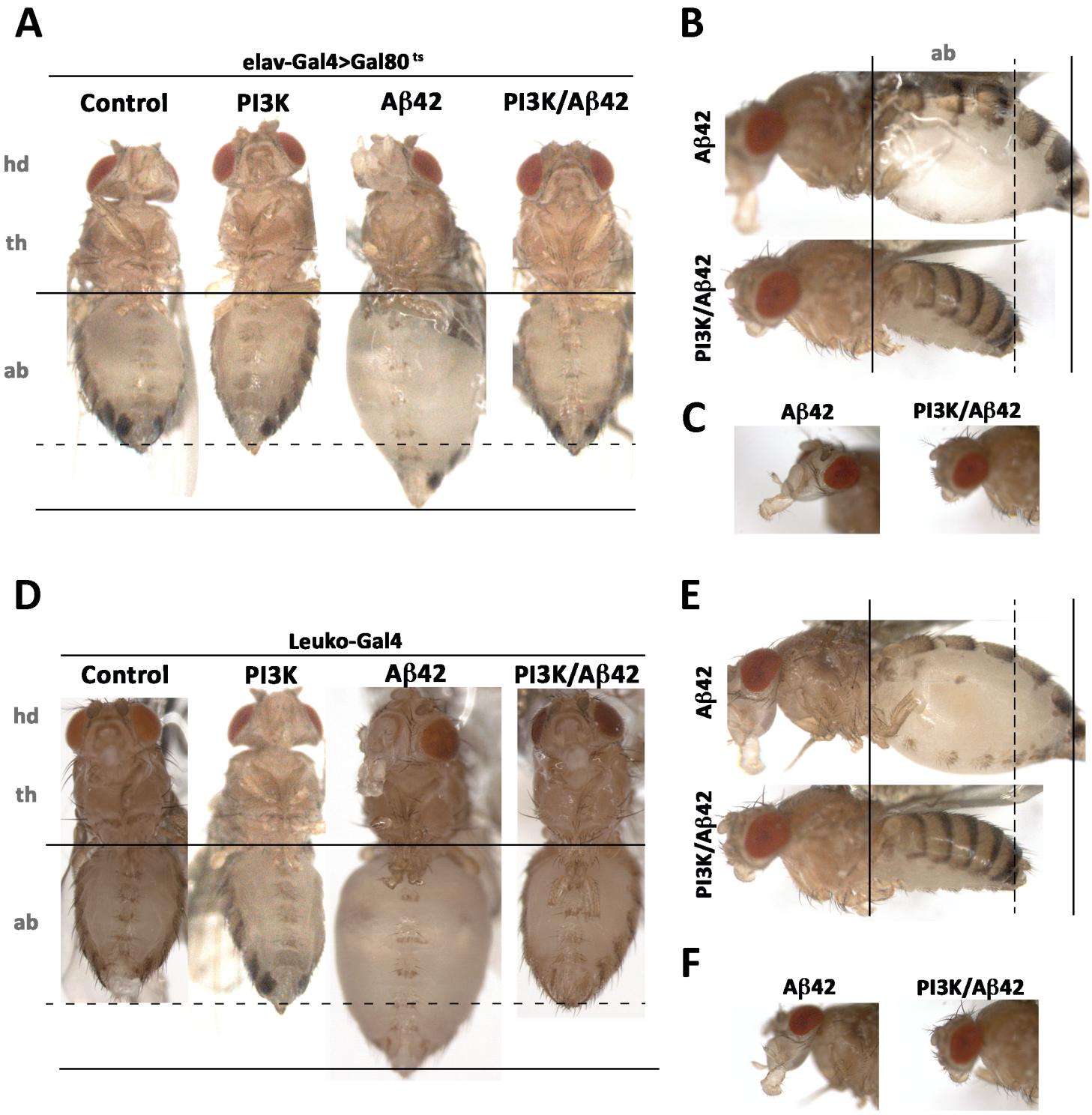
A
elav-Gal4>Gal80ts
Control
PI3K
Aβ42
PI3K/Aβ42
hd
th
ab
B
ab
Aβ42
PI3K/Aβ42
C
Aβ42
PI3K/Aβ42
D
Leuko-Gal4
Control
PI3K
Aβ42
PI3K/Aβ42
hd
th
ab
E
Aβ42
PI3K/Aβ42
F
Aβ42
PI3K/Aβ42

Fig. R16

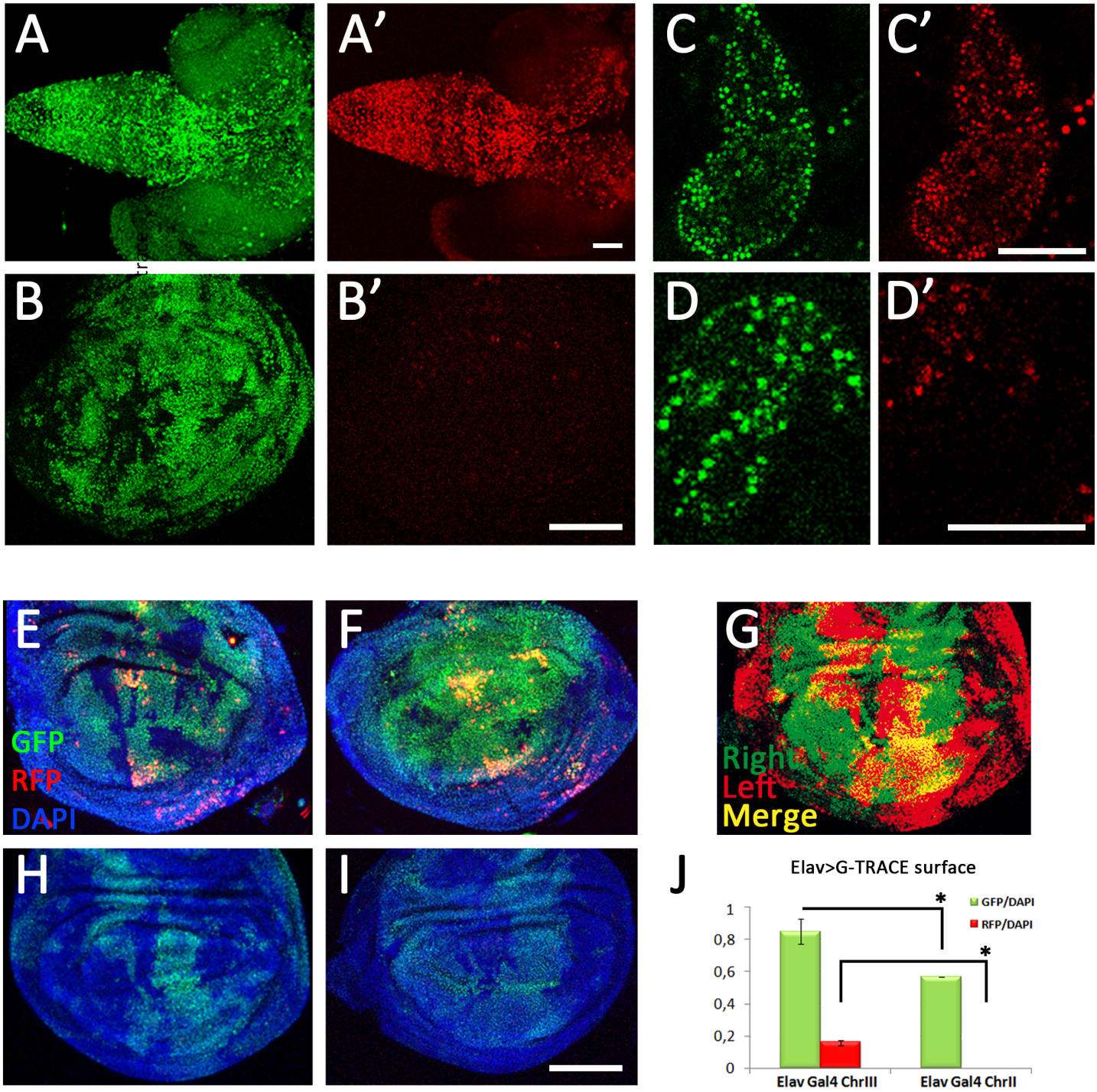
A
A'
C
C'
B
B'
D
D'
E
GFP
RFP
DAPI
F
G
Right
Left
Merge
H
I
J
Elav>G-TRACE surface
GFP/DAPI
RFP/DAPI
1
0,8
0,6
0,4
0,2
0
*
*
Elav Gal4 ChrIII
Elav Gal4 ChrII
K
GFP
RFP
DAPI
K'
Elav
L
GFP
RFP
DAPI
L'
Elav

Fig. R17

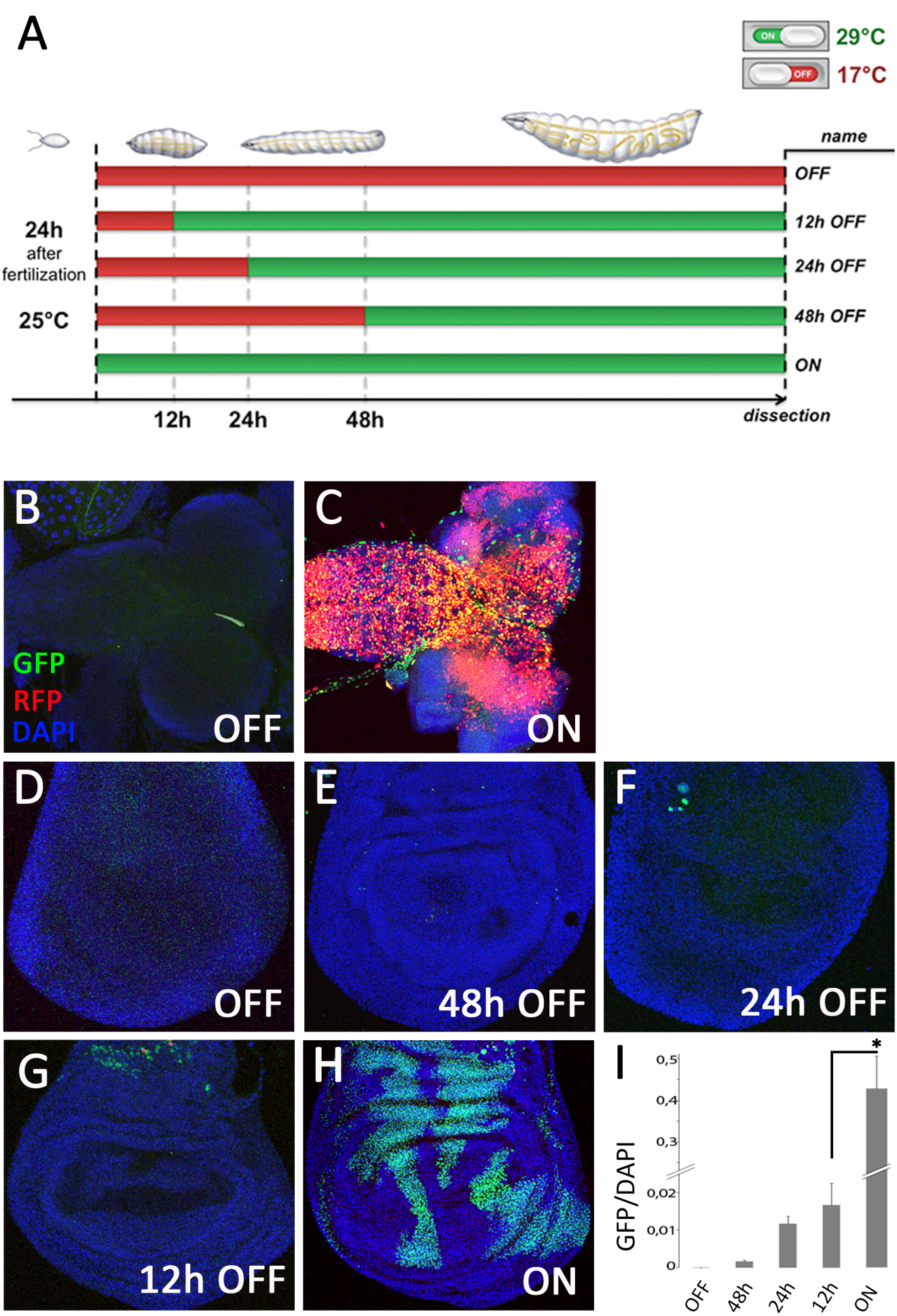
A
ON
29°C
OFF
17°C
name
OFF
12h OFF
24h OFF
48h OFF
ON
24h
after
fertilization
25°C
12h
24h
48h
dissection
B
GFP
RFP
DAPI
OFF
C
ON
D
OFF
E
48h OFF
F
24h OFF
G
12h OFF
H
ON
I
GFP/DAPI
0,5
0,4
0,3
0,02
0,01
0
*
OFF
48h
24h
12h
ON

Fig. R18

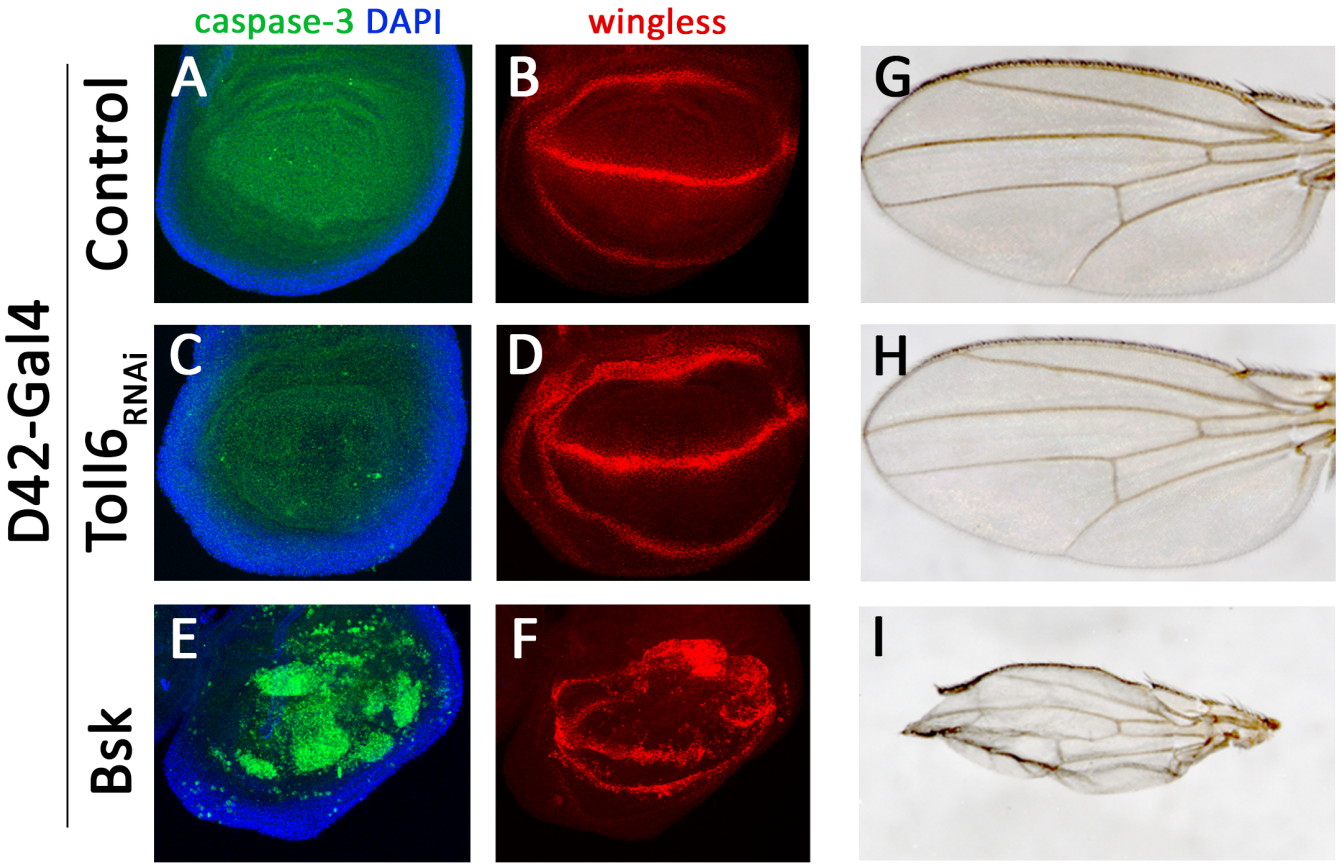
caspase-3 DAPI
wingless
D42-Gal4
Control
Toll6RNAi
Bsk
A
B
C
D
E
F
G
H
I

Fig. R19

Fig. R20

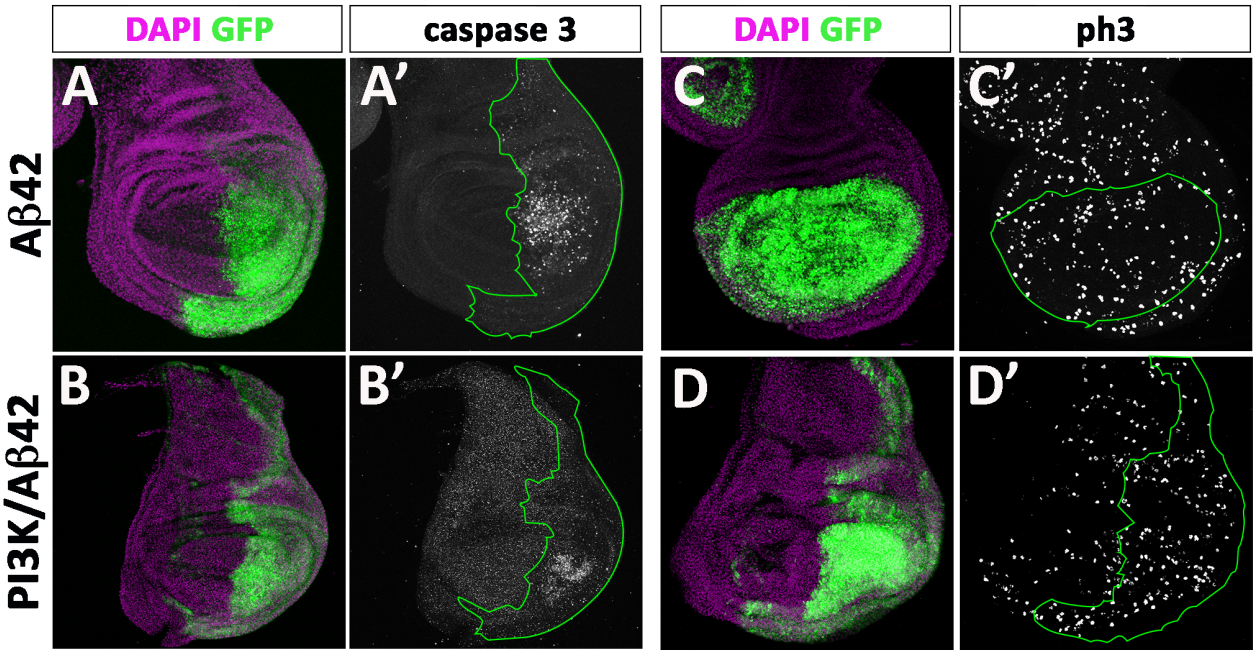

Fig. R21

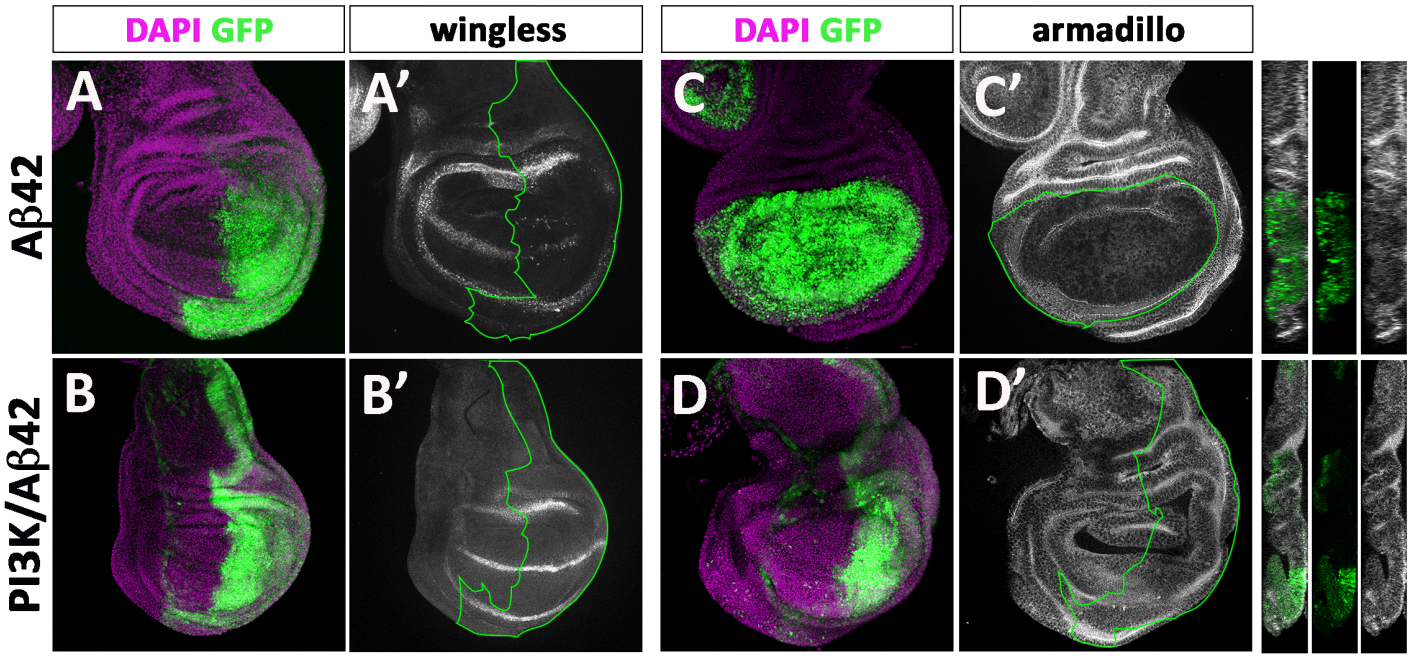
DAPI GFP
wingless
DAPI GFP
armadillo
Aβ42
PI3K/Aβ42
A
A'
C
C'
B
B'
D
D'

Fig. R22

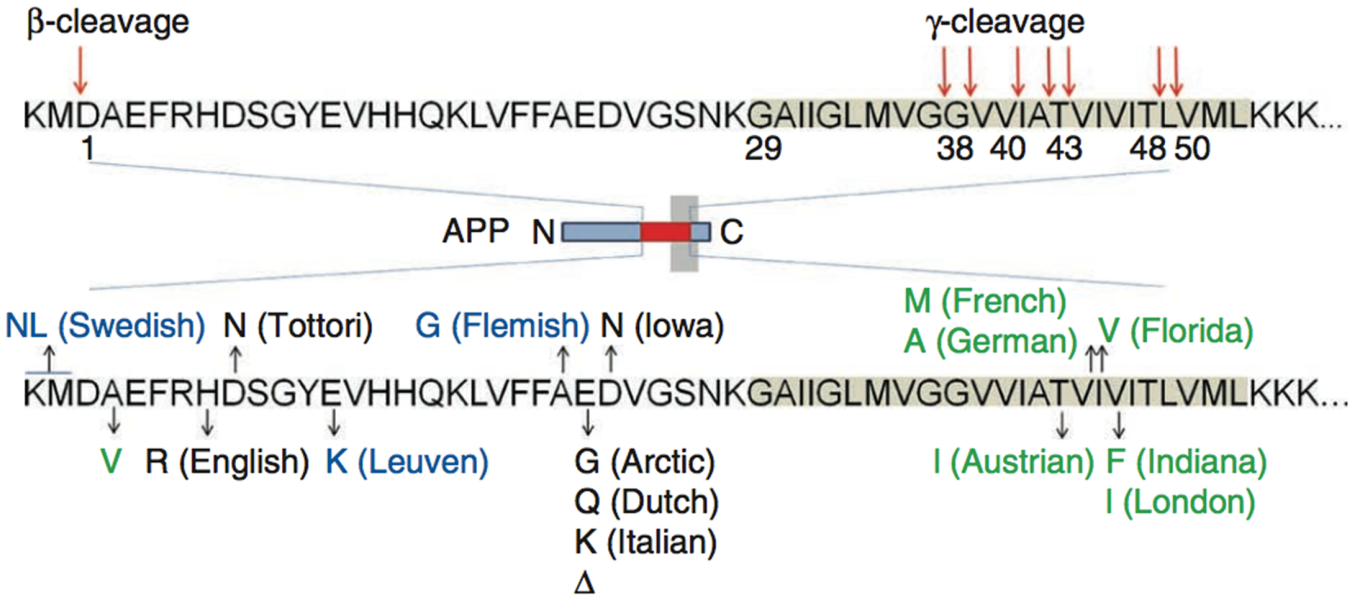
β-cleavage
γ-cleavage
KMDAEFRHDSGYEVHHQKLVFFAEDVGSNKGAIIGLMVGGVVIATVIVITLVMLKKK...
1
29
38 40 43
48 50
APP N C
NL (Swedish)
N (Tottori)
G (Flemish)
N (Iowa)
M (French)
A (German)
V (Florida)
KMDAEFRHDSGYEVHHQKLVFFAEDVGSNKGAIIGLMVGGVVIATVIVITLVMLKKK...
V
R (English)
K (Leuven)
G (Arctic)
Q (Dutch)
K (Italian)
Δ
I (Austrian)
F (Indiana)
I (London)

Fig. D1